



República Federativa do Brasil
Ministério da Economia
Instituto Nacional da Propriedade Industrial

(21) BR 102017021032-4 A2



(22) Data do Depósito: 29/09/2017

(43) Data da Publicação Nacional: 16/04/2019

(54) Título: MÉTODO DE SÍNTESE DE GRAFENO 3D A PARTIR DO POLITEREFTALATO DE ETILENO (PET)

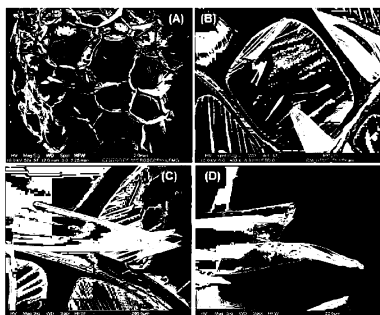
(51) Int. Cl.: C01B 32/184.

(52) CPC: C01B 32/184.

(71) Depositante(es): UNIVERSIDADE FEDERAL DE MINAS GERAIS.

(72) Inventor(es): LUIZ ORLANDO LADEIRA; CAMILA DE OLIVEIRA VIANA; TARCOZO DA CRUZ COSTA DE SOUZA; SÉRGIO LUÍS LIMA DE MORAES RAMOS.

(57) Resumo: MÉTODO DE SÍNTESE DE GRAFENO 3D A PARTIR DO POLITEREFTALATO DE ETILENO (PET). A presente tecnologia refere-se ao processo de síntese de uma estrutura tridimensional de carbono constituída de finas folhas de carbono em arranjo aleatório de baixa densidade e alta área superficial específica, aqui denominada de grafeno tridimensional ou grafeno 3D ou espuma de carbono. Este processo de síntese basicamente utiliza como precursor de carbono o polímero politereftalato de etileno também denominado PET que juntamente com um agente de expansão termodecompõem numa mesma faixa de temperatura próxima as temperaturas de amolecimento e de carbonização do PET. Este processo sincronizado de amolecimento, expansão e carbonização do PET é realizado sob pressão atmosférica em atmosfera inerte ou não, dependendo da sua aplicação pós-síntese. Este material, aqui denominado grafeno 3D, pode ser aplicado em várias áreas, tais como: suporte para fixação de elementos e compostos para catálise, como elemento de filtração e purificação de água, na fabricação de tintas condutoras, na área de armazenamento de energia, como fertilizante agrícola e como elemento de incorporação em matrizes poliméricas e cerâmicas.



“MÉTODO DE SÍNTESE DE GRAFENO 3D A PARTIR DO POLITEREFTALATO DE ETILENO (PET)”

[001] A presente tecnologia refere-se ao processo de síntese de uma estrutura tridimensional de carbono constituída de finas folhas de carbono em arranjo aleatório de baixa densidade e alta área superficial específica, aqui denominada de grafeno tridimensional ou grafeno 3D ou espuma de carbono. Este processo de síntese basicamente utiliza como precursor de carbono o polímero politereftalato de etileno também denominado PET que juntamente com um agente de expansão termodecompõem numa mesma faixa de temperatura próxima as temperaturas de amolecimento e de carbonização do PET. Este processo sincronizado de amolecimento, expansão e carbonização do PET é realizado sob pressão atmosférica em atmosfera inerte ou não, dependendo da sua aplicação pós-síntese. Este material, aqui denominado grafeno 3D, pode ser aplicado em várias áreas, tais como: suporte para fixação de elementos e compostos para catálise, como elemento de filtração e purificação de água, na fabricação de tintas condutoras, na área de armazenamento de energia, como fertilizante agrícola e como elemento de incorporação em matrizes poliméricas e cerâmicas.

[002] A ligação carbono-carbono pode ocorrer de duas formas distintas a saber: em coordenação tetraédrica denominada fase diamante ou em coordenação planar denominada grafite. Em condições de temperatura e pressão ambiente a forma estável é a fase grafite que é a forma planar constituída por um arranjo de empilhamento de múltiplas camadas de carbono. Uma única camada de carbono é denominada de grafeno cujas propriedades mecânicas, eletrônicas e químicas mostram um enorme potencial de aplicações em ciência e tecnologia. (Duplock, E. J.; Scheffler, M.; Lindan, P. J. D. *Hallmark of Perfect Graphene*. *Phys. Rev. Lett.* 92, 225502 – Published 3 June 2004), (Papageorgiou, D. G.; Kinloch, I. A.;

Young, R. J. *Mechanical properties of graphene and graphene-based nanocomposites. Progress in Materials Science 90 (2017) 75-127.*

[003] O grafeno apresenta-se atualmente como um material muito promissor para diversas aplicações tecnológicas em função de suas características e propriedades e atualmente ocorre um intenso esforço técnico/científico no desenvolvimento de novas tecnologias que permitam a sua aplicação a nível industrial. (Duplock, E. J.; Scheffler, M.; Lindan, P. J. D. *Hallmark of Perfect Graphene. Phys. Rev. Lett. 92, 225502 – Published 3 June 2004*), (Papageorgiou, D. G.; Kinloch, I. A.; Young, R. J. *Mechanical properties of graphene and graphene-based nanocomposites. Progress in Materials Science 90 (2017) 75-127*).

[004] Neste cenário, rotas de síntese para produção do grafeno tridimensional (3D) - também chamado de espumas, esponjas, redes ou quadros de grafeno - foram propostas por diversos pesquisadores, sendo este um nanomaterial versátil, pois mesmo sendo macroscópico, ou seja, um material expandido tal que tem a possibilidade de ser manipulado pela mão humana, exibe ainda as propriedades microscópicas do grafeno (Żelechowska, K.; Kondratowicz, I.; Sadowski, W. *3D porous graphene-based structures - synthesis and applications. Chapter 9, Carbon Nanotechnology. Editor Milne, W. I. One Central Press, 2013*).

[005] Aplicações diversas do grafeno 3D são mencionadas na literatura científica nas áreas como eletrônica, química, ciência dos materiais e biotecnologia. As principais formas de obtenção deste material envolvem a pirólise de precursores de carbono, naturais ou sintéticos. O processo de pirólise pode se dar utilizando “moldes” ou não para sua estruturação tridimensional. Por exemplo, é possível utilizar uma estrutura já tridimensional, tais como espumas de níquel ou esferas de sílica como moldes a para síntese do grafeno 3D e depois, eliminar tais arcabouços, resultando somente no grafeno tridimensional. Também, é possível produzir

a estruturas de grafeno já expandida, sem utilização de moldes através da redução de óxidos de grafeno em grafeno em alta temperatura (gelificação hidrotermal), ou utilizando processos de evaporação em vácuo, fermentação, filtração à vácuo, e moldagens à partir do açúcar, por sopro. (Wang, X., Zhang, Y., Zhi, C., Wang, X., Tang, D., Xu, Y, Bando, Y. *Three-dimensional strutted graphene grown by substrate-free sugar blowing for high-power-density supercapacitor.* *Nature communications.* 2013), (Żelechowska, K.; Kondratowicz, I.; Sadowski, W. *3D porous graphene-based structures - synthesis and applications. Chapter 9, Carbon Nanotechnology.* Editor Milne, W. I. One Central Press, 2013).

[006] Levantamentos realizados por pesquisadores ou instituições de proteção ambiental mostram um aumento vertiginoso da poluição dos oceanos por resíduos plásticos, sendo o PET um dos principais poluidores. (Jambeck, J. R.; Geyer R.; Wilcox C.; Siegler, T. R.; Perryman, M.; Andrade A.; Narayan R.; Law, K. L. *Plastic waste inputs from land into the ocean,* 2016. Science, Vol. 347, Issue 6223, pp. 768-771).

[007] O documento de patente US2017218166, de 2017, “*Polyethylene terephthalate – graphene nanocomposites*”, refere-se a um material nanocompósito composto de politereftalato de etileno (PET) como um polímero base e uma nanopartícula adicionada a ele, de modo aumentar a resistência mecânica do polímero base, não comprometendo a atividade inventiva da tecnologia, pois o politereftalato de etileno é usado como polímero base e não como precursor de carbono para obtenção do grafeno.

[008] O documento de patente CN101837972A, de 2010, intitulado “*Graphene three-dimensional structure and preparation method thereof*”, descreve a síntese do grafeno a partir de óxido de grafeno utilizando íons metálicos. No entanto, o processo produtivo e os materiais utilizados são diferentes da presente invenção em questão.

[009] O documento de patente CN101982408A, de 2011, intitulado "*Graphene three-dimensional material as well as preparation method and application thereof*", descreve a síntese do grafeno a partir de óxido de grafeno seguida de liofilização, diferenciando-se da tecnologia proposta nesta invenção.

[010] A patente CN102674321 (A), de 2012, intitulado "*Graphene foam with three dimensional fully connected network and macroscopic quantity preparation method thereof*", descreve a síntese do grafeno pelo método de Deposição Química da fase de Vapor (CVD) usando um molde metálico para obtenção da estrutura tridimensional, diferenciando-se da tecnologia proposta nesta invenção.

[011] O documento de patente CN101993056, de 2011, com o seguinte título "*Graphene-based porous macroscopic carbon material and preparation method thereof*", descreve a síntese do grafeno a partir de óxido de grafeno e álcool polivinílico seguida de redução hidrotermal, diferenciando-se da tecnologia proposta nesta invenção.

[012] O artigo "Green synthesis of graphene from recycled PET bottle wastes for use in the adsorption of dyes in aqueous solution", 2017, descreve a síntese de uma estrutura de grafeno com o uso do PET e de um catalisador. No entanto, o processo utilizado diferencia-se do proposto nesta tecnologia devido a necessidade de um sistema de autoclave, da qualidade do material e da pequena taxa de produção (El Essawy, N. A; Alib, S. F.; Faragc, H. A.; Konsowac, A. H.; Elnoubyd, M.; Hamade, H. A. Green synthesis of graphene from recycled PET bottle wastes for use in the adsorption of dyes in aqueous solution. Ecotoxicology and Environmental Safety, 145. 57-68. 2017).

[013] O artigo intitulado "*Three-dimensional struttured graphene grown by substrate-free sugar blowing for high-power-density supercapacitor*" utiliza um método similar à da presente invenção para a síntese do grafeno,

utilizando o açúcar como precursor de carbono e não o PET (Wang, X., Zhang, Y., Zhi, C., Wang, X., Tang, D., Xu, Y., Bando, Y. *Nature communications*. 2013), diferenciando-se da tecnologia proposta nesta invenção.

[014] O artigo “*3D Oxidized Graphene Frameworks for Efficient Nano Sieving*”, de 2016, trata-se da síntese de uma estrutura de grafeno 3D, sem moldes, utilizando o bagaço de cana de açúcar como precursor de carbono e não o PET como descrito nesta tecnologia (Pawar, P. B., Saxena, S., Badhe, D. K., Chaudhary, R. P., Shukla, S. *3D Oxidized Graphene Frameworks for Efficient Nano Sieving. Scientific Reports*, 2013).

[015] Apesar do enorme potencial de aplicação, os processos de síntese de grafeno propostos e desenvolvidos no ambiente científico/acadêmico não possuem reproduzibilidade em ambiente industrial. A produção em larga escala é hoje o maior desafio para a aplicação deste revolucionário nanomaterial em diversos setores industriais.

[016] Na presente tecnologia grafeno tridimensional (grafeno 3D) é obtido utilizando o polímero politereftalato de etileno (PET) como precursor de carbono. Portanto, apesar de já existirem métodos para a produção de grafeno tridimensional (3D), ainda não foi mencionado no estado da técnica métodos utilizando o PET como precursor de carbono.

[017] O método proposto nesta invenção não requer moldes e é similar à moldagem do açúcar por sopro. Para a síntese do grafeno 3D é utilizado além do PET, um agente de expansão, seja um sal inorgânico ou orgânico, que se decompõe termicamente gerando gases e vapores sob condições oxidantes ou não oxidantes. O processo é análogo ao açúcar soprado sendo que inicialmente, o agente de expansão, age de forma a aumentar o volume do material amolecido, decompondo-se e gerando gases, sendo o responsável pela expansão do material. Em seguida, dá-se início ao processo de carbonização seguido ou não de grafitização.

[018] Portanto, os processos envolvidos nesta síntese são originais e facilmente executáveis que, consequentemente, servirão como base tecnológica para o estabelecimento de um processo de produção de grafeno 3D com viabilidade de ser executado em escala industrial e à baixo custo, que é objeto desta patente. Ademais, por fazer uso do PET como material precursor de carbono, enquadra-se como um processo de reciclagem/reaproveitamento de resíduos de PET, caracterizando-se como uma “tecnologia verde” e de impacto muito positivo na sustentabilidade ambiental.

[019] Além do método proposto apresentar baixo custo, ele pode utilizar montagens relativamente simples e insumos facilmente empregados no meio industrial. O grafeno 3D produzido na presente invenção apresenta alto potencial de uso e interesse comercial abrangendo aplicações diversas como: purificação, filtração, tintas e materiais condutores. Além de outras como energia em supercapacitores, baterias e em ciência dos materiais (compósitos poliméricos e cimentícios).

BREVE DESCRIÇÃO DAS FIGURAS

[020] A **Figura 1** apresenta imagens MEV da estrutura tridimensional do material após o processo de carbonização, com os aumentos de 52 vezes (A), 403 vezes (B), 686 vezes (C), 5617 vezes (D).

[021] A **Figura 2** apresenta o espectro EDS, à esquerda, representativo da imagem obtida por MEV mostrada à direita com um aumento de 244 vezes.

[022] A **Figura 3** apresenta o perfil de perda de massa (linha sólida; eixo da esquerda) e sua derivada (linha tracejada; eixo da direita) obtidos por análise termogravimétrica.

[023] A **Figura 4** apresenta o espectro de espalhamento Raman.

[024] A **Figura 5** apresenta uma imagem obtida por microscopia eletrônica de transmissão (MET) (A) e o padrão de difração de elétrons da área selecionada (B).

DESCRÍÇÃO DETALHADA DA TECNOLOGIA

[025] A presente tecnologia refere-se a método de preparação de grafeno tridimensional (3D) utilizando o polímero politereftalato de etileno (PET) como precursor de carbono.

[026] Mais especificamente, a presente invenção refere-se a uma rota de síntese para obtenção de grafeno 3D. Esta síntese é realizada em um reator com atmosfera e temperatura controladas ou não, onde os insumos, o PET e um agente de expansão (um sal inorgânico ou orgânico) que se decompõem termicamente gerando gases e vapores sob condições atmosféricas oxidantes ou não oxidantes.

[027] O método proposto para a obtenção do grafeno 3D a partir do politereftalato de etileno (PET) realizado com o controle da atmosfera no reator compreende as seguintes etapas:

- a. Retirar todo o oxigênio presente no reator com a injeção de um fluxo de um gás inerte, durante 30 a 60 minutos, preferencialmente 40 minutos;
- b. Triturar o PET até obter uma granulometria entre 0,3 e 1,5 mm, preferencialmente 0,3 mm;
- c. Misturar o agente expansivo, sais ou ácidos que se decompõem termicamente e geram gases na faixa de 150°C a 480°C, com o material processado;
- d. Pré-aquecer o material em conjunto com o agente de expansão durante 20 a 30 minutos, preferencialmente 30 minutos;
- e. Aquecer o reator em temperaturas de 150 a 480 °C, preferencialmente 260 °C, a uma taxa de 1 a 50 °C/min, preferencialmente 5°C/min, por um período entre 5 e 600 minutos, preferencialmente 60 minutos;
- f. Caso a aplicação tenha a necessidade de um material com alta condutividade térmica e elétrica é necessário aquecer e manter o

reator entre 700 a 1500 °C, preferencialmente 1500 °C por 120 a 220 minutos, preferencialmente 180 minutos;

- g. Refriar o reator a temperatura ambiente, e retirar o material obtido.

[028] O método proposto para obtenção do grafeno 3D realizado em atmosfera oxidante compreende as seguintes etapas:

- a. Triturar o PET até obter uma granulometria entre 0,3 e 1,5 mm, preferencialmente 0,3 mm;
- b. Misturar o agente expansivo, sais ou ácidos que se decompõem termicamente e geram gases na faixa de 150°C a 380°C, com o material processado;
- c. Pré-aquecer o material em conjunto com o agente de expansão durante 20 ou 30 minutos, preferencialmente 30 minutos;
- d. Aquecer o reator em temperaturas de 150 a 380 °C, preferencialmente 260 °C, a uma taxa de 1 a 50 °C/min, preferencialmente 5 °C/min, por um período entre 5 e 600 minutos, preferencialmente 60 minutos.

EXEMPLO 1 – Método de preparação de grafeno tridimensional (3D) utilizando o polímero politereftalato de etileno (PET) como precursor de carbono e diferentes tipos de agentes expansivos.

[029] Este processo pode ser realizado com a injeção ou não de um fluxo de um gás inerte (argônio, nitrogênio, etc.) ou gases redutores como monóxido de carbono, amônia, hidrogênio ou outros gases durante um tempo determinado ou até que se verifique a inexistência de oxigênio no sistema. O processo é análogo ao do açúcar soprado, sendo que inicialmente, o agente de expansão gere gases que permita o aumento de volume do material.

[030] O PET foi primeiramente processado de forma a obter uma granulometria adequada (0,3 mm) e posteriormente misturada com o

agente de expansão (sais ou ácidos que se decompõem termicamente e geram gases na faixa de 150°C a 480°C) e então esta mistura foi colocada no reator. Os parâmetros temperatura de pré-aquecimento foram ajustadas para 260°C por 30 minutos para realizar a síntese. Antes de iniciar o processo em si, foi necessário a purga do reator, retirando o oxigênio existente dentro do mesmo, durante 40 minutos. Este tempo pode variar dependendo do volume de material a ser carbonizado. Para um reator de diâmetro aproximado de 200 mm e comprimento de 1500 mm o tempo de 40 minutos é ideal.

[031] Após a purga, o reator foi aquecido a partir da temperatura ambiente até alcançar temperatura superior à temperatura de amolecimento do polímero (~260°C), a uma taxa de 5 °C/min ou menor. A temperatura foi mantida acima deste valor por um tempo aproximado de 60 min. Nesta etapa ocorreu a expansão volumétrica deste material gerando uma espuma de carbono na faixa 480 °C. Em seguida, deu-se início ao processo de carbonização. Para isto, o reator foi aquecido a uma taxa aproximada 5 °C/min até alcançar temperaturas na faixa de 700 a 1500 °C preferencialmente 750 °C para completar o processo de deshidrogenação e eliminação de outros grupos químicos do polímero. Após o resfriamento do reator, retirou-se o material.

[032] O processo acima descrito utilizou como agente expansivo o sal cloreto de amônio. Como teste efetivo, nesta rota de obtenção de grafeno tridimensional, o PET triturado foi misturado com o cloreto de amônio na proporção de 1:1 em massa, pré-aquecido a 300 °C por 30 minutos, pirolisado, por 2 horas a 750 °C e grafitizado por 1h a 1500 °C em atmosfera de argônio.

[033] O material obtido a partir deste processo é altamente poroso, contendo poros com tamanhos variados - de 0,3 mm a 1,4 mm de diâmetro

- como demonstrado na imagem de Microscopia Eletrônica de Varredura de elétrons (MEV), Figura 1.

[034] O material possui em sua composição apenas os elementos carbono e oxigênio, conforme demonstrado na Figura 2, pela análise de Espectroscopia por Dispersão de Energia de Raios X (EDS) realizada na imagem de microscopia eletrônica de varredura.

[035] Ainda, a análise de termogravimetria (TGA) ilustrada na Figura 3, mostra que este material é constituído por aproximadamente 93 % de carbono puro e sua decomposição térmica, com início na temperatura de 500 °C e término em 950 °C, ocorre em dois estágios indicando um material semicristalino.

[036] Através da técnica de Espectroscopia Raman, verifica-se que o material obtido a partir da presente invenção exibe características espectrais de um material caracterizado por uma estrutura cristalina ou semi-cristalina de grafite, possuindo picos característicos de grafeno e de estruturas grafíticas - especificamente a presença das bandas D, G, G', como ilustra a Figura 4.

[037] Com o objetivo de verificar o arranjo cristalino da estrutura do material sintetizado, a amostra foi avaliada pela técnica de microscopia eletrônica de transmissão (MET). A Figura 5 apresenta a imagem obtida, juntamente com o padrão de difração de elétrons da mesma.

REIVINDICAÇÕES

1. MÉTODO DE SÍNTESE DE GRAFENO 3D caracterizado pela obtenção do grafeno 3D a partir do politereftalato de etileno (PET) com controle da atmosfera no reator, compreendendo as seguintes etapas:

- a) Retirar todo o oxigênio presente no reator com a injeção de um fluxo de um gás inerte, durante 30 a 60 minutos, preferencialmente 40 minutos;
- b) Triturar o PET até obter uma granulometria entre 0,3 e 1,5 mm, preferencialmente 0,3 mm;
- c) Misturar o agente expansivo, sais ou ácidos que se decompõem termicamente e geram gases na faixa de 150°C a 480°C, com o material processado;
- d) Pré-aquecer o material em conjunto com o agente de expansão durante 20 a 30 minutos, preferencialmente 30 minutos;
- e) Aquecer o reator em temperaturas de 150 a 480 °C, preferencialmente 260 °C, a uma taxa de 1 a 50 °C/min, preferencialmente 5°C/min, por um período entre 5 e 600 minutos, preferencialmente 60 minutos;
- f) Caso a aplicação tenha a necessidade de um material com alta condutividade térmica e elétrica é necessário aquecer e manter o reator entre 700 a 1500 °C, preferencialmente 1500 °C por 120 a 220 minutos, preferencialmente 180 minutos;
- g) Resfriar o reator a temperatura ambiente, e retirar o material obtido.

2. MÉTODO DE SÍNTESE DE GRAFENO 3D caracterizado pela obtenção do grafeno 3D a partir do politereftalato de etileno (PET) com atmosfera oxidante compreendendo as seguintes etapas:

- a) Triturar o PET até obter uma granulometria entre 0,3 e 1,5 mm, preferencialmente 0,3 mm;

- b) Misturar o agente expansivo, sais ou ácidos que se decompõem termicamente e geram gases na faixa de 150°C a 380°C, com o material processado;
- c) Pré-aquecer o material em conjunto com o agente de expansão durante 20 ou 30 minutos, preferencialmente 30 minutos;
- d) Aquecer o reator em temperaturas de 150 a 380 °C, preferencialmente 260 °C, a uma taxa de 1 a 50 °C/min, preferencialmente 5 °C/min, por um período entre 5 e 600 minutos, preferencialmente 60 minutos.

DESENHOS

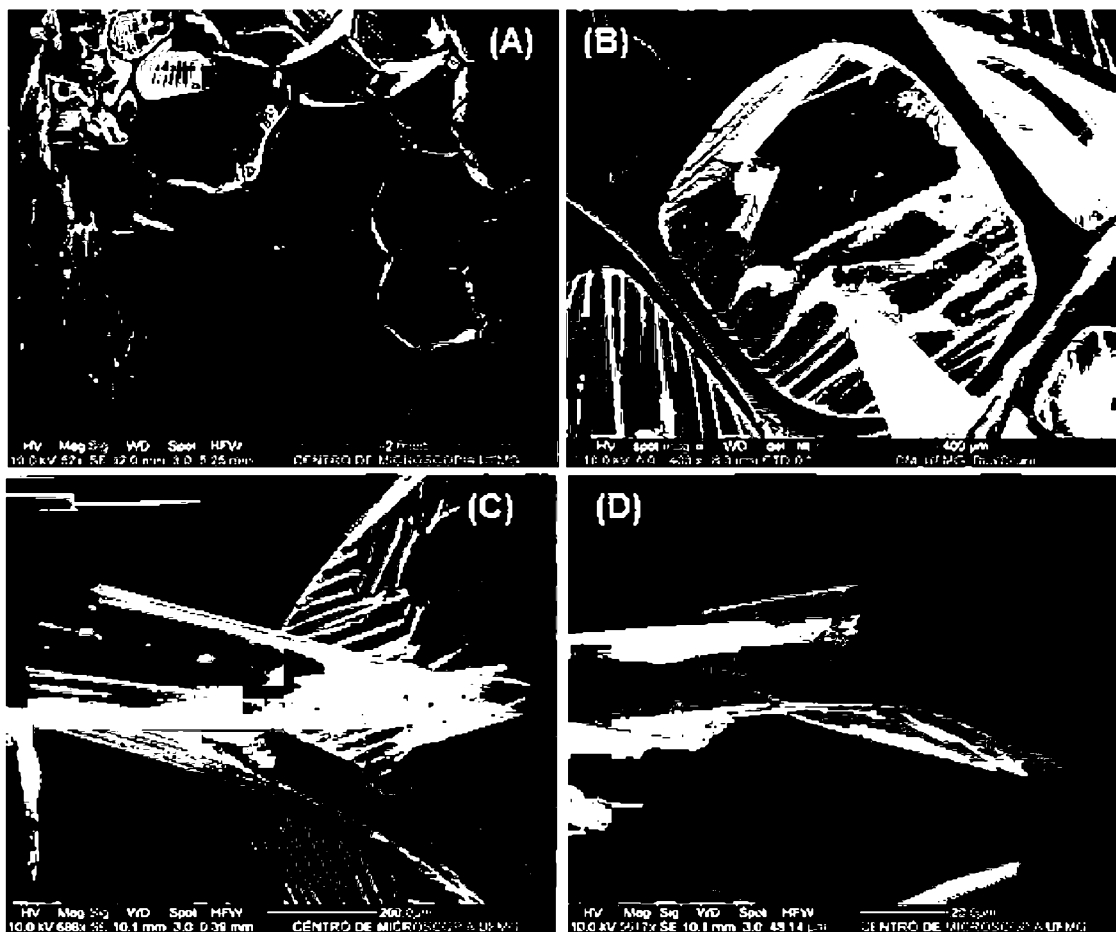


FIGURA 1

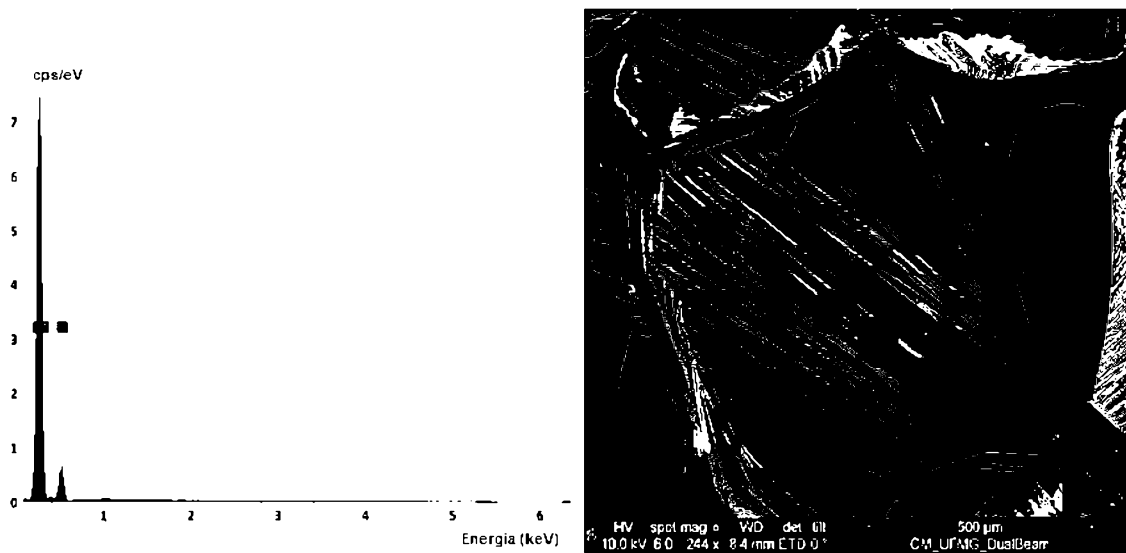
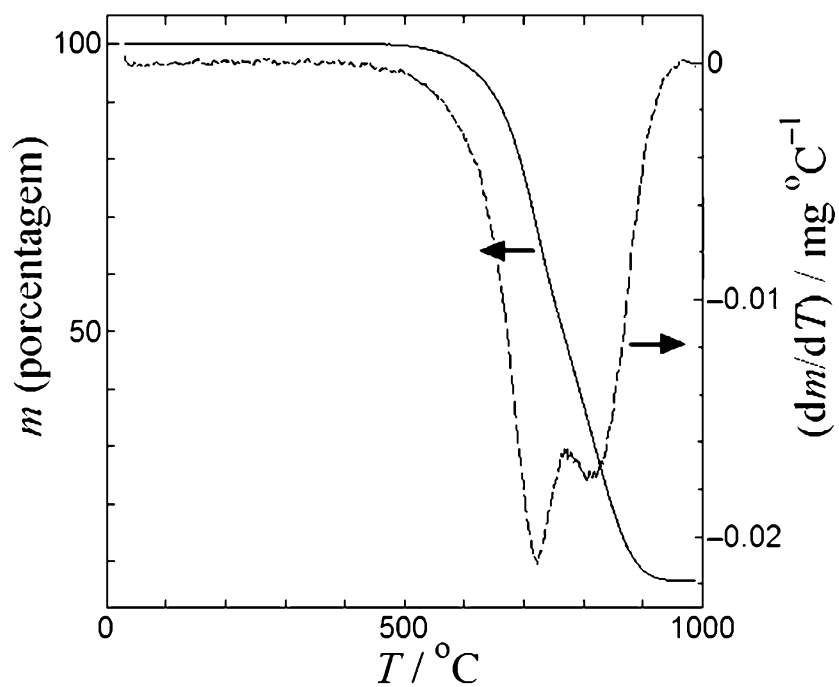
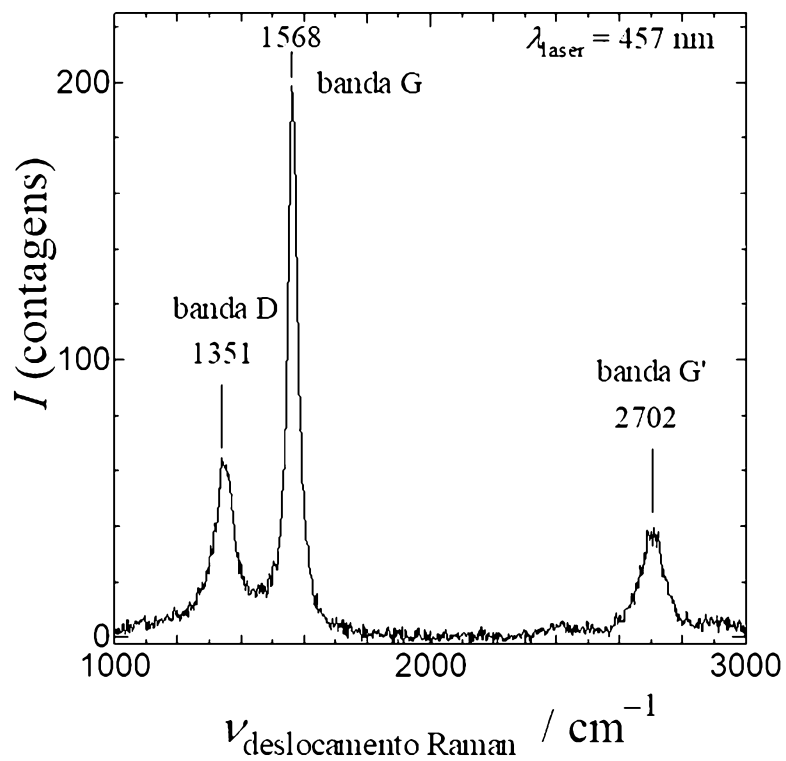


FIGURA 2

**FIGURA 3****FIGURA 4**

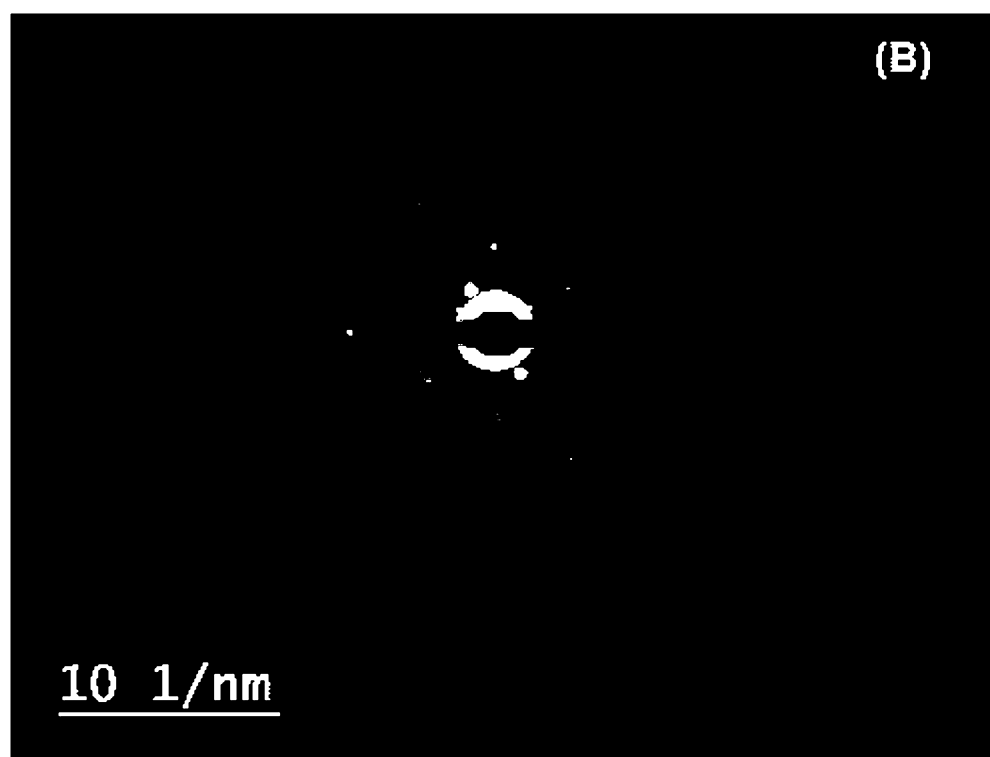
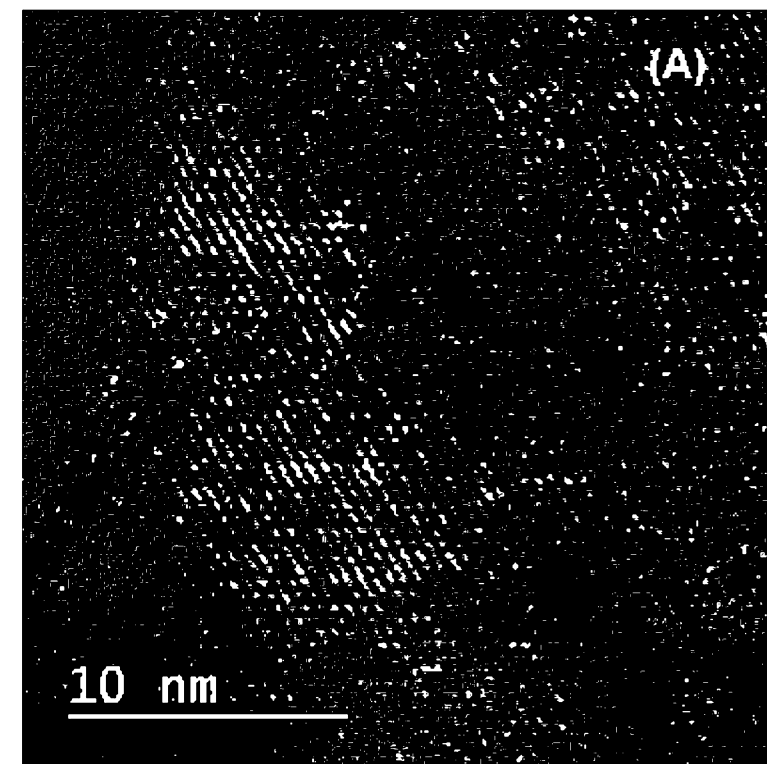


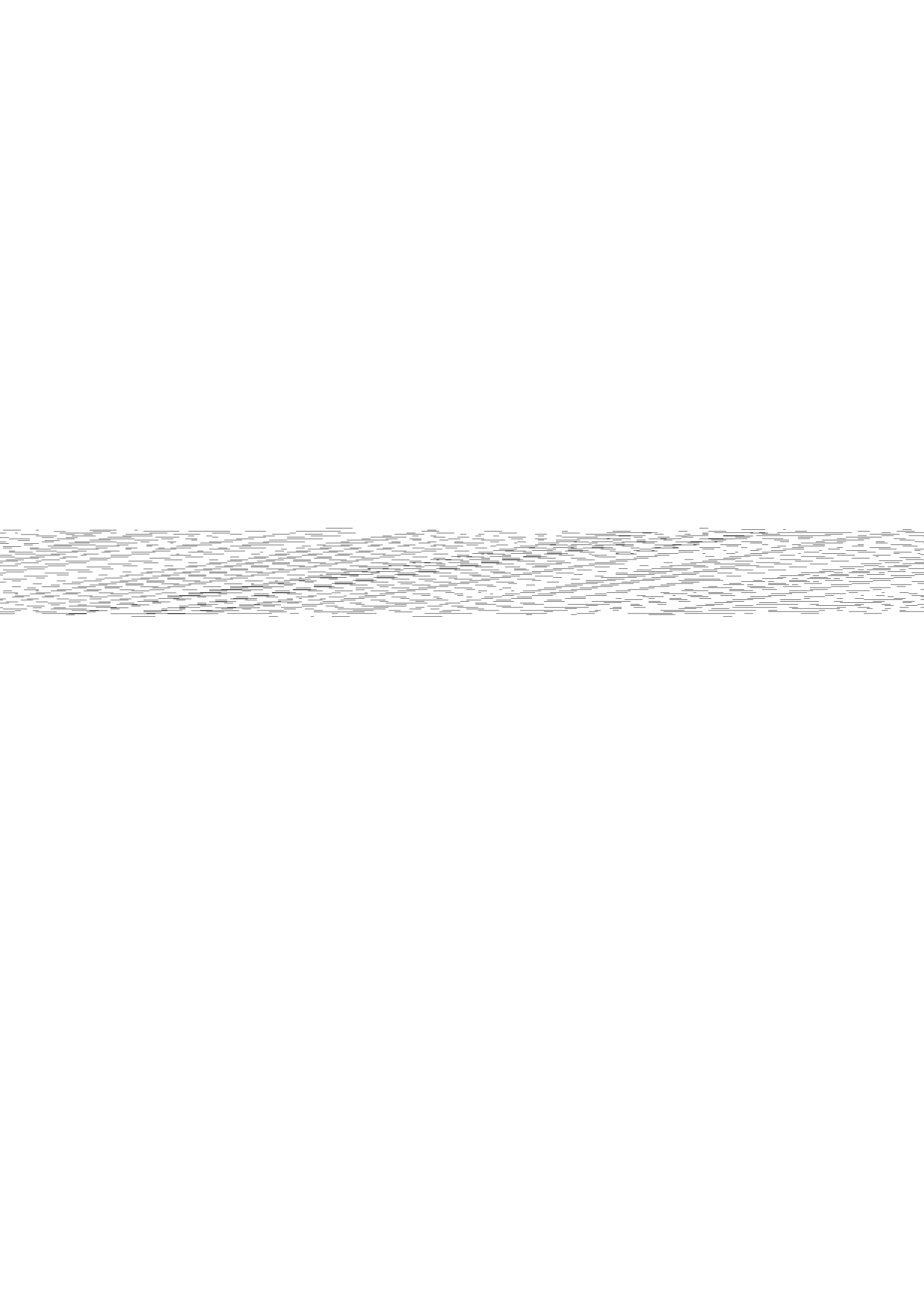
FIGURA 5

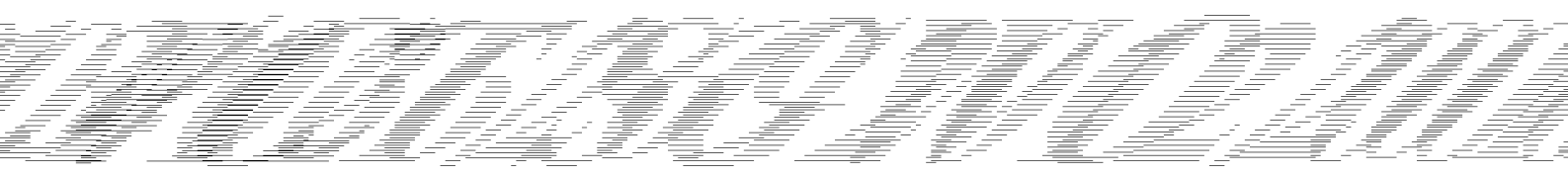
RESUMO

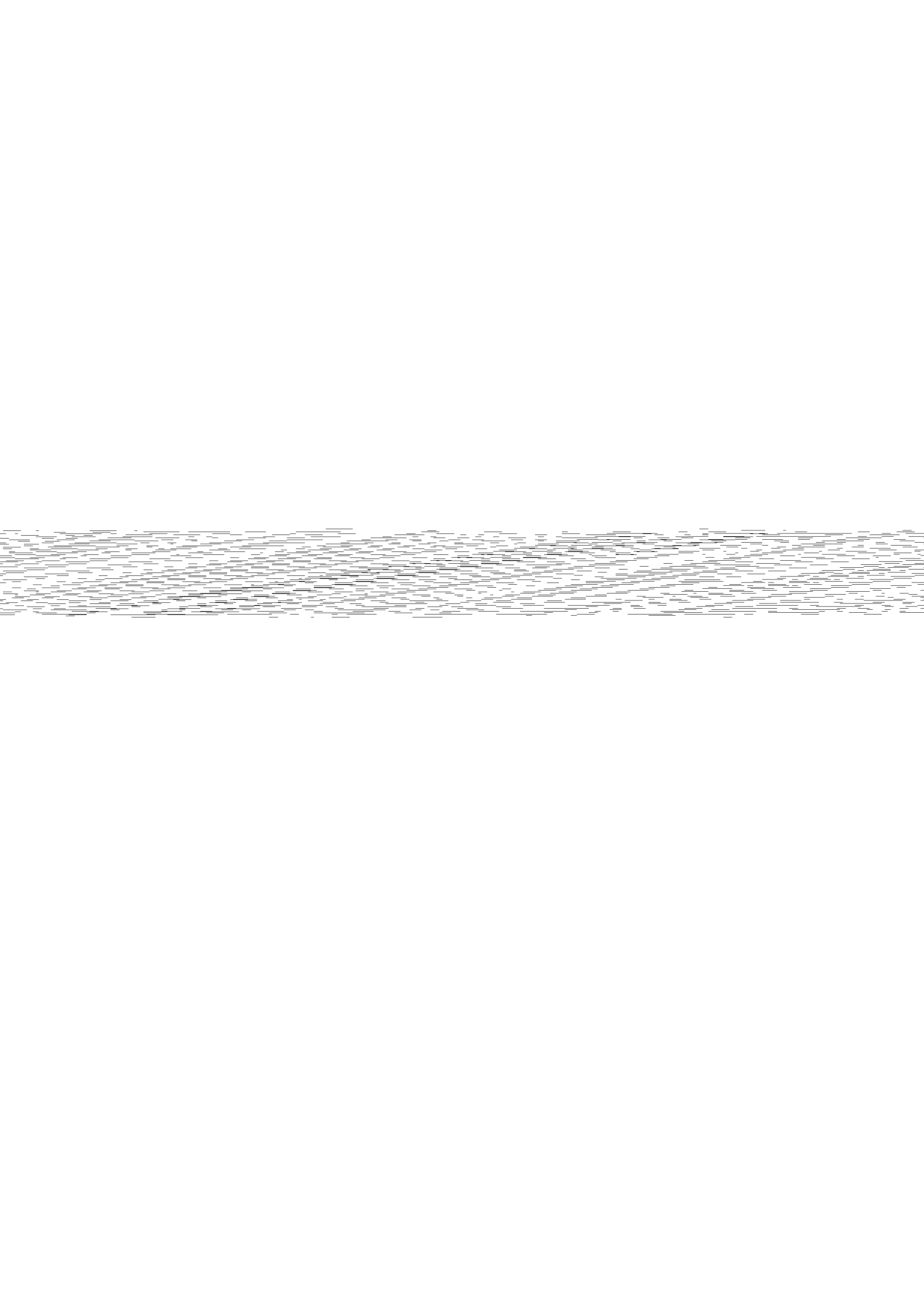
“MÉTODO DE SÍNTESE DE GRAFENO 3D A PARTIR DO POLITEREFTALATO DE ETILENO (PET)”

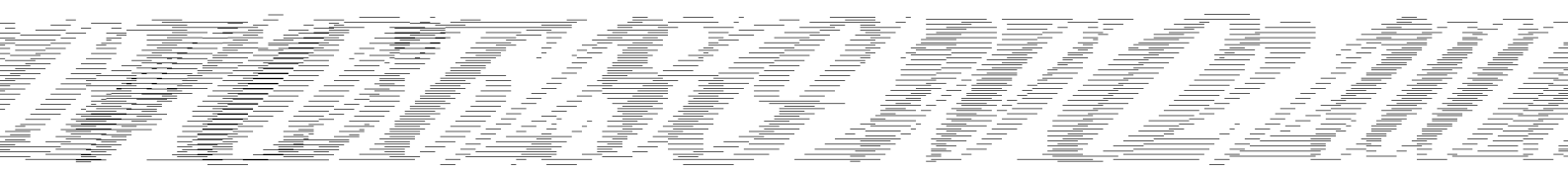
A presente tecnologia refere-se ao processo de síntese de uma estrutura tridimensional de carbono constituída de finas folhas de carbono em arranjo aleatório de baixa densidade e alta área superficial específica, aqui denominada de grafeno tridimensional ou grafeno 3D ou espuma de carbono. Este processo de síntese basicamente utiliza como precursor de carbono o polímero politereftalato de etileno também denominado PET que juntamente com um agente de expansão termodecompõem numa mesma faixa de temperatura próxima as temperaturas de amolecimento e de carbonização do PET. Este processo sincronizado de amolecimento, expansão e carbonização do PET é realizado sob pressão atmosférica em atmosfera inerte ou não, dependendo da sua aplicação pós-síntese. Este material, aqui denominado grafeno 3D, pode ser aplicado em várias áreas, tais como: suporte para fixação de elementos e compostos para catálise, como elemento de filtração e purificação de água, na fabricação de tintas condutoras, na área de armazenamento de energia, como fertilizante agrícola e como elemento de incorporação em matrizes poliméricas e cerâmicas.

Today's **Butcher**

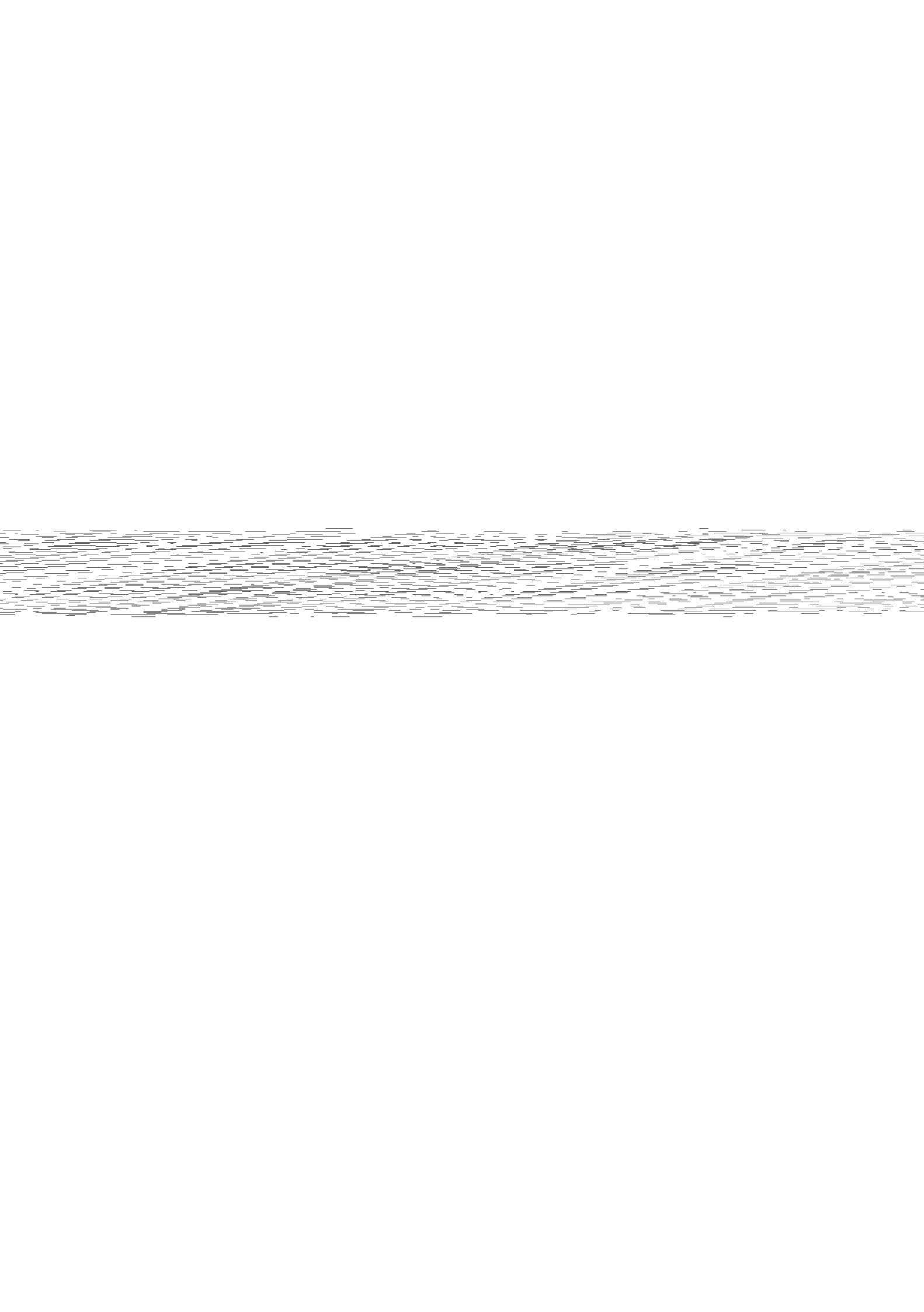




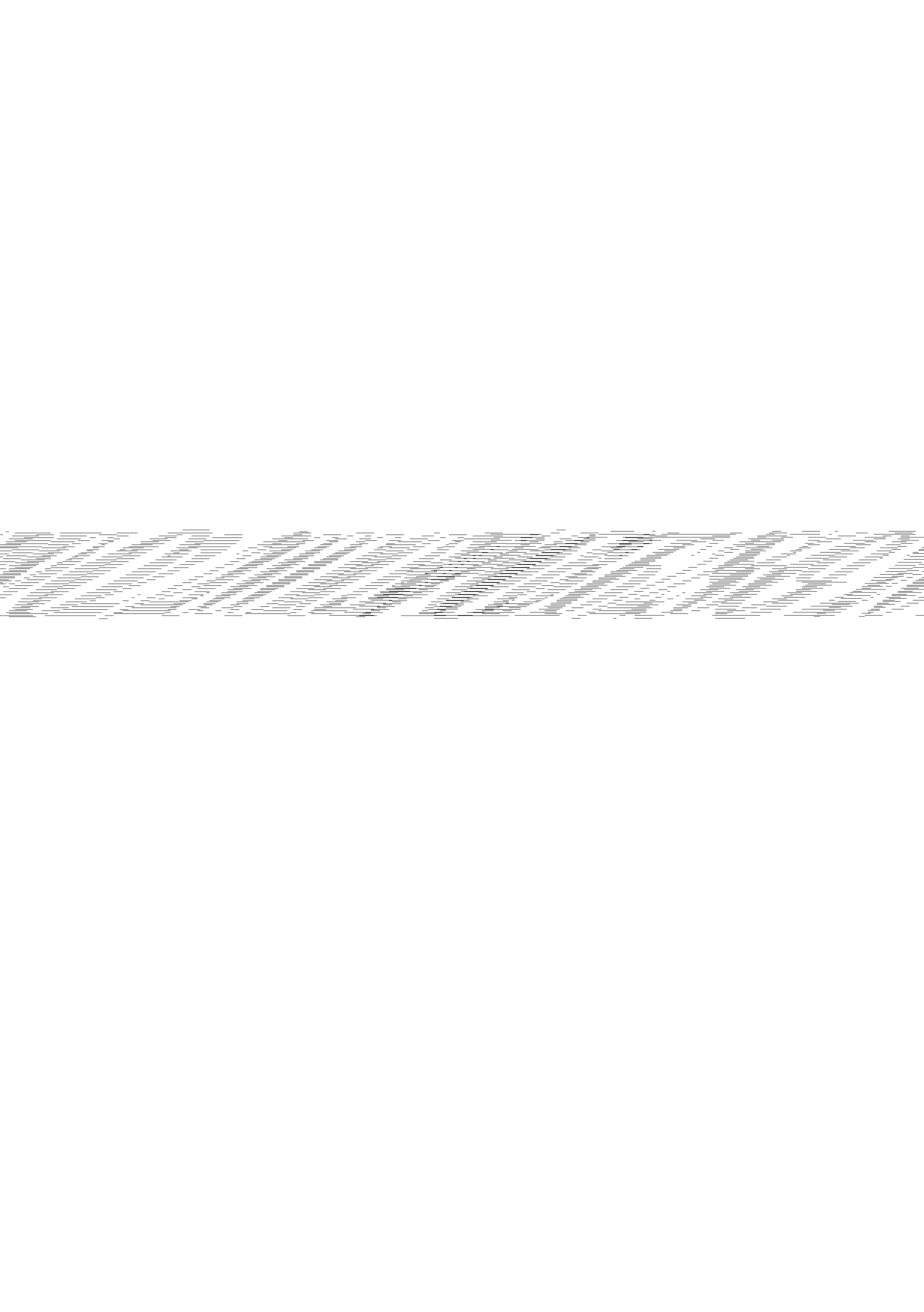


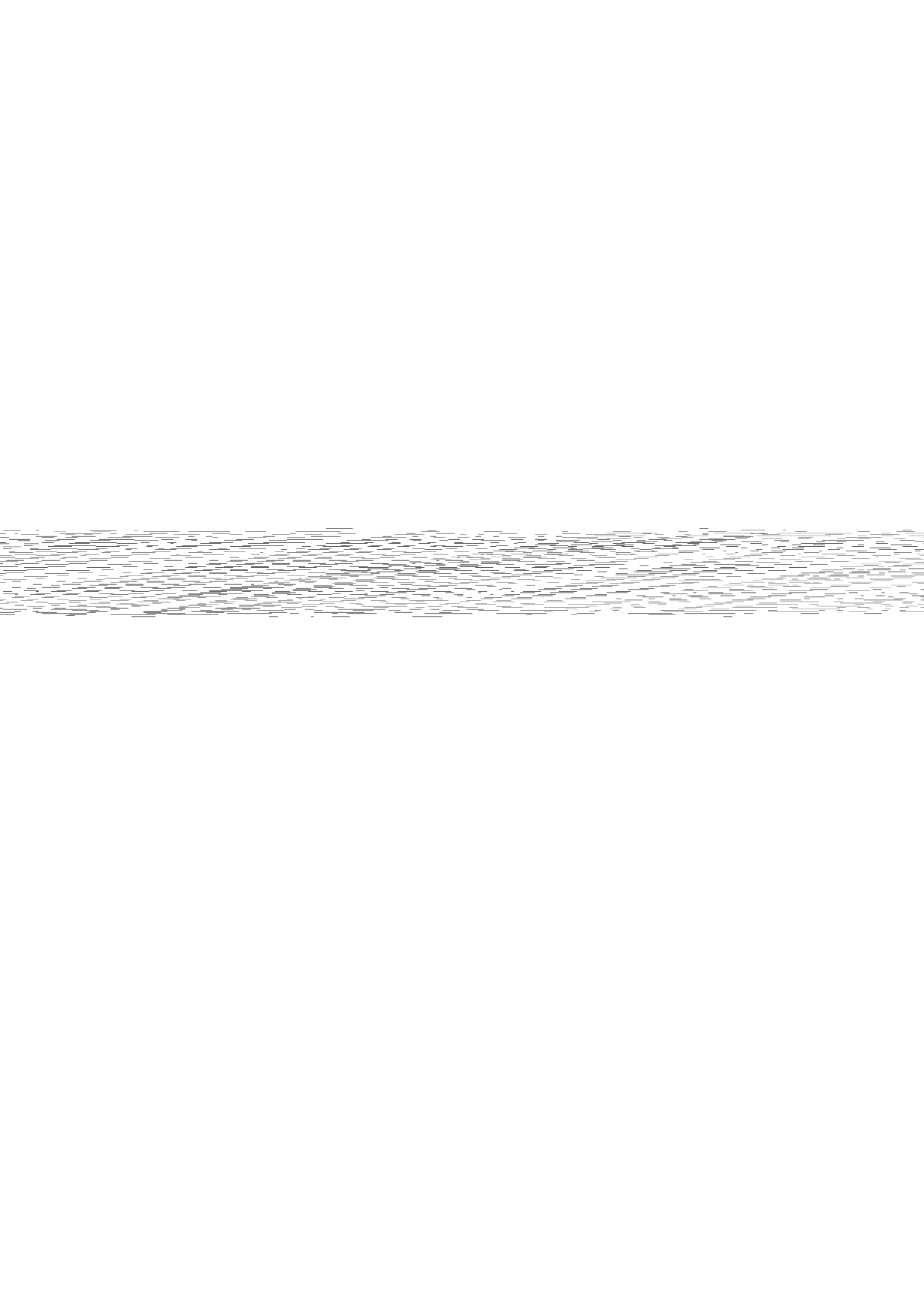


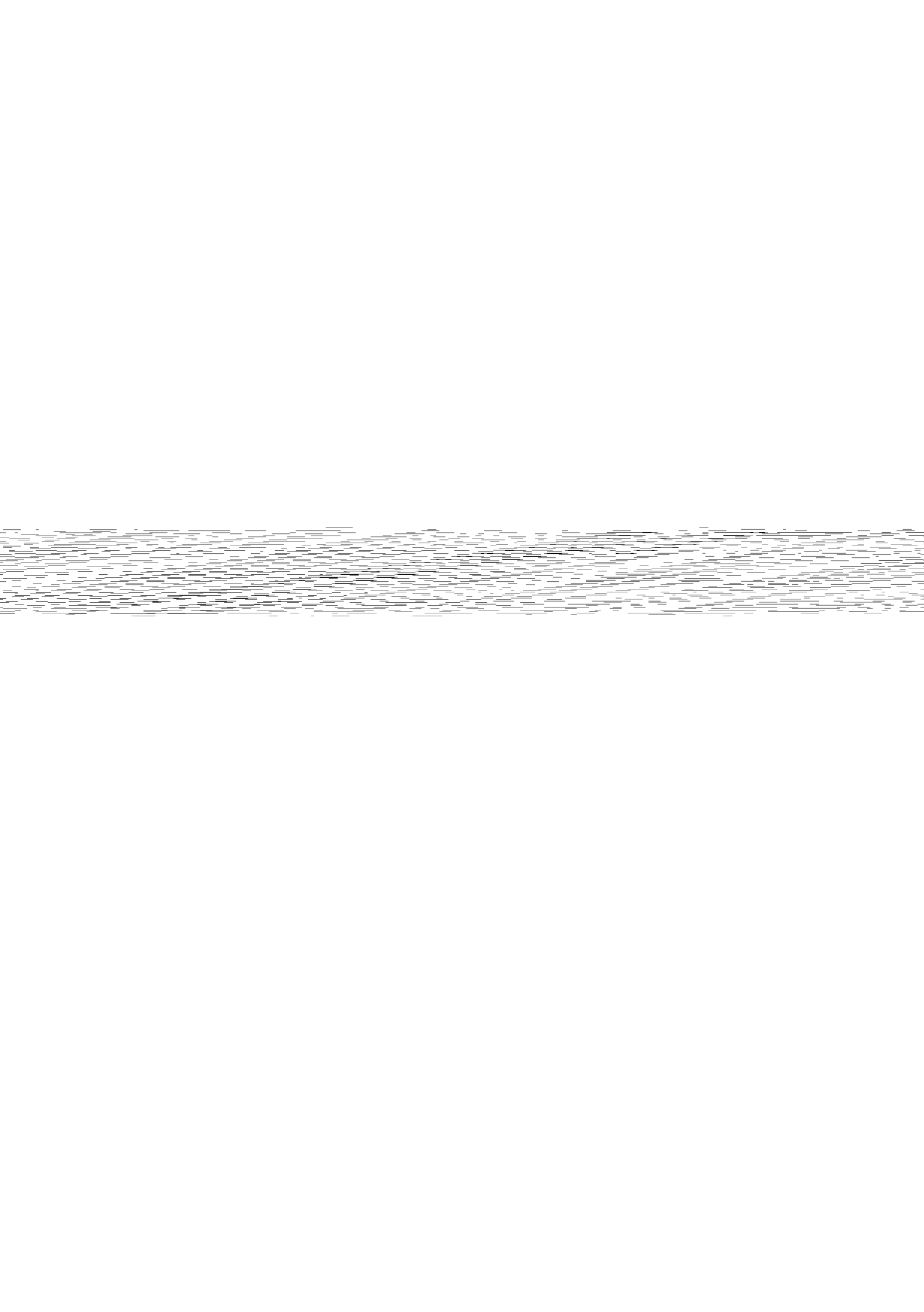




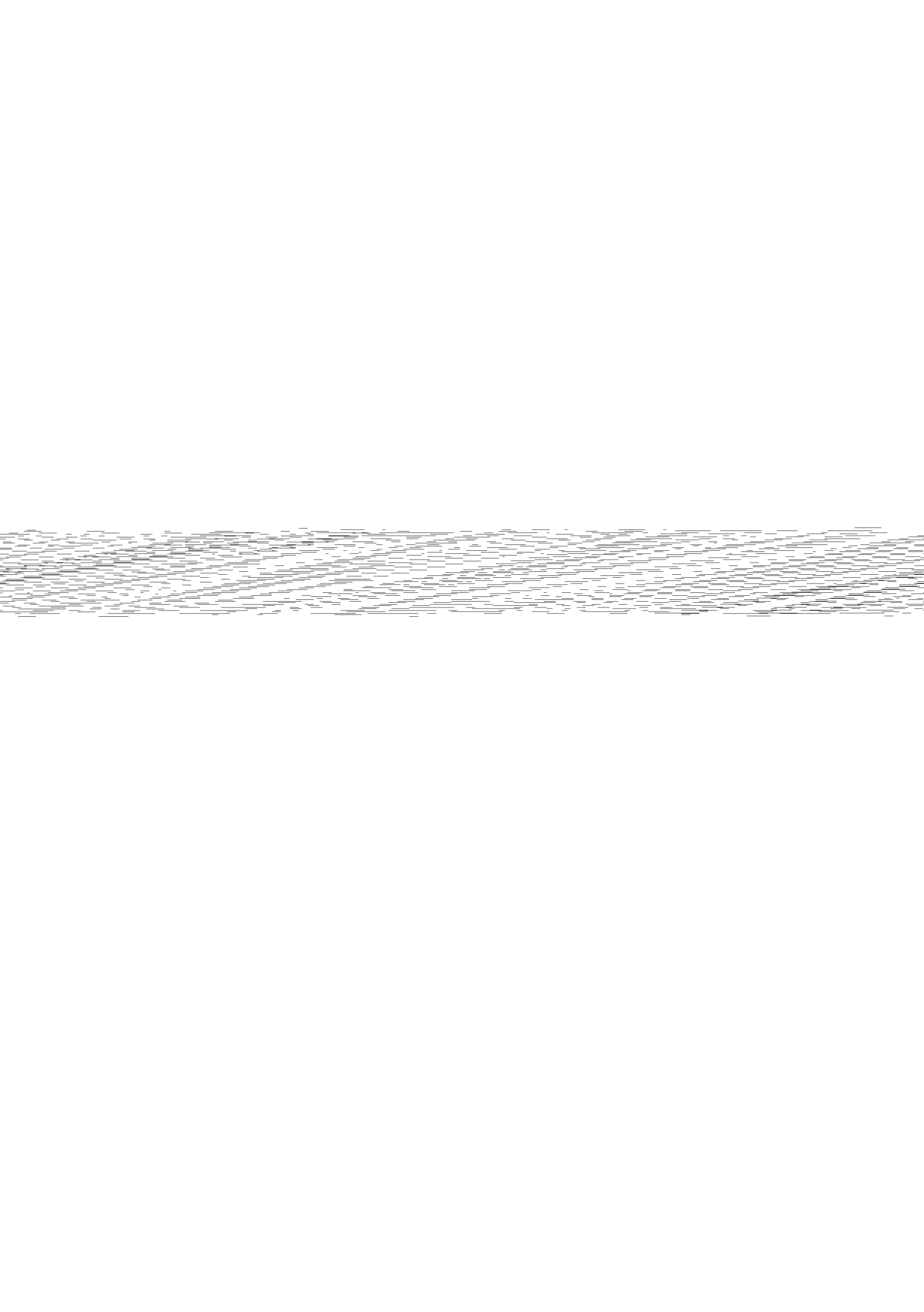
2012 02 0000000000

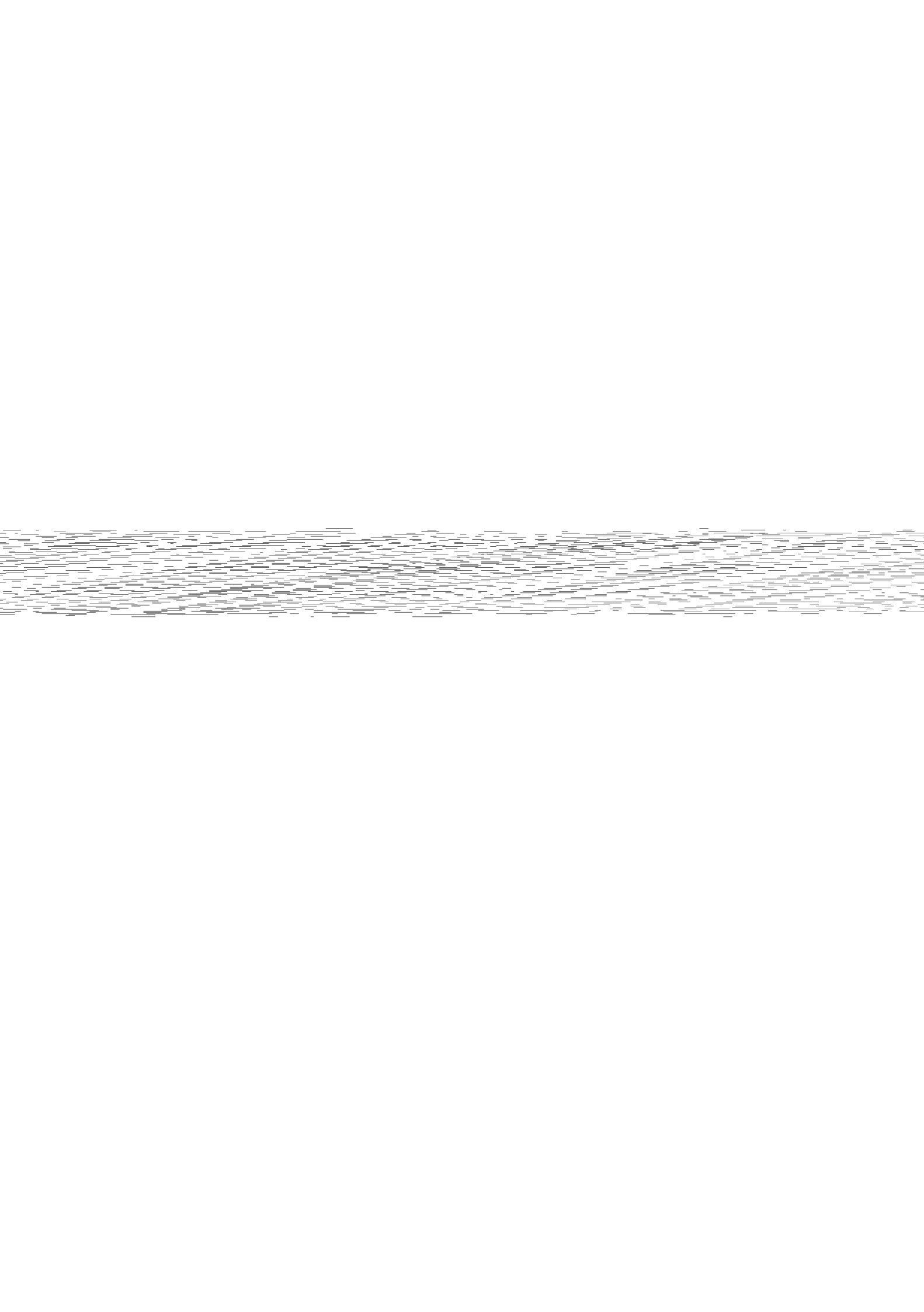


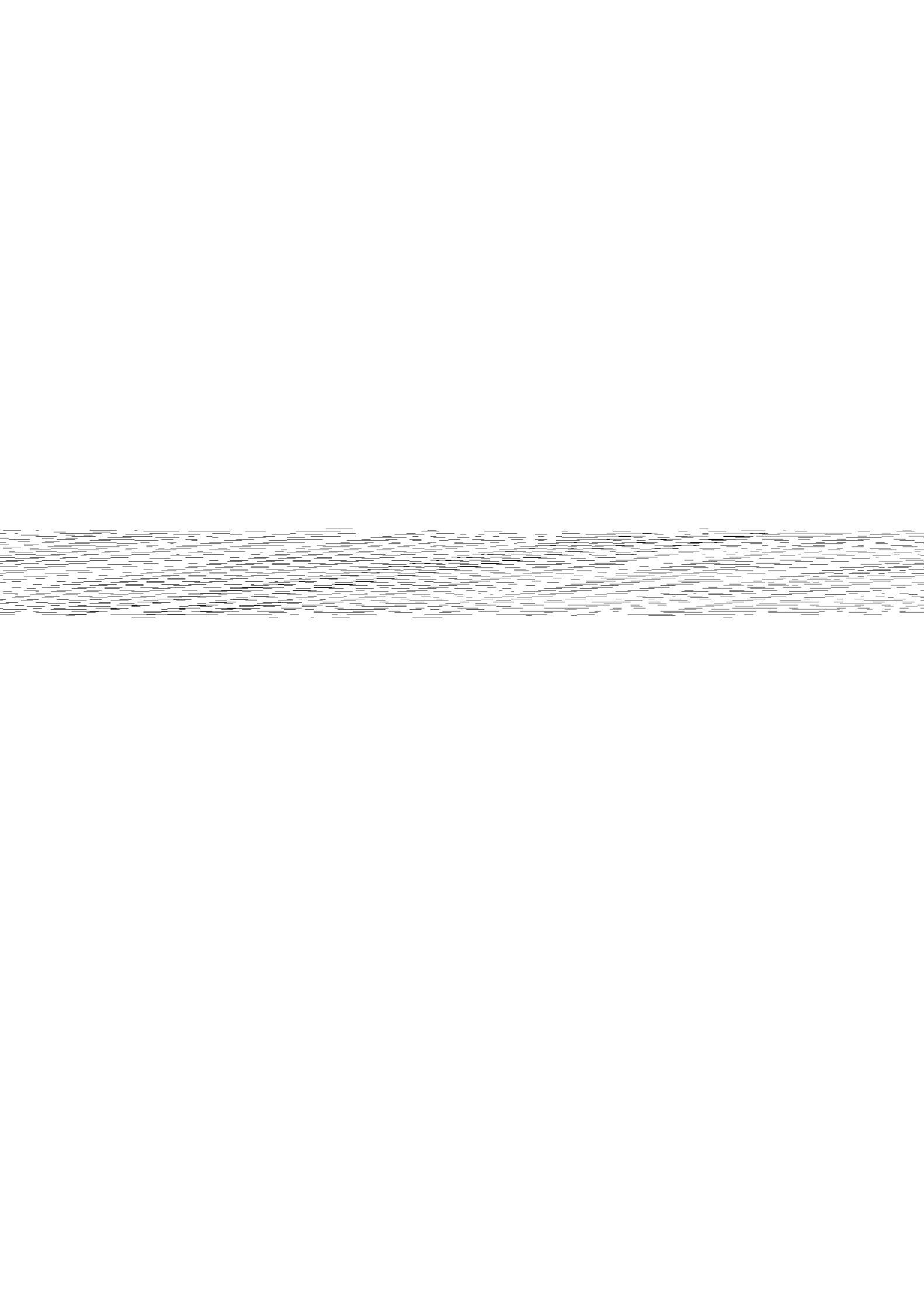


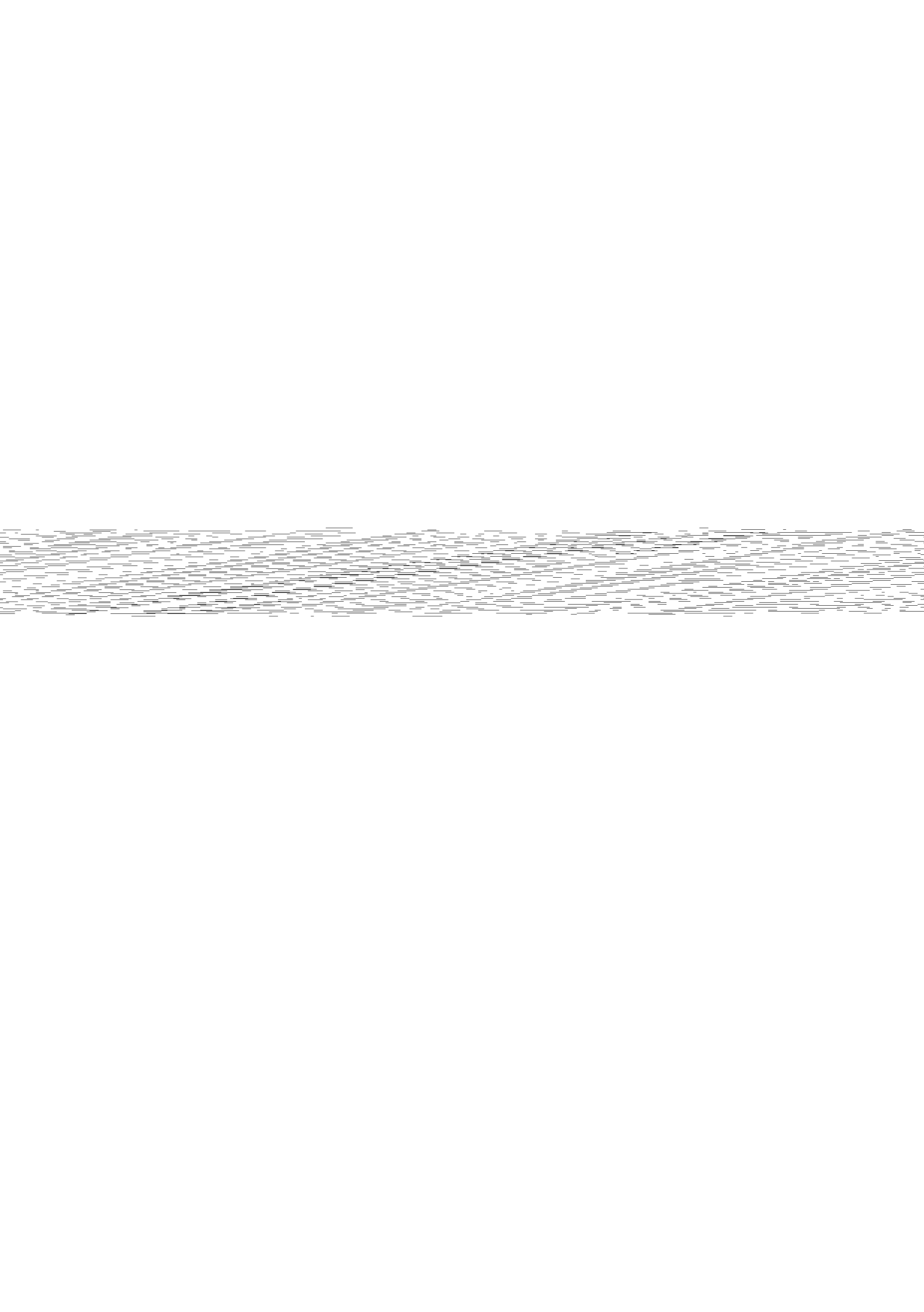


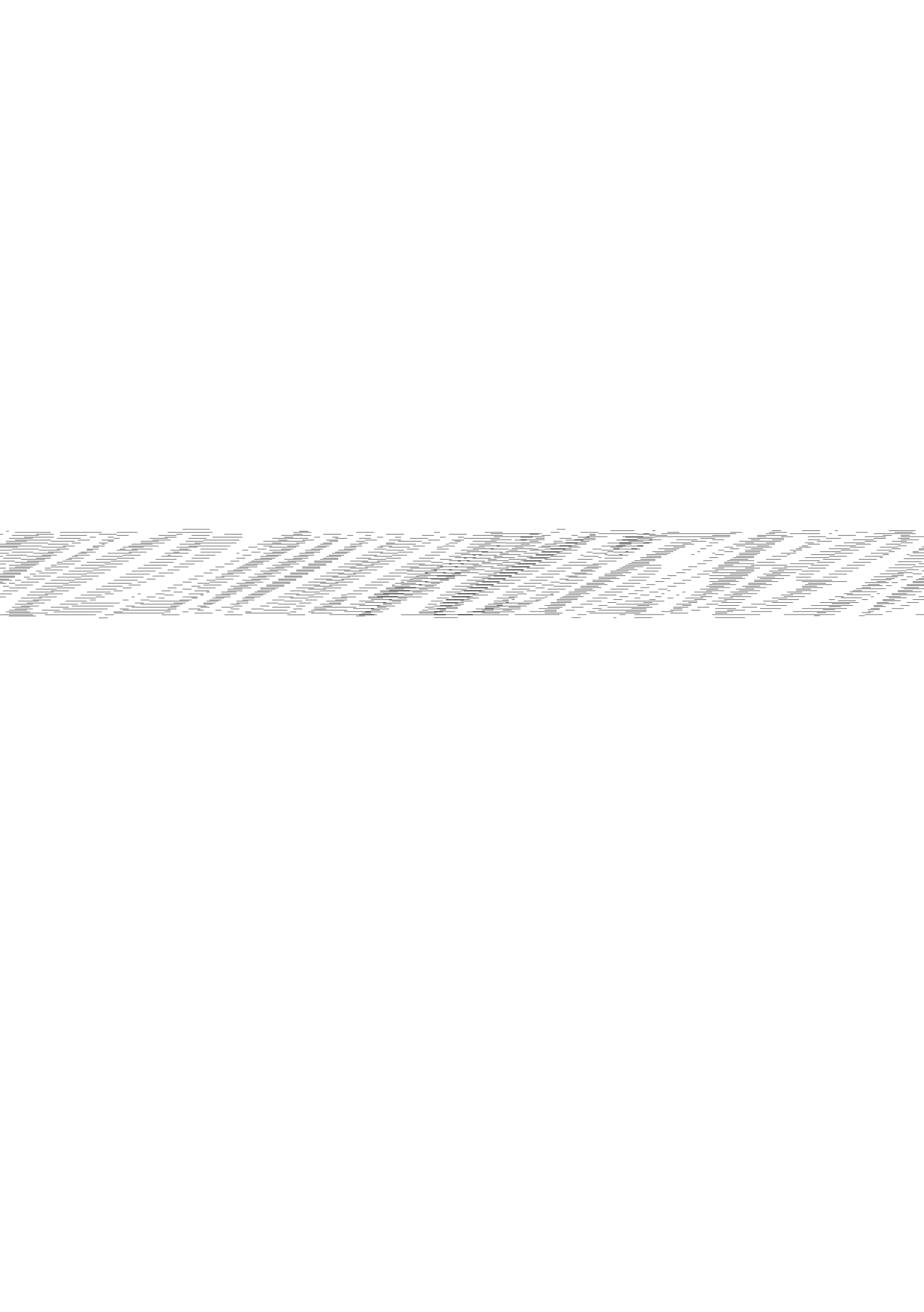


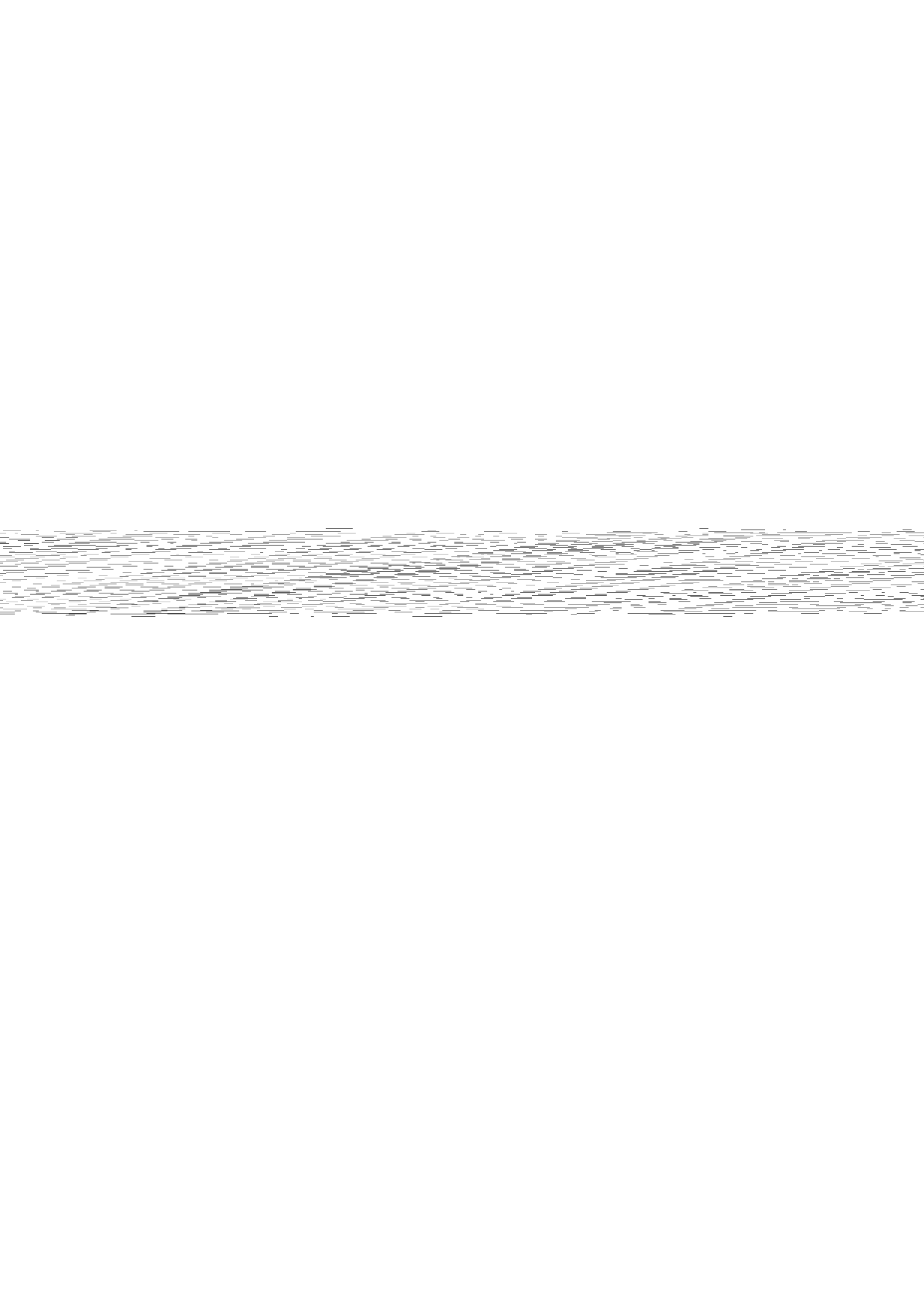




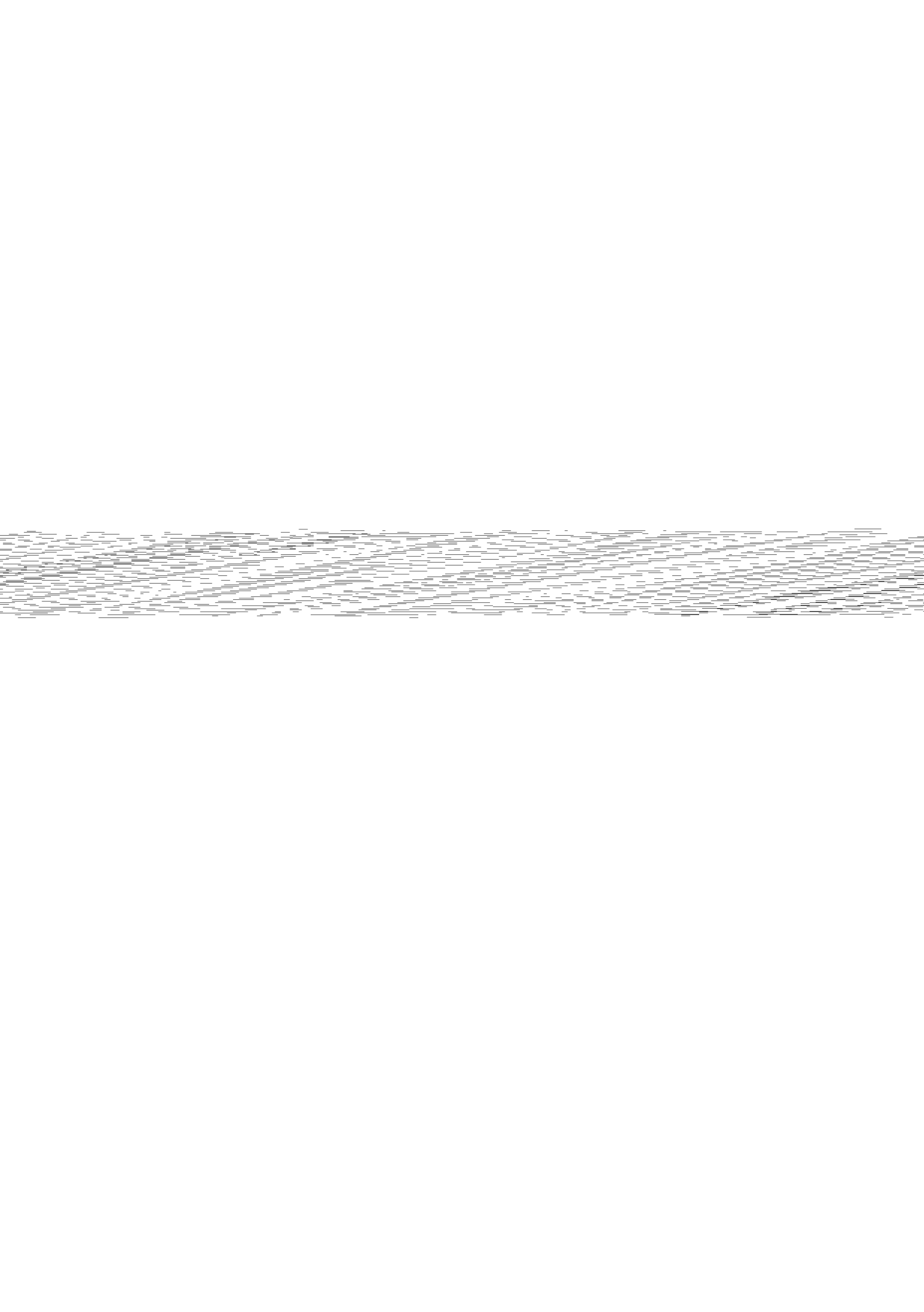




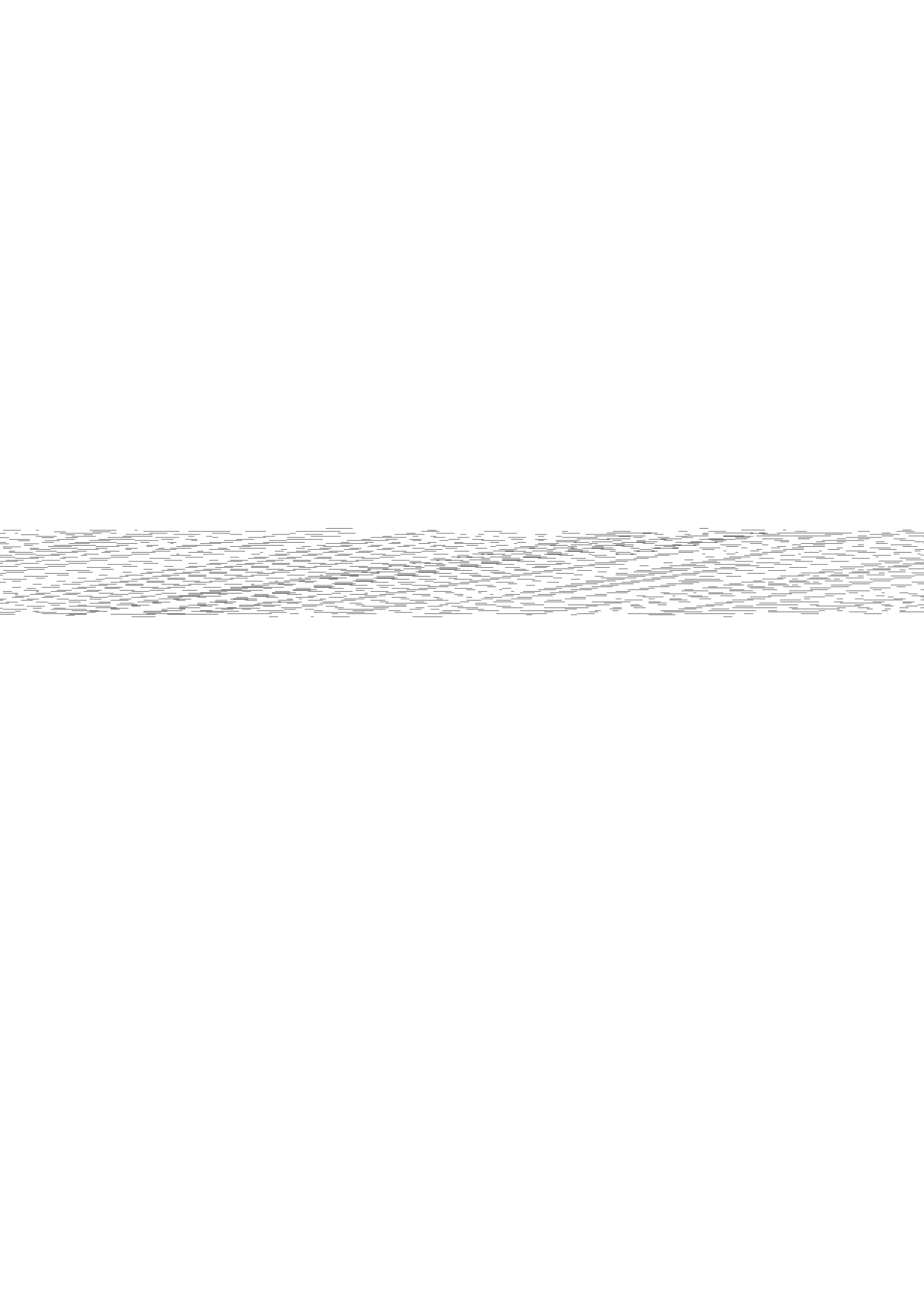


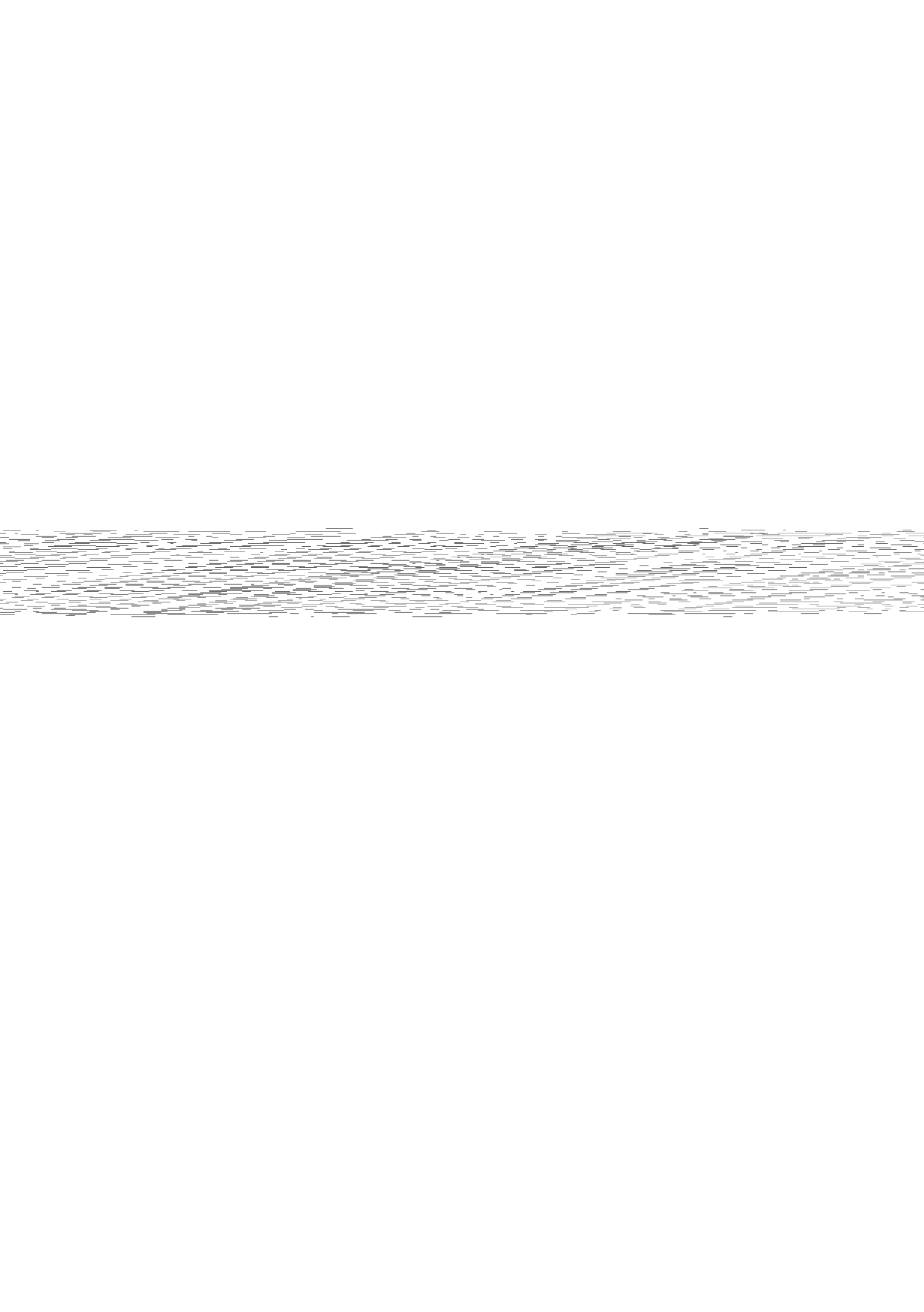




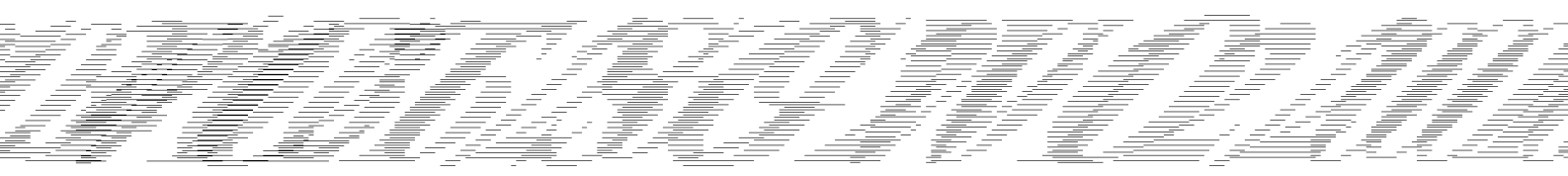


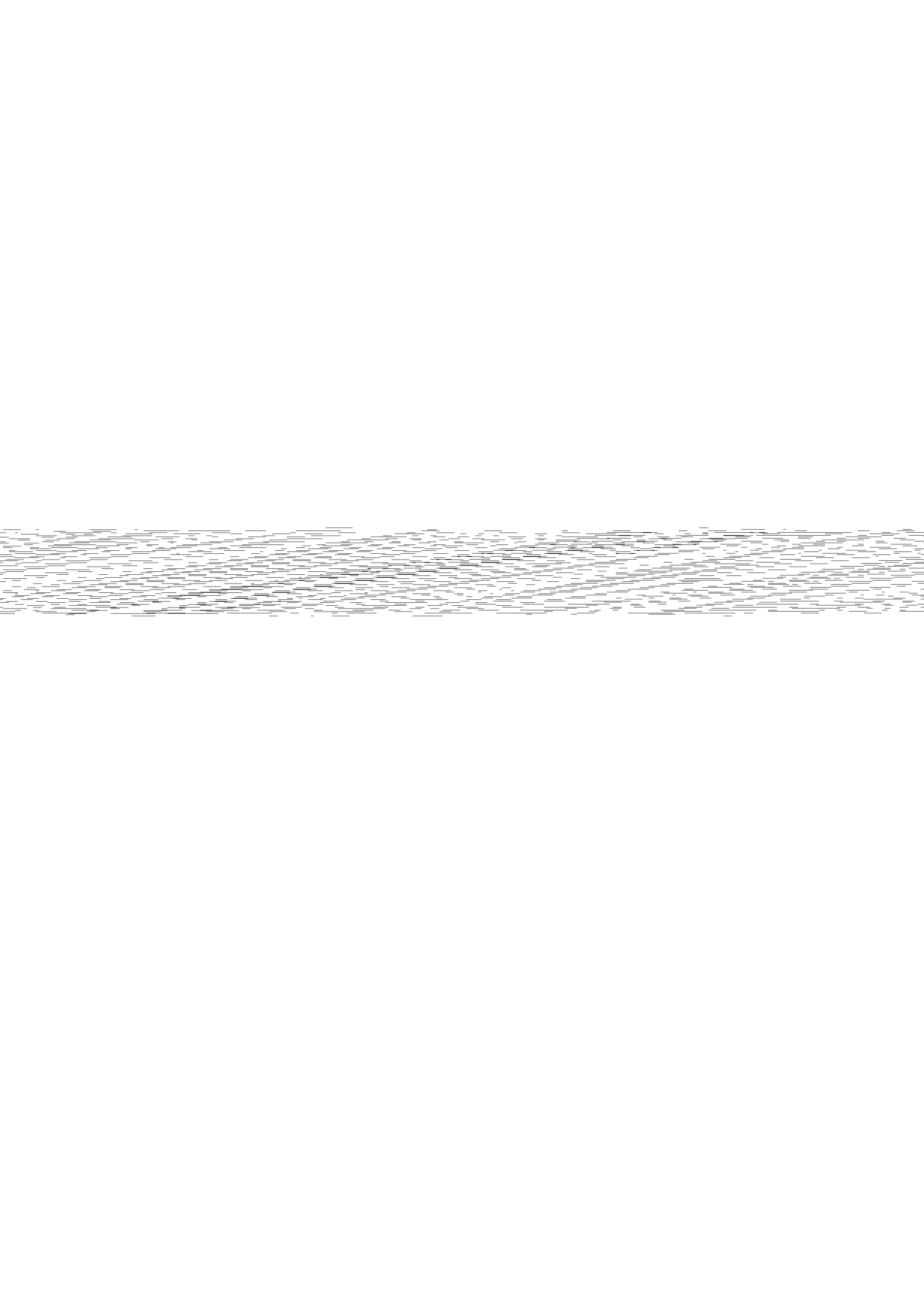




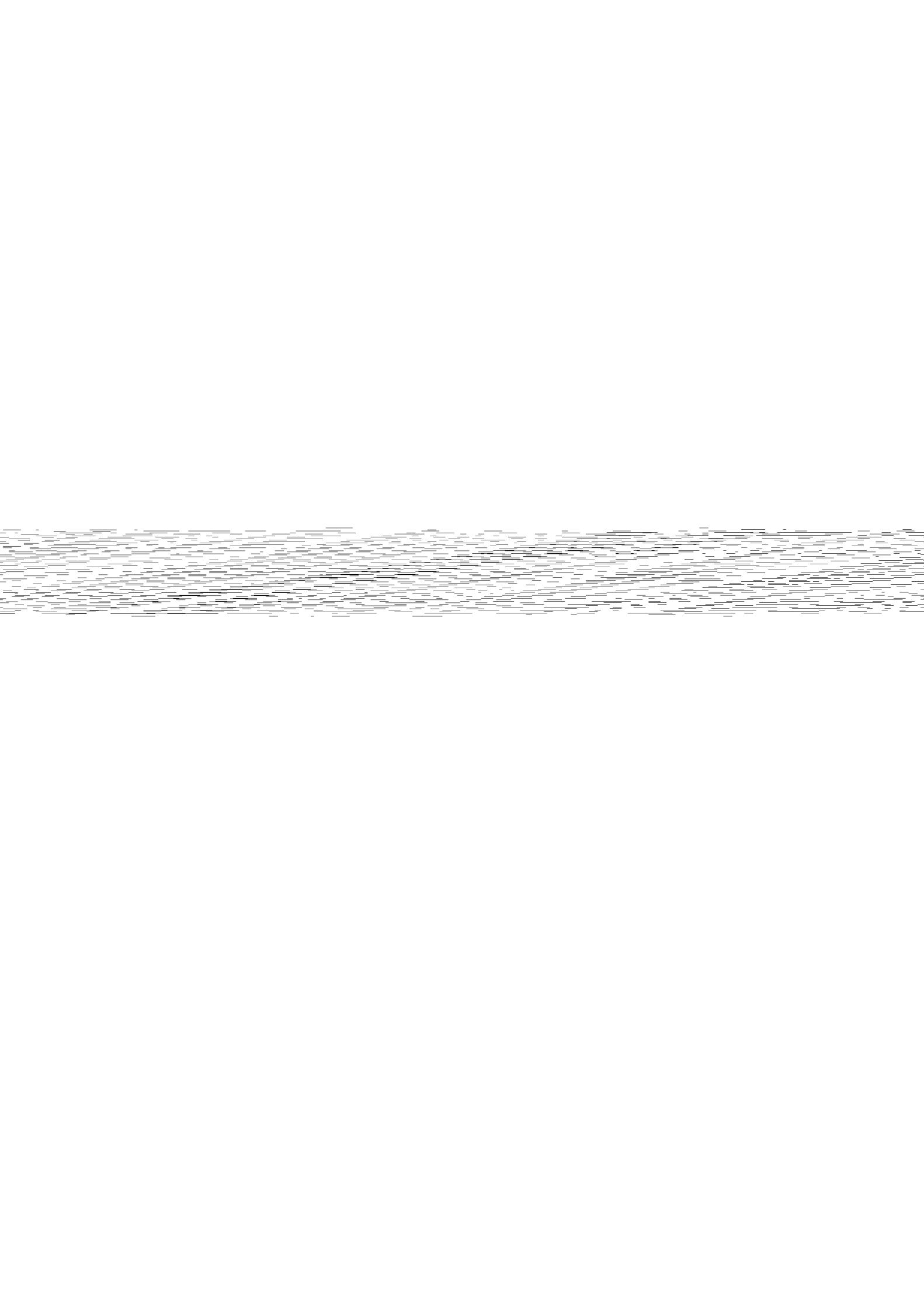


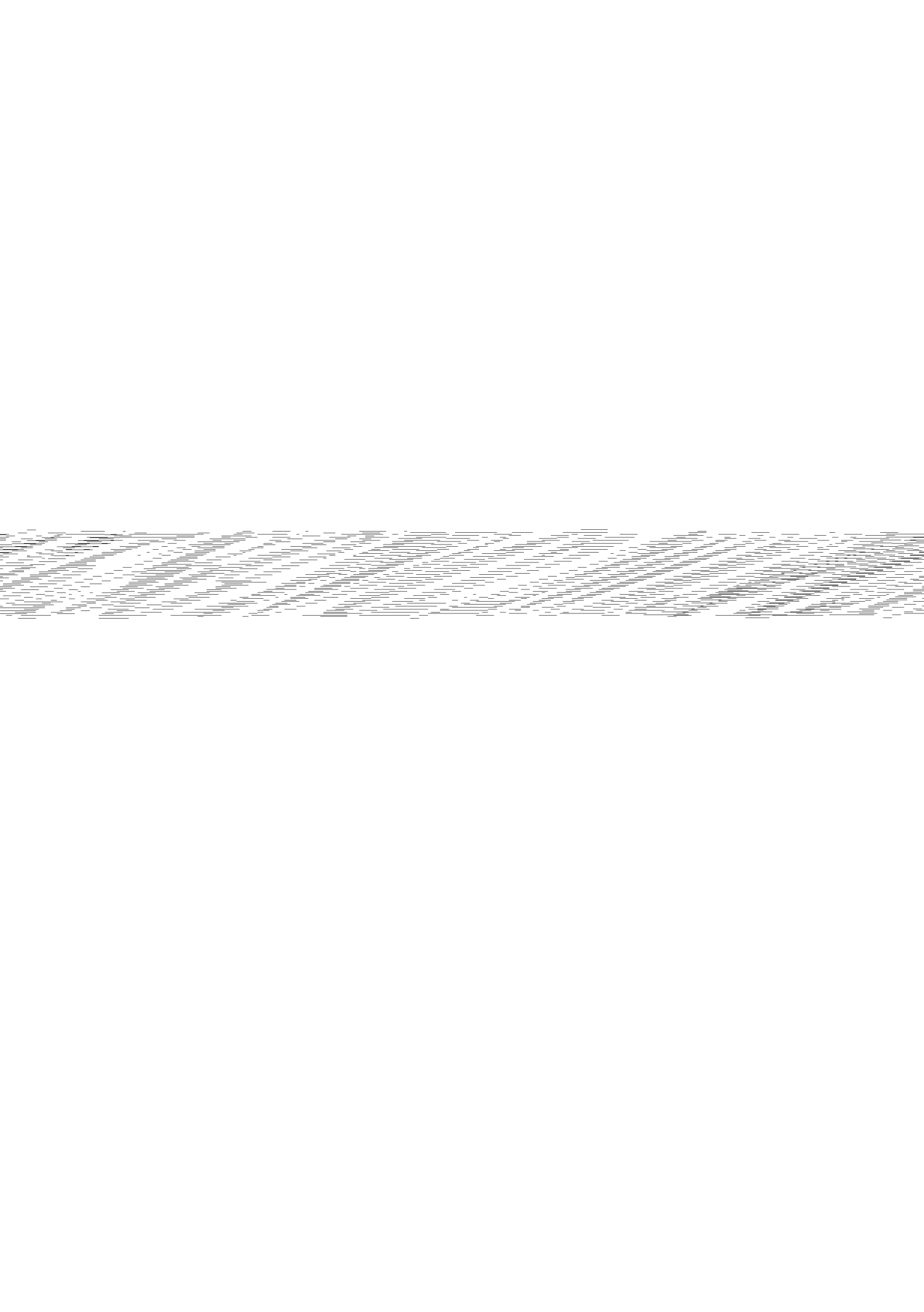


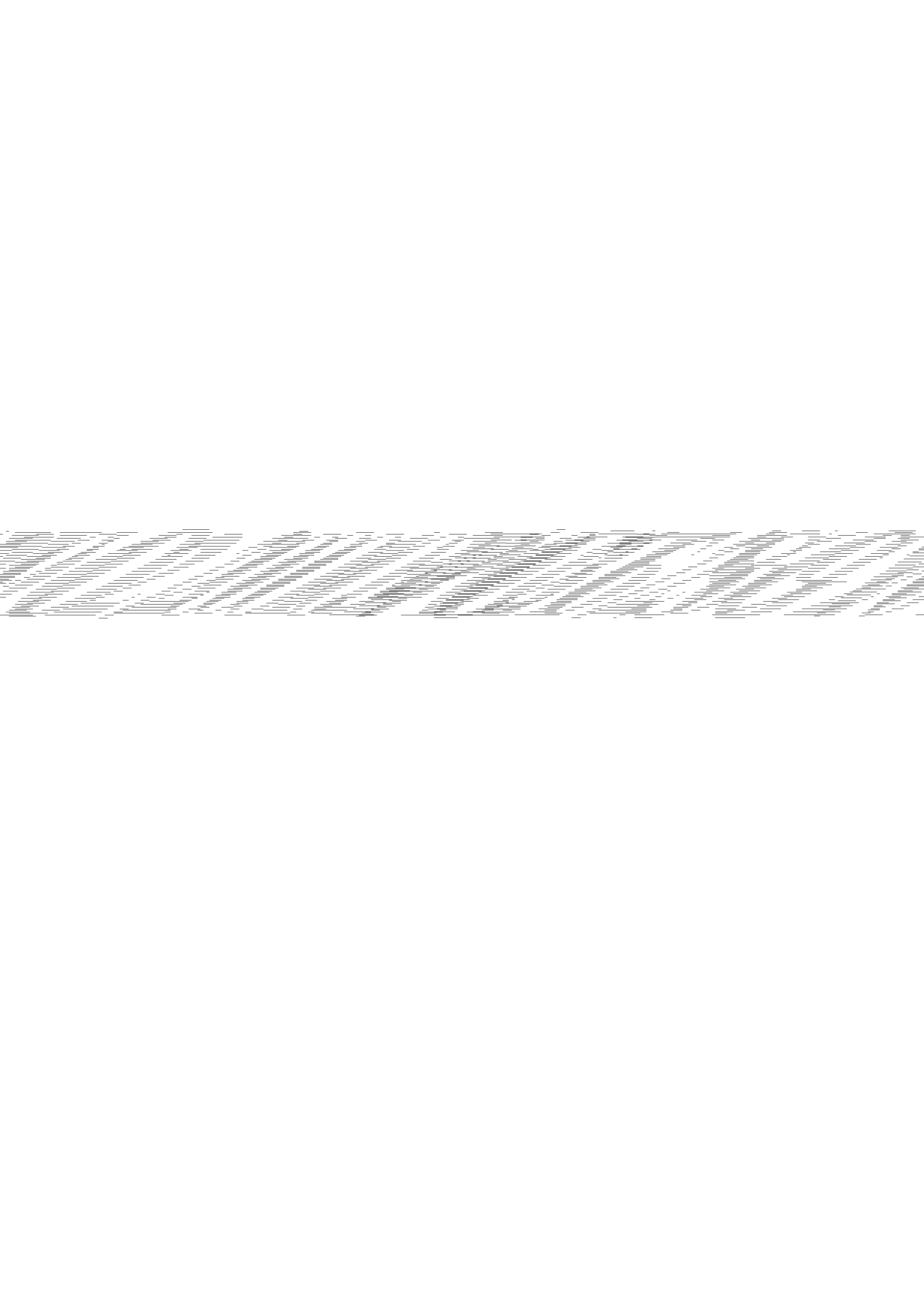


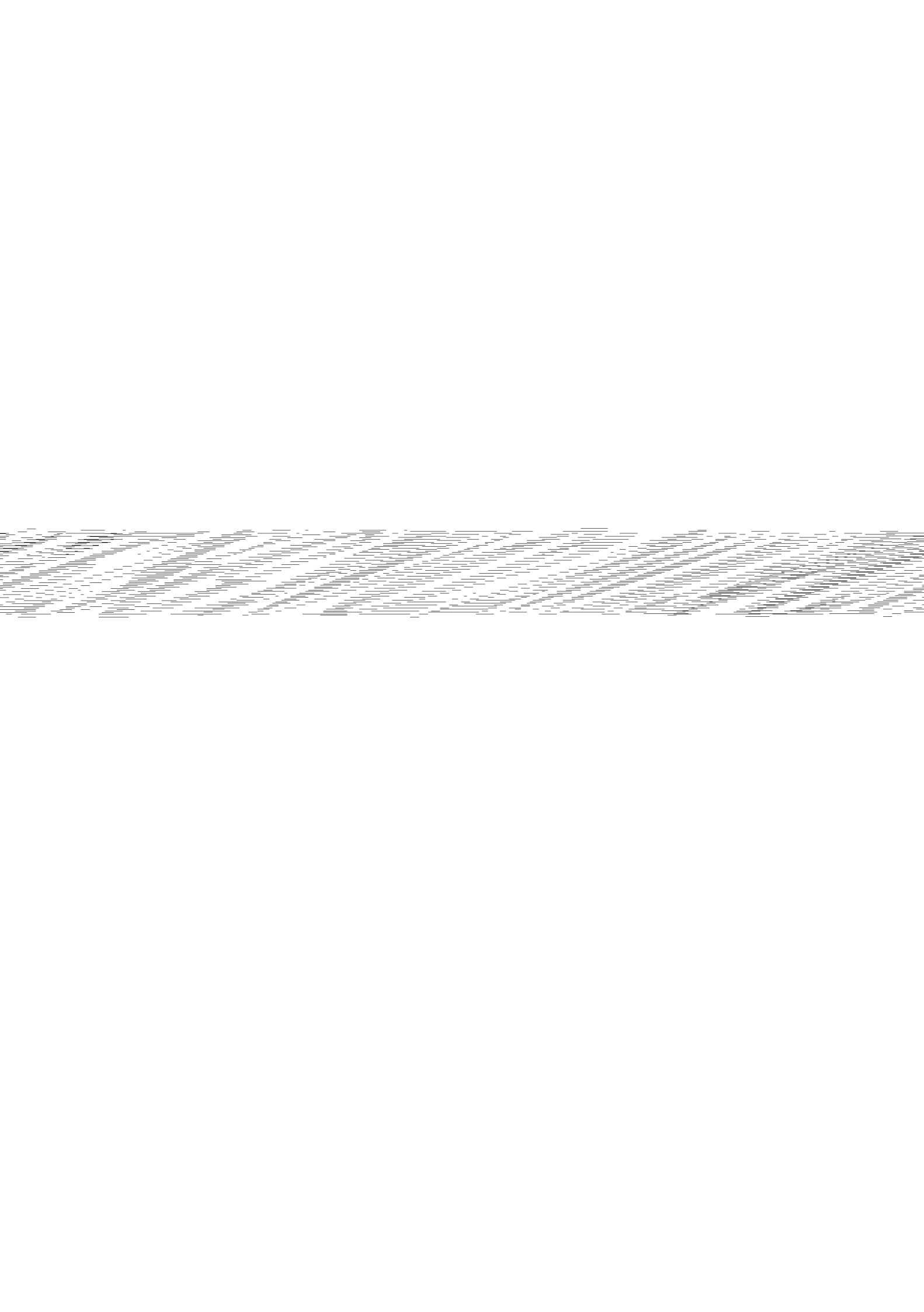


2020-02-20 10:00:00





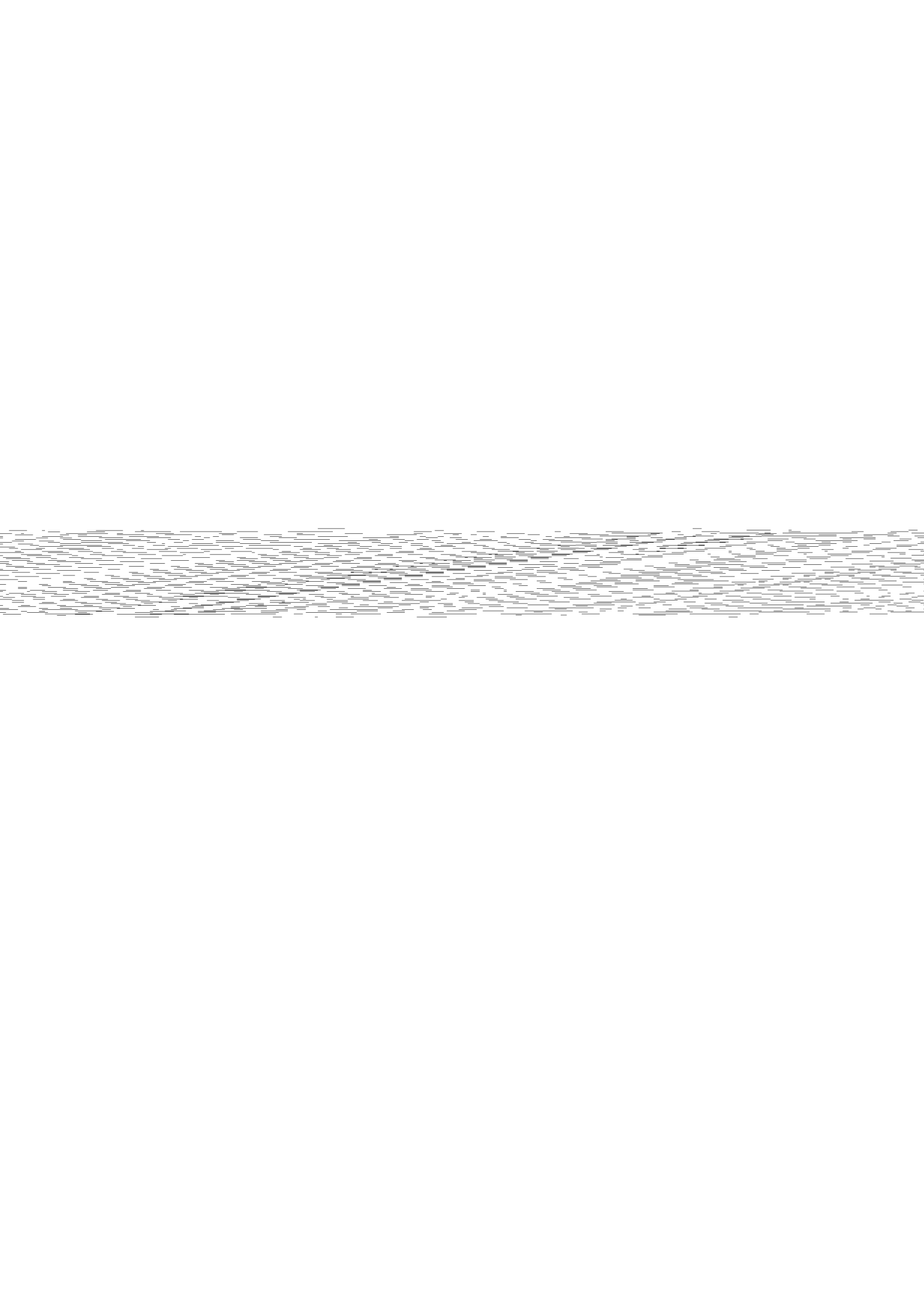


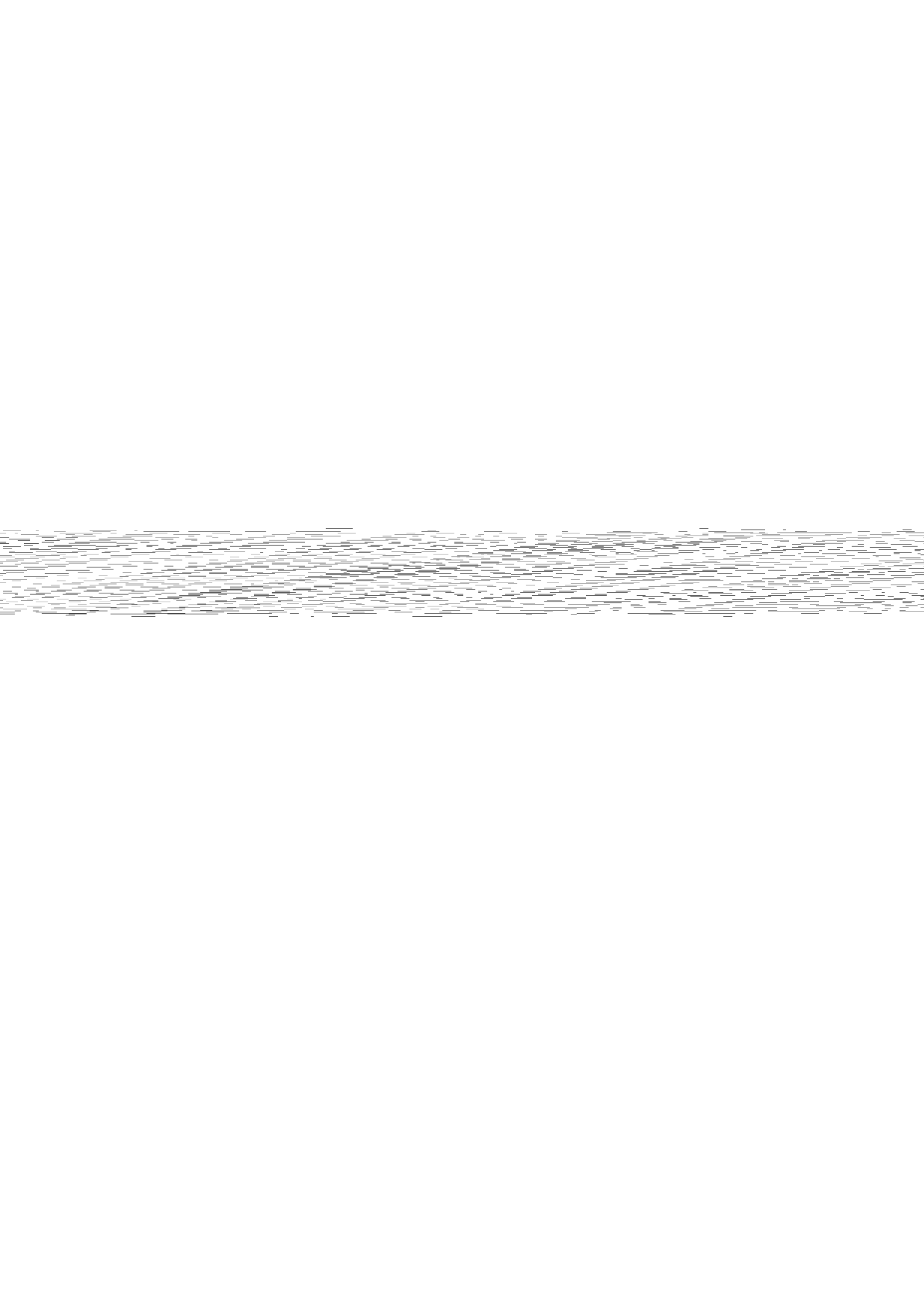


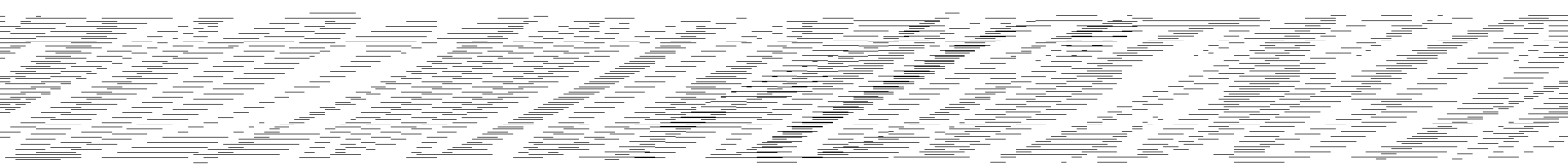




20200220103162





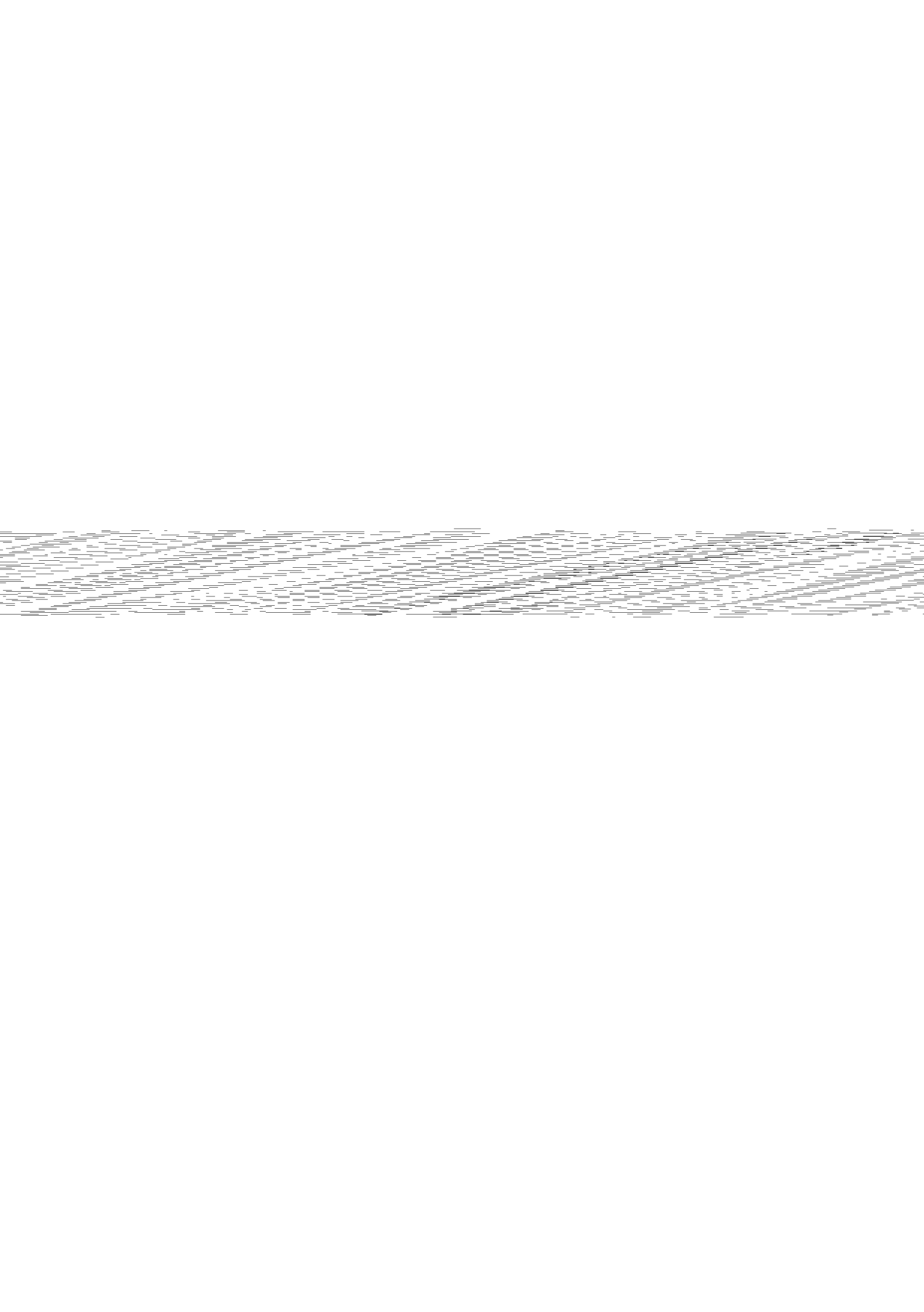


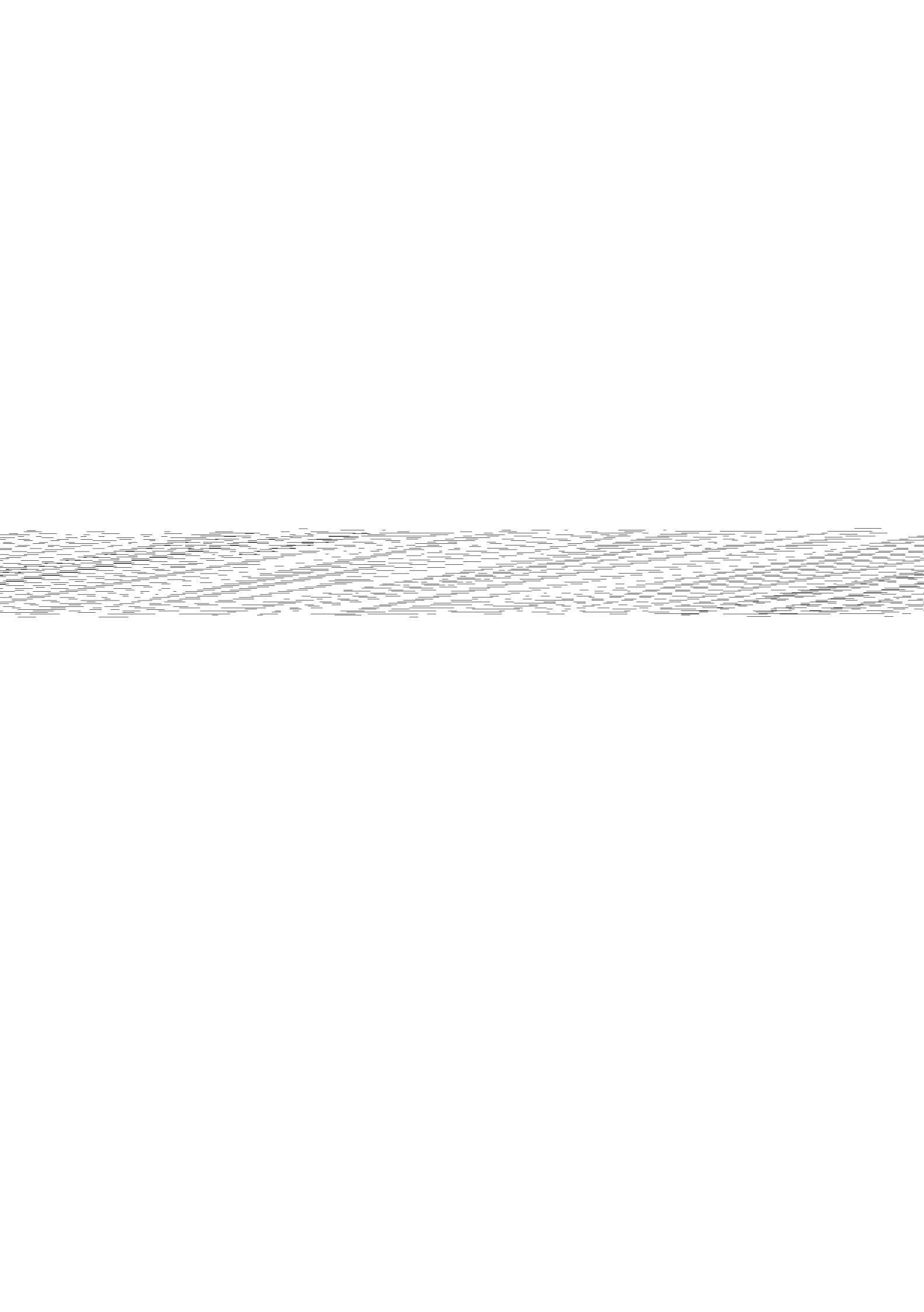
2012 02 0000000000

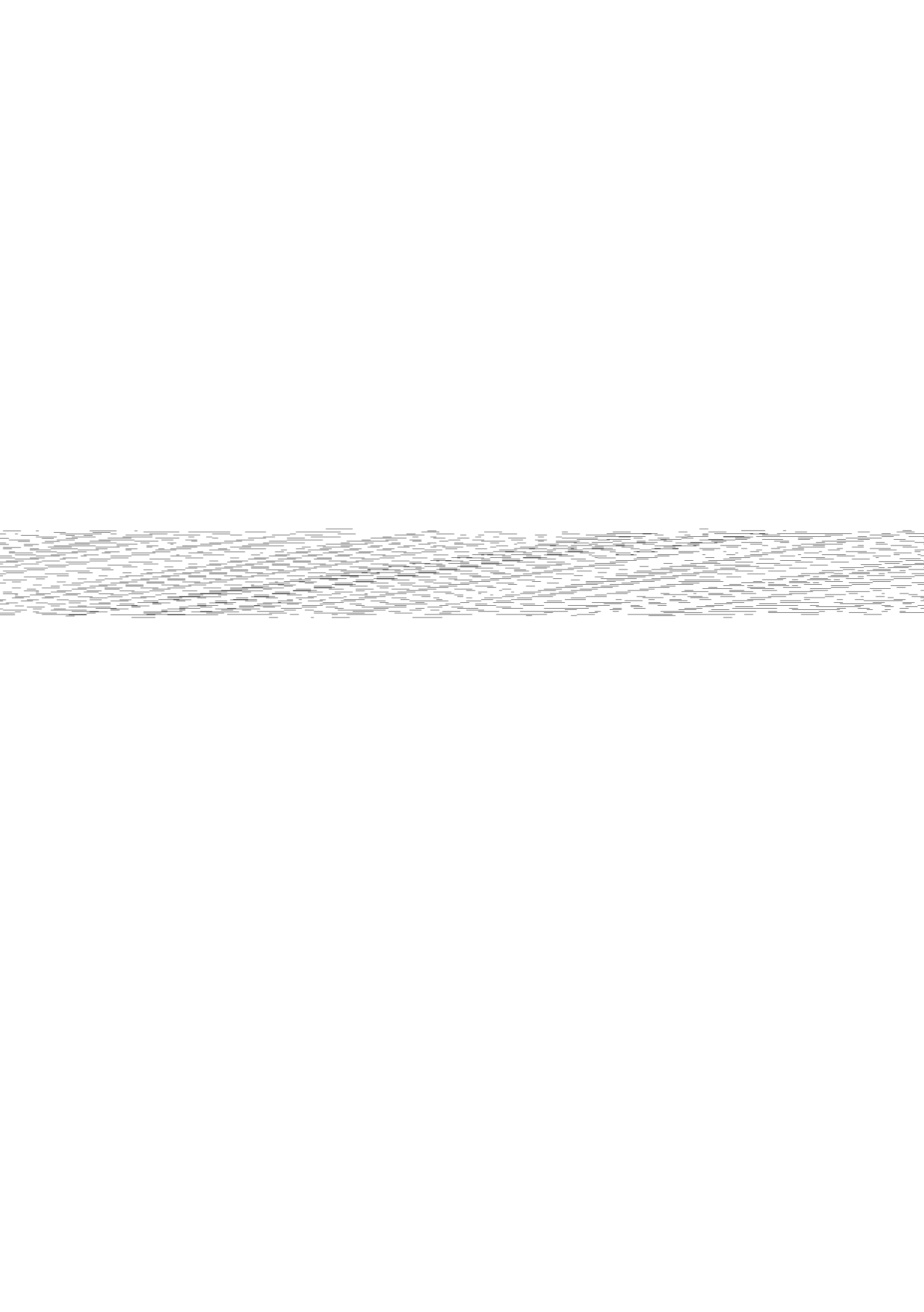


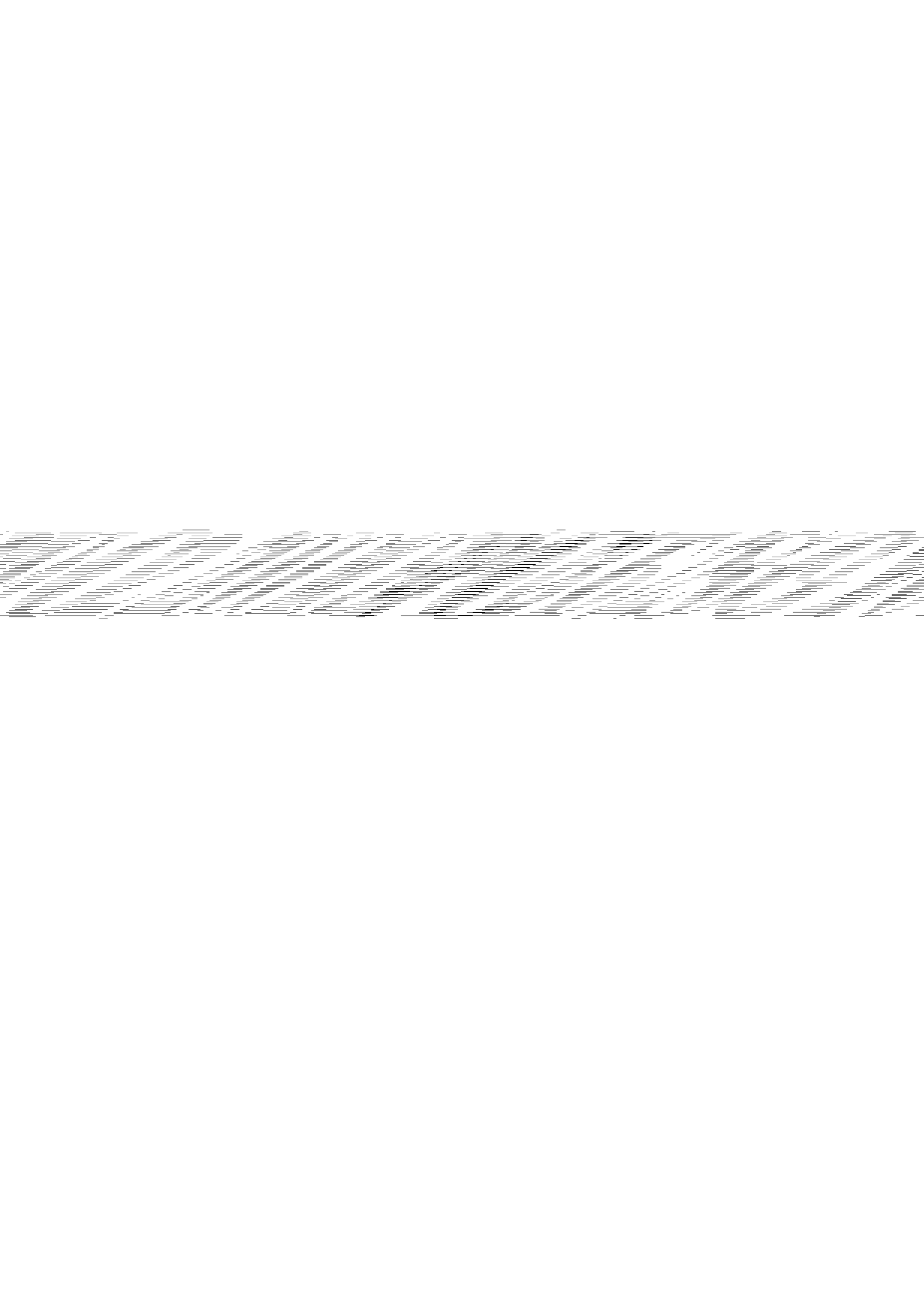
2012 000120260

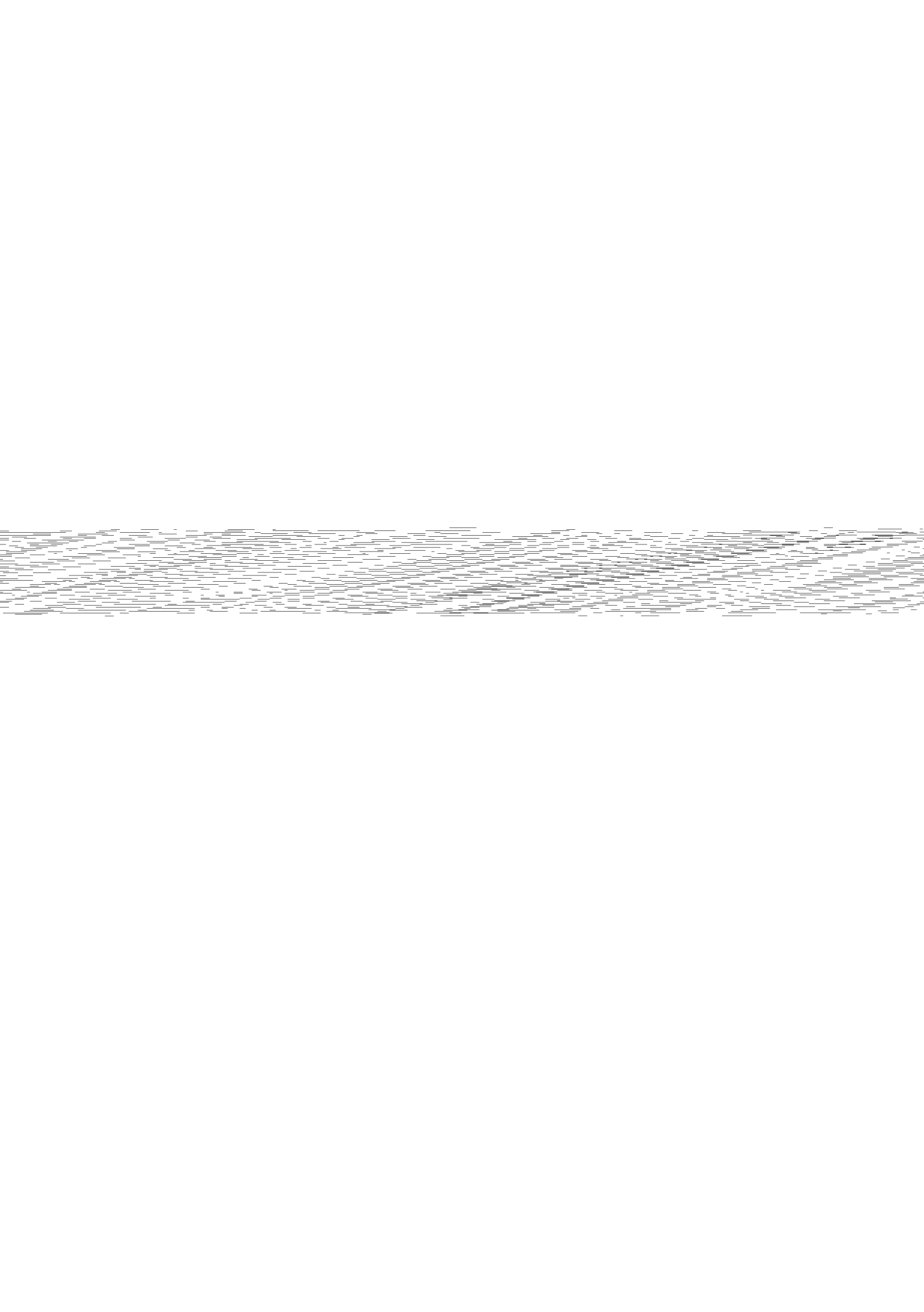
2020-2021 2020-2021 2020-2021

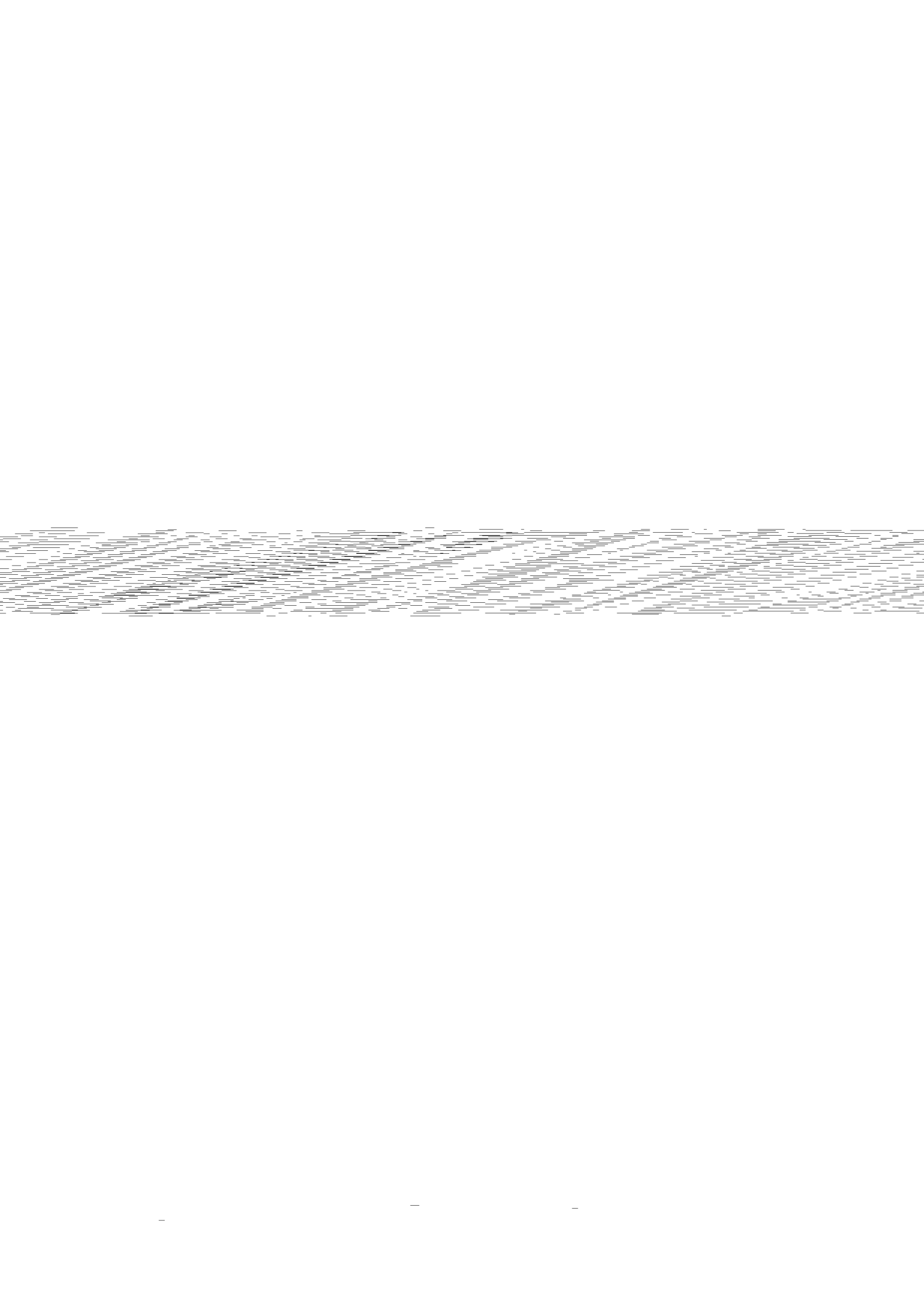


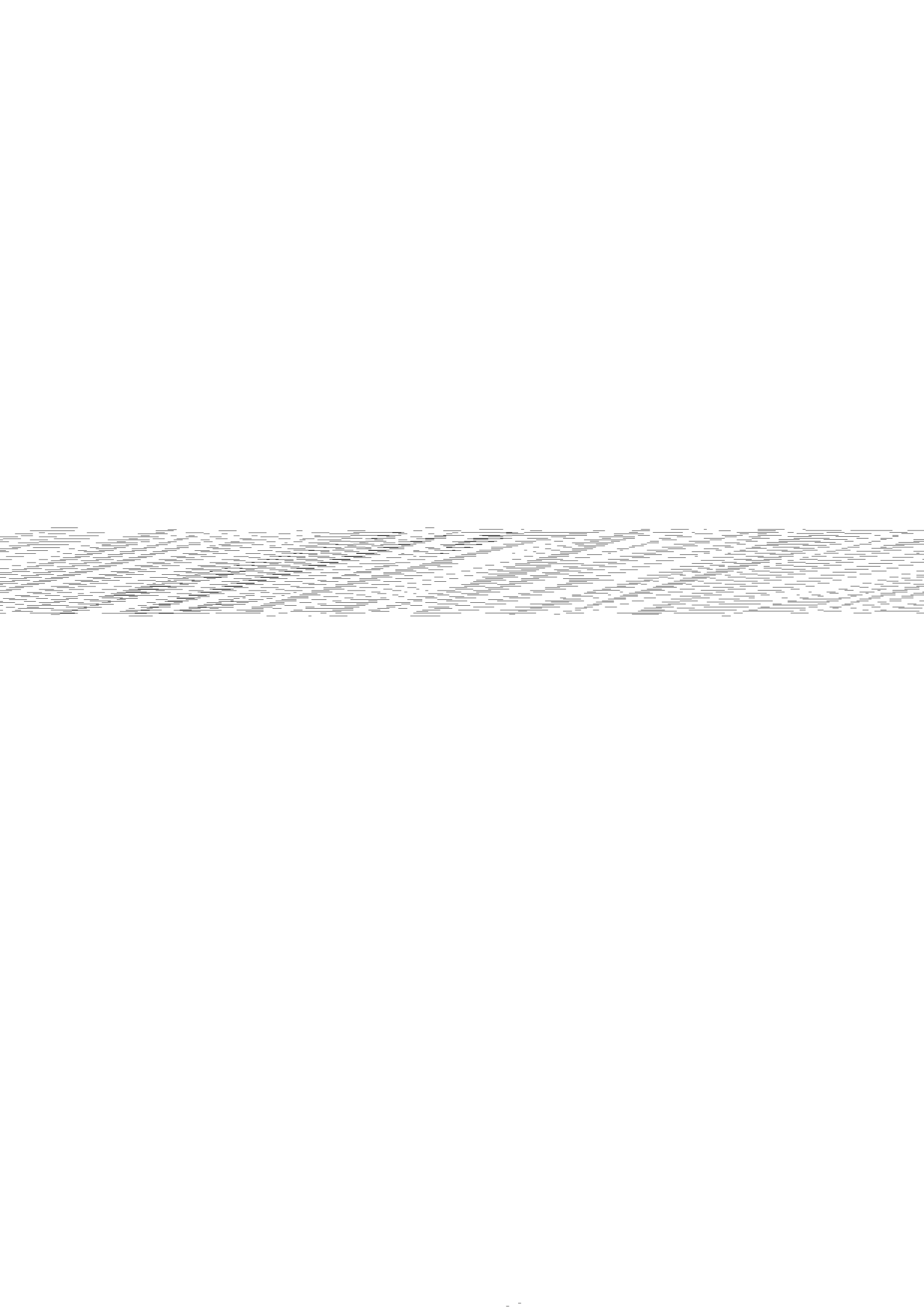


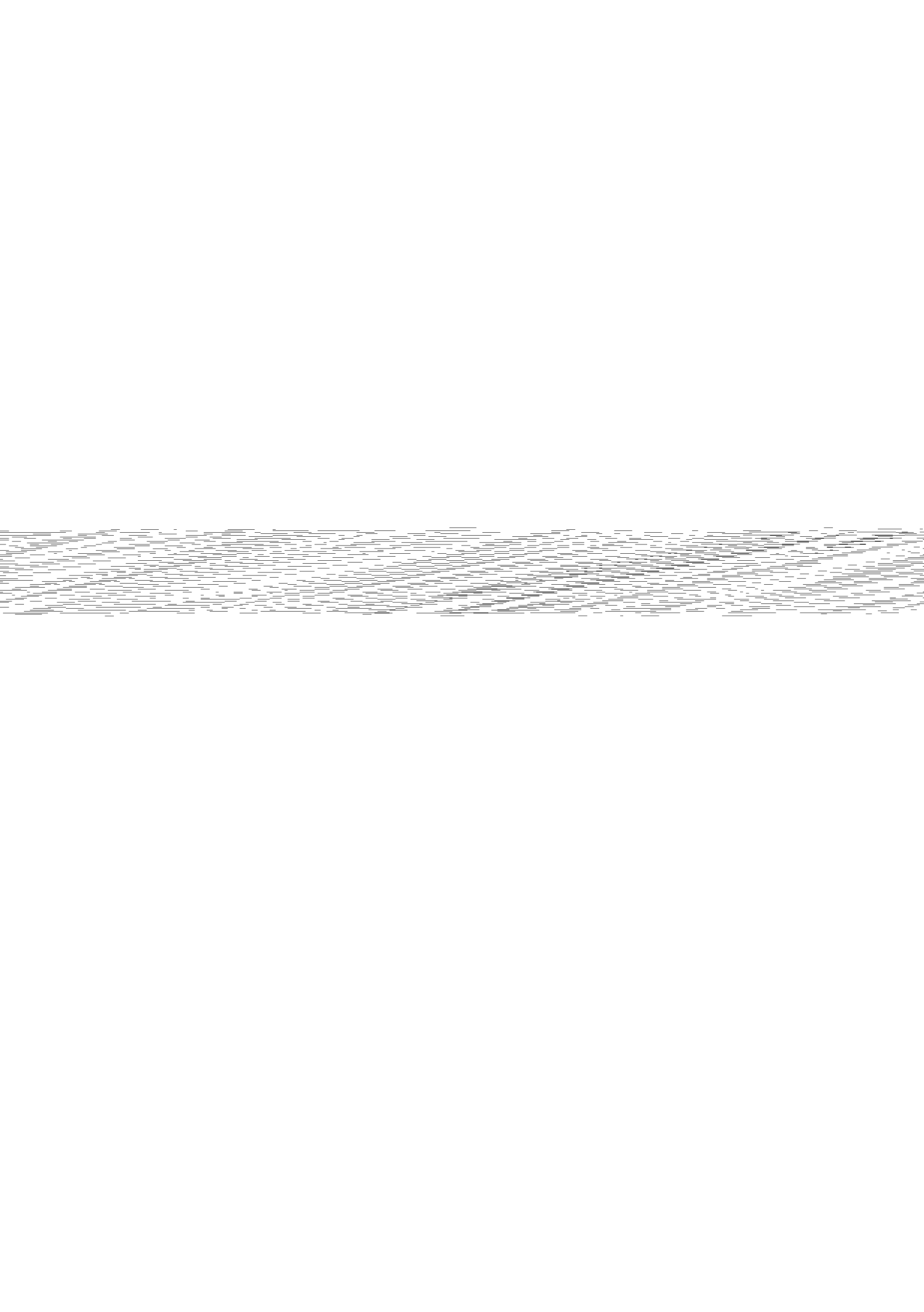


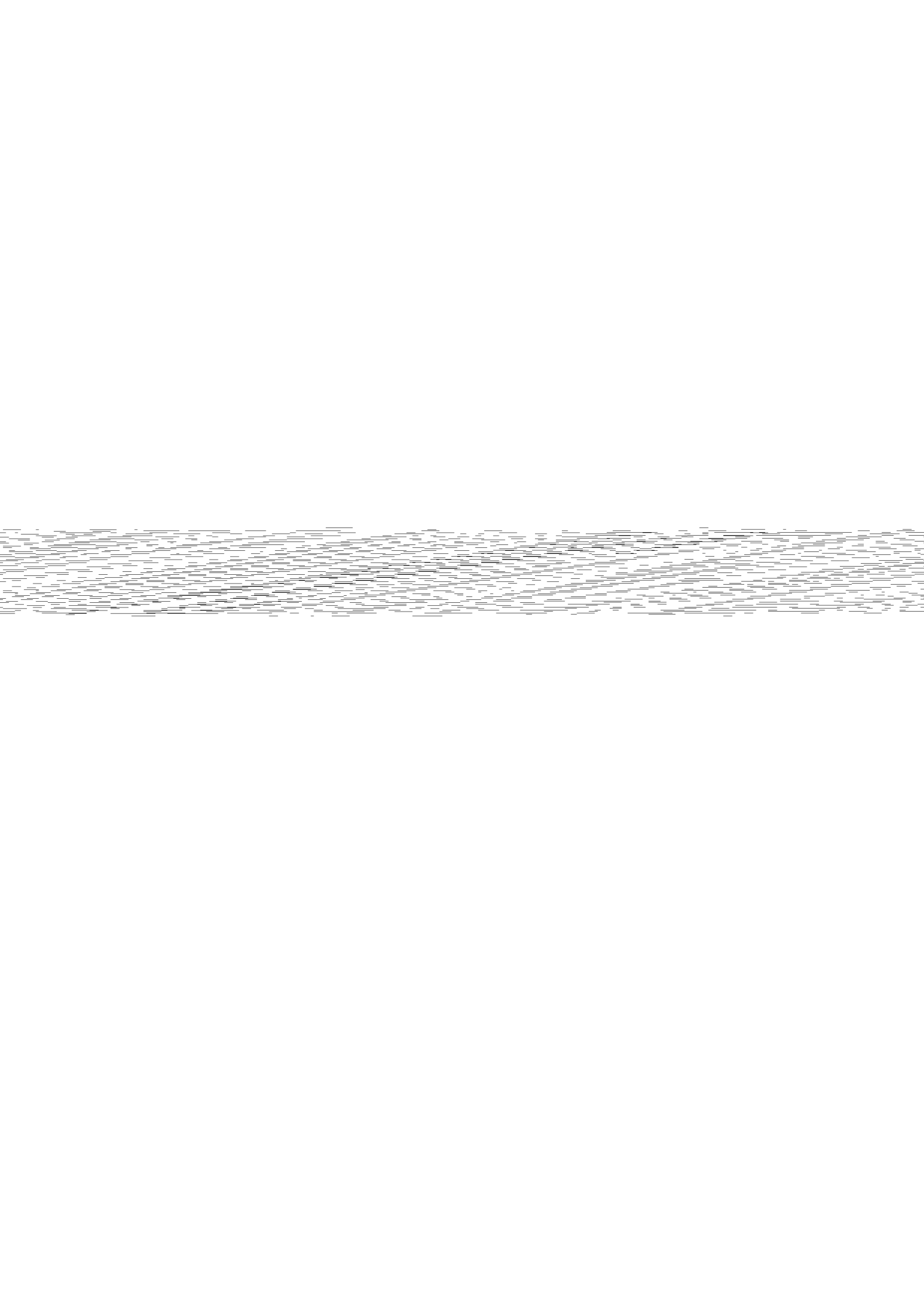








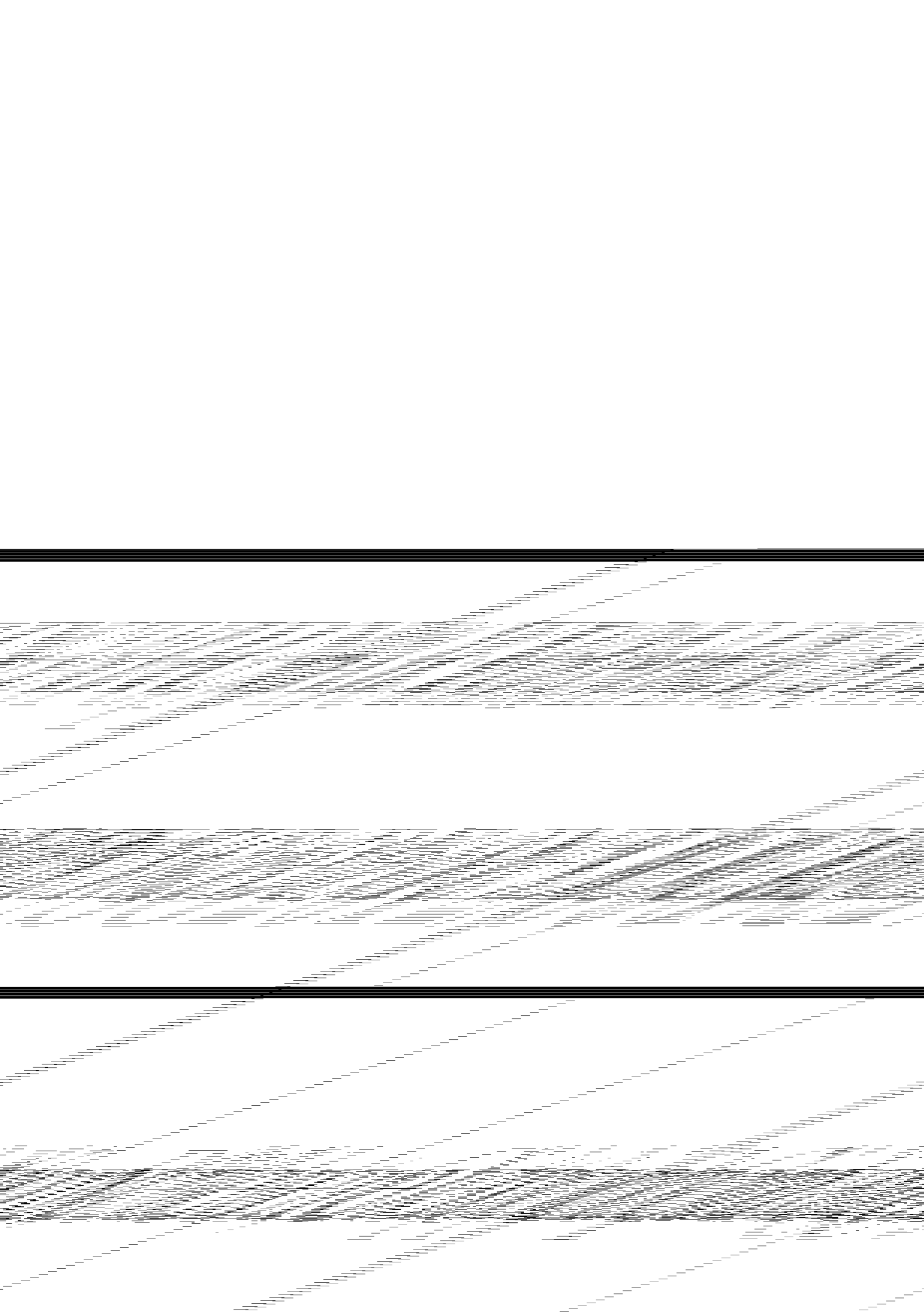


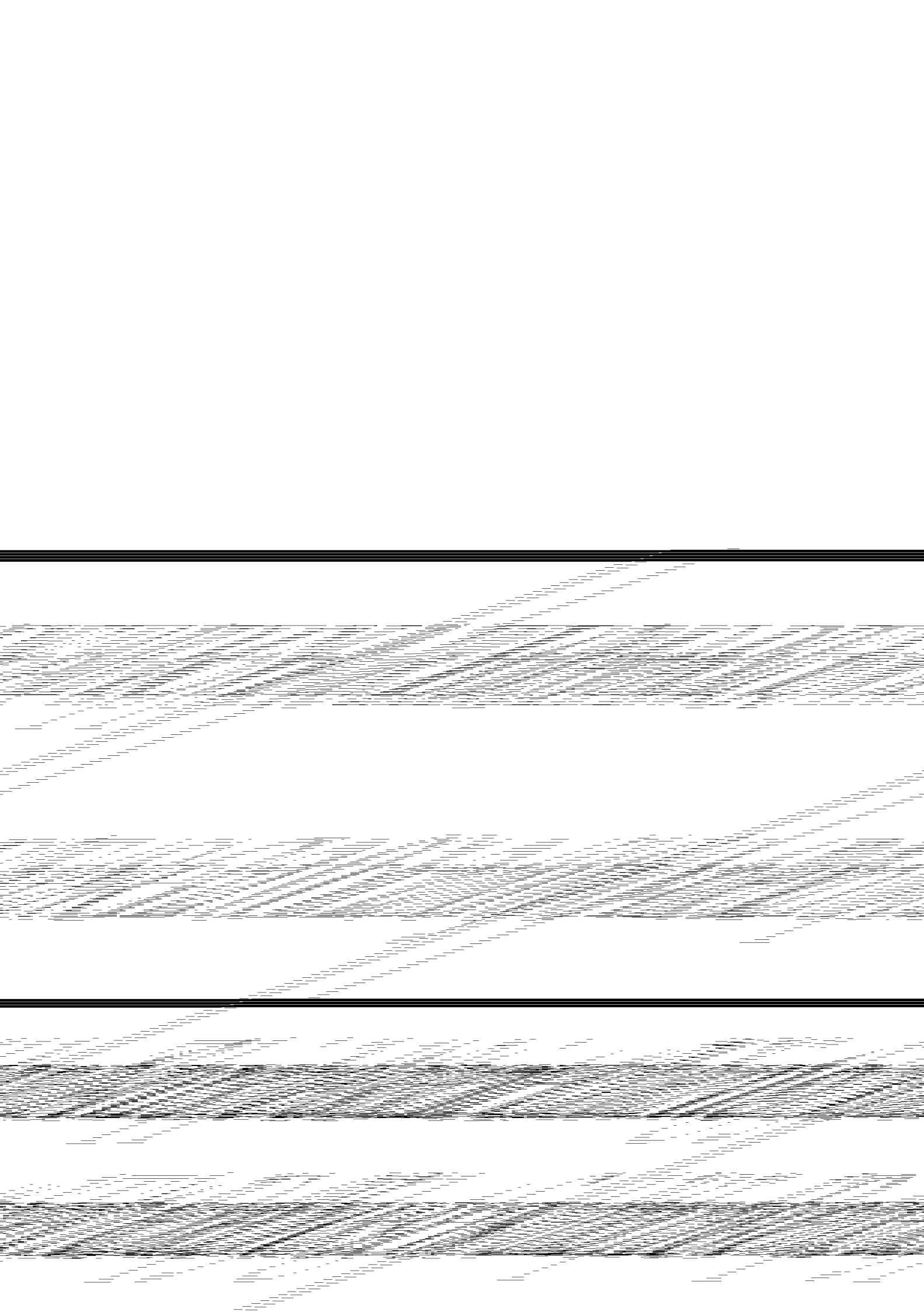


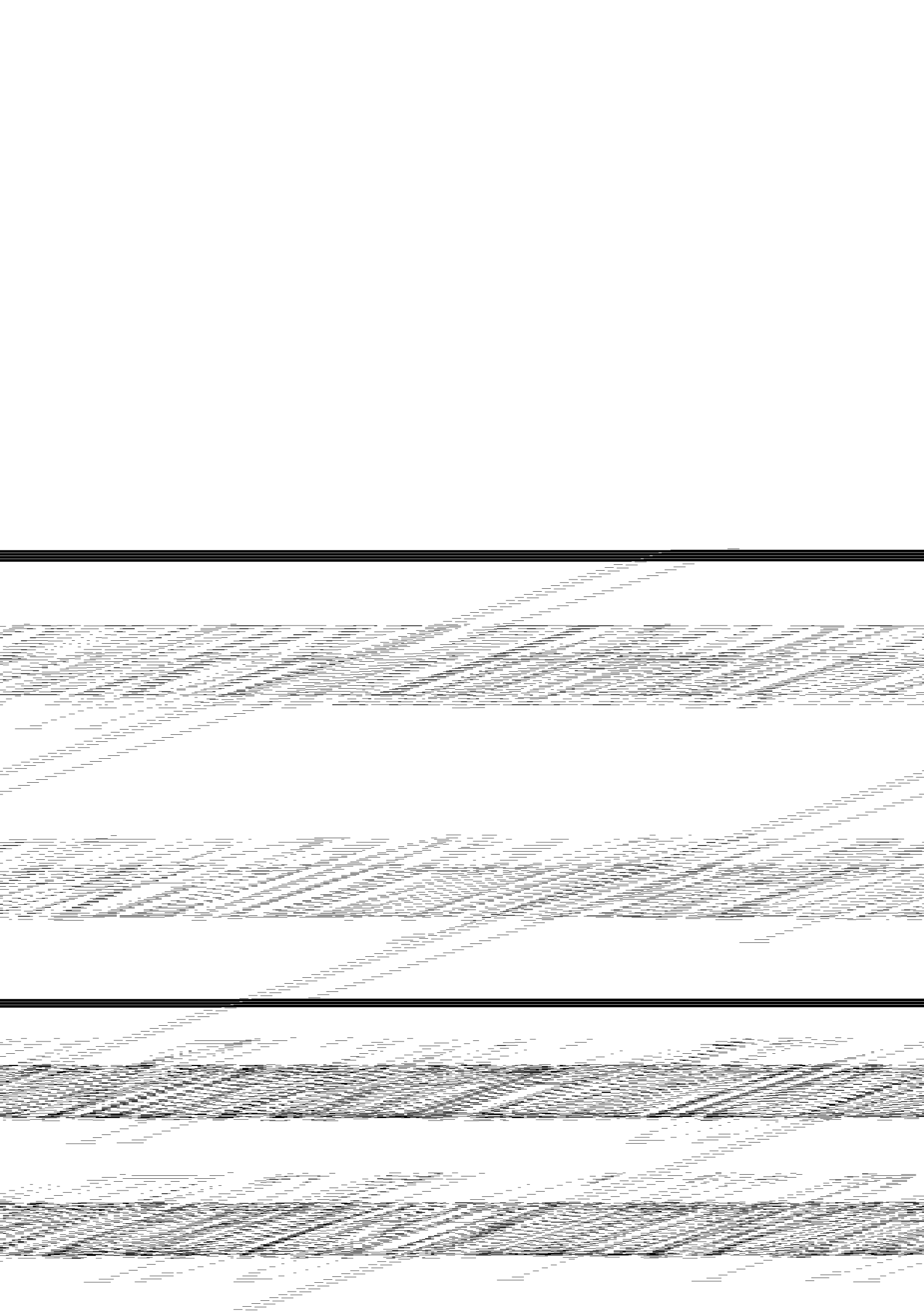


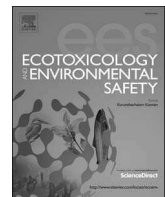












Green synthesis of graphene from recycled PET bottle wastes for use in the adsorption of dyes in aqueous solution

Noha A. El Essawy^{a,*}, Safa M. Ali^b, Hassan A. Farag^c, Abdelaziz H. Konsowa^c, Mohamed Elnoubey^d, Hesham A. Hamad^{e,*1}

^a Advanced Technology and New Materials Research Institute (ATNMRI), City for Scientific Research and Technological Applications (SRTA-City), New Borg El-Arab City, 21934 Alexandria, Egypt

^b Nucleic Acid Research Department, Genetic Engineering and Biotechnology Research Institute (GEBRI), City for Scientific Research and Technological Applications (SRTA, City), New Borg El-Arab, 21934 Alexandria, Egypt

^c Chemical Engineering Department, Faculty of Engineering - Alexandria University, Alexandria 21544, Egypt

^d Nanomaterials and Composites Research Department, Advanced Technology and New Materials Research Institute (ATNMRI), City for Scientific Research and Technological Applications (SRTA-City), New Borg El-Arab City, 21934, Alexandria, Egypt

^e Fabrication Technology Research Department, Advanced Technology and New Materials Research Institute (ATNMRI), City for Scientific Research and Technological Applications (SRTA-City), New Borg El-Arab City, 21934, Alexandria, Egypt



ARTICLE INFO

Keywords:

PET
Waste management
Graphene
Adsorption
Cationic dye
Anionic dye

ABSTRACT

Polyethyleneterephthalate (PET) is an important component of post-consumer plastic waste. This study focuses on the potential of utilizing "waste-treats-waste" by synthesis of graphene using PET bottle waste as a source material. The synthesized graphene is characterized by SEM, TEM, BET, Raman, TGA, and FT-IR. The adsorption of methylene blue (MB) and acid blue 25 (AB25) by graphene is studied and parameters such as contact time, adsorbent dosage were optimized. The Response Surface Methodology (RSM) is applied to investigate the effect of three variables (dye concentration, time and temperature) and their interaction on the removal efficiency. Adsorption kinetics and isotherm are followed a pseudo-second-order model and Langmuir and Freundlich isotherm models, respectively. Thermodynamic parameters demonstrated that adsorption of dye is spontaneous and endothermic in nature. The plastic waste can be used after transformation into valuable carbon-based nanomaterials for use in the adsorption of organic contaminants from aqueous solution.

1. Introduction

Over the last decades, made-up polymers have become a sophisticated part of our community. Polyethylene terephthalate (PET) is one of the most common, abundant industrial and municipal wastes. It is related to the thermoplastic polyester that enormous consumed markedly in the last few years in pharmaceutical, food and soft drink bottles and containers industries due to its excellent properties such as; high thermal stability, transparency, low cost, easy to handle, flexibility in design, inertness towards food, negligible permeability to CO₂ and malleability resistance to both weak and strong mineral acids, oxidizing agents, sunlight and microorganisms (Association of Plastic Manufacturers in Europe, 2001; Parra et al., 2004).

Although the significant fastest expansion rate in the plastic residue production, it led to severe an environmental issue. PET is considered is one of the most abundant municipal and industrial wastes that may be

returned to the valuable application of PET as a waste is limited because unsuitable mechanical properties, thermal stability as well as the low of electrical conductivity (Dutt and Soni, 2013; Mallakpour and Behranvand, 2016). Therefore, the disposal of this waste represents a major challenge for all over the world, especially in developing countries for waste and environmental management. The most popular approach to eliminate the PET waste is by means of incineration with energy recovery, chemical recycling or feedstock recycling to produce gaseous and liquid products and carbon-enriched materials (Mishra et al., 2003). For several years, incineration in landfill sites has been a common practice in the handling process of PET residues. However, this method may also negatively affect the environment as it carries out with air consumption and the release of heat and volatile compounds (Saha and Ghoshal, 2005). Another alternative would be the use of the spare PET bottles as an excellent candidate to be used a promising precursor in the synthesis of carbon-based materials as, for instance,

* Corresponding authors.

E-mail addresses: nony_essawy@yahoo.com (N.A. El Essawy), heshamaterials@hotmail.com (H.A. Hamad).

¹ Present address: Departamento de Química Inorgánica, Facultad de Ciencias, Universidad de Granada, 18071 Granada, Spain.

carbon microspheres, carbon nanotubes (Bazargan and McKay, 2012) or activated carbons (Mendoza-Carrasco et al., 2016) due to it has a high content of carbon and negligible amounts of mineral impurities in its chemical constitution. (Nakagawa et al., 2004).

In order to promote a more competitive carbon material, it is vital to consider developing carbon based materials from the renewable resources as waste polymers and agriculture waste (El Essawy et al., 2016; Deng et al., 2016). The main motivation of utilizing these sources is to provide “green and sustainable” alternatives with low-cost raw materials for large scale production of clean carbon based structures.

An assortment of dyes is used extensively in many industries, such as dyeing, printing, paper and pulp, textiles, plastics, leather, cosmetics, and food industries. Many of the dyes and their products are harmful and pose severe environmental problems. Dyes usually have complex aromatic molecular structures which make them more stable, resistant to fading, difficult to bio-degradation and inhibit sunlight penetration into the stream which is affecting the aquatic ecosystem. Moreover, they are toxic to some microorganisms and may cause destruction of their catalytic capabilities (Forgacs et al., 2004). Thus, treating the effluents of these industries before they are released into the water system is a must.

Various techniques have been used to treat dye-polluted water, including chemical precipitation, ion exchange (Sheng et al., 2016a, b, c; Elkady et al., 2014, 2016), membrane filtration (Giardelli et al., 2001), adsorption (Sheng et al., 2016a, b, c; Abd Elhafez et al., 2017), TiO₂-photo-catalytic degradation (Hamad et al., 2015a, 2015b, 2016; Fathy et al., 2016), solid-phase extraction (Wu et al., 2015a), microbiological decomposition and electrochemical technologies (Bassyouni et al., 2017). However, many synthetic dyes are chemically stable and resistant to photodegradation and biodegradation (Forgacs et al., 2004; Rafatullah et al., 2010). Most of dye removal methods have some limitations such as high capital investment and operation costs.

Adsorption is found to be an alternative technique for removing dyes from wastewater (Yu et al., 2014; Idris et al., 2011; Sivukumar and Palanisamy, 2009). In fact, a chemical or physical bonding retains the atoms, molecules, or ions on the surfaces of solids. A number of adsorbents have been used for the removal of dyes from polluted water; such as activated carbon (Nasuha and Hameed, 2011), carbon nanotubes (Yu et al., 2014; Wu et al., 2015b), graphene (Kui et al., 2012; Yu et al., 2015, 2016a), graphene oxide nanosheet (Yu et al., 2016b), reduced graphene oxide and its magnetic composite (Jin et al., 2015); nano zerovalent iron (Hu et al., 2016) and immobilized on carbon nanotubes (Sheng et al., 2016a, b, c). Therefore, the development of new effective, low-cost and eco-friendly adsorbent with high efficiency for dye removal from the water system is attracting the increased attention of the researchers worldwide.

Therefore, the aim of the present novel work is to prepare graphene from PET bottle waste by simple, reproducible and affordable method which involves the thermal decomposition of PET waste in a closed system under autogenic pressure. The adsorption behavior of the prepared graphene is evaluated for cationic and anionic dye removal. Methylene Blue (MB) is selected as a model for basic dye (cationic dye) and Acid Blue 25 (AB25) as a model for acidic dye (anionic dye). The effects of important factors including, initial dye concentration, time, temperature and solution pH are examined as input variables on the dye removal efficiency through the Response Surface Methodology (RSM) as a powerful statistical technique which has shown a growing interest among different researchers worldwide (Rahimodkht et al., 2016). In addition, the kinetics, equilibrium, and thermodynamics studies of the adsorption process have been discussed. Wastes-treats –wastes are a demanding area as it has double benefits which are water treatment and waste management.

2. Materials and experimental procedure

2.1. Starting materials and reactants

Mineral water bottles waste (Baraka-Nestle bottled water company in Egypt) as a source for PET were used in the present study. All the reagents used were commercially available and used without further purification. Acid blue 25 (AB25) and methylene blue (MB) were obtained from Sigma-Aldrich (USA). Properties and structure of MB and AB25 dyes were shown in Table S1. All solutions were prepared with ultra-pure water under ambient conditions.

2.2. Graphene synthesis from PET bottle wastes

First, waste PET bottles were crushed and sieved to obtain the desired size fractions (1–3 mm) using a conventional sieve-shaker. Then 2 g of raw PET waste was introduced into an enclosed 50 mL stainless steel autoclave reactor (SS316). The closed stainless steel reactor was placed inside the center of an electric furnace and heated to 800 °C with a rate of 8 °C min⁻¹ and maintained at this temperature for 1 h. After that the system was left to cool overnight. The resulted dark products were collected and crushed. As it was illustrated in Fig. 1, the bottle wastes were used as a precursor for the synthesis of graphene.

2.3. Characterization of the prepared graphene

The prepared sample was characterized using different physical and chemical techniques. Scanning electron microscope (SEM) is used to investigate the surface topography of the prepared sample with JEOL, model: JSM 6360 LA, Japan. Prior to the investigation, the sample was coated with gold using sputtering coater (model: S150B, Edwards High Vacuum Ltd., England) in order to avoid the buildup of local electrical charges.

Transmission electron microscope (TEM) (TECNAL G20, Super twin, Double tilt, FEI, Netherland with EDAX) was employed to obtain images for studying the nanostructure and elemental analysis (qualitative and semi-quantitative analysis) of the prepared sample. In order to prepare the sample for TEM analysis, approximately 1 mg of the dry black powder was dispersed in 15 mL of ethanol using an ultrasonicator and 10 µL of this dispersion was put on a coated copper grid. The dried grid was then examined under an electron microscope (HR-TEM, high resolution transmission electron microscope operating at 200 kV).

Two different modes of imaging were employed; the bright field at electron accelerating voltage 200 kV using lanthanum hexaboride (LaB₆) electron source gun and diffraction pattern imaging. Eagle CCD camera with (4k*4k) image resolution was used to acquire and collect transmitted electron images. TEM Imaging and Analysis (TIA) software was used for spectrum acquisition and analysis of EDAX peaks.

Crystallographic information about the micro-structure of sample was obtained from powder X-ray diffraction (XRD) data collected with a (Schimadzu-7000, U.S.A.) with CuK α radiation beam ($\lambda = 0.154060$ nm). The finely powdered sample was packed into a flat aluminum sample holder, where the X-ray is generated at 30 kV and

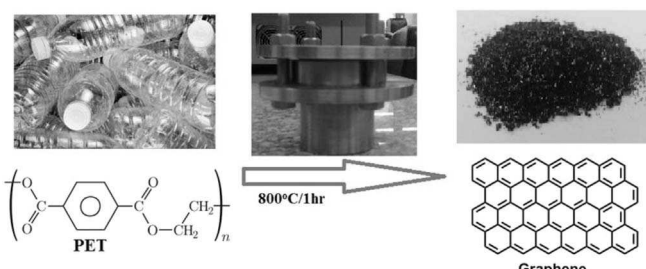


Fig. 1. Schematic representation of synthesis of graphene from PET recycle bottles.

30 mA with a copper target. Scans are performed at 4°min^{-1} for 20 values between 10 and 80.

Thermal characteristics of PET and produced graphene were measured by TGA-50H, Shimadzu (Japan) with heating rate $10^{\circ}\text{C}/\text{min}$ (30 mL/min) up to 800°C under air atmosphere.

Raman spectroscopy was performed on the dried sample at room temperature using Senterra Raman spectrometer, Bruker- Germany with a 514.5 nm excitation wavelength and power output of 10 mW to determine the extent of graphitic disorder within the prepared material. Each measurement was taken for 60 s and repeated four times in the range of wave numbers from 40 to 3500 cm^{-1} .

Fourier transform infrared (FTIR) analysis was applied to determine the surface functional groups, using a Bruker ALFA FTIR spectrometer (Bruker Corporation, Ettlingen, Germany), where the spectra were recorded from 400 to 4000 cm^{-1} .

Finally, The Brunauer-Emmett-Teller (BET) surface area and total pore volume were determined using BET and the Barret- Joyner- Halenda (BJH) adsorption methods.

2.4. Adsorption tests

Stock solutions of MB and AB25 of 500 mg L^{-1} were prepared by dissolving 0.5 g of dye in 1 L of ultrapure water. The effects of contact time, initial dye concentration, adsorbent dose, solution pH, and temperature of the dye adsorption process using the prepared material were investigated. Desired temperature was controlled by using a temperature-controlled water bath shaker. All pH measurements were carried out using a pH meter and solution pH were adjusted using 0.1 M HCl and 0.1 M NaOH.

At a certain time, the supernatant was taken out and filtered, and the final dye concentration was determined using UV-Vis spectrometer at the wavelength of 650 and 600 nm for MB and AB25 dyes, respectively. The following formula was used to determine the adsorbed dye amounts per gm of the prepared graphene (q) either at equilibrium (q_e) or at specific times (q_t):

$$q_e = \frac{(C_0 - C_e)}{m} V \quad (1)$$

$$q_t = \frac{(C_0 - C_t)}{m} V \quad (2)$$

Where; q_e and q_t (mg g^{-1}) are the amounts of dye adsorbed per unit weight of the adsorbent at equilibrium and t time, respectively; C_0 , C_e and C_t ($\text{ppm} = \text{mg L}^{-1}$) are the dye concentrations at initial, equilibrium and t time, respectively; V (L) is the volume of dye solution; and m (g) is the weight of the adsorbent.

While dye removal efficiency ($R\% \%$) was calculated using the following equations:

$$R\% = \frac{C_0 - C_t}{C_0} \times 100 \quad (3)$$

2.5. Adsorption procedure by response surface methodology (RSM)

The response surface methodology which was described in the experiment of a Box-Behnken design (Box and Behnken, 1960), used to determine the optimum conditions for MB and AB25 dye removal using prepared graphene from waste PET bottles. The design matrix with 13 trials was chosen to evaluate the interaction of different operating conditions (Pajootan et al., 2014). Box-Behnken design with three factors at three levels (-1, 0 and 1) was taken into consideration with regard to the adsorption process and a total number of 13 experimental runs were conducted to evaluate the effect of three independent variables (X1: time (min), X2: dye concentration (mg L^{-1}) and X3: temperature ($^{\circ}\text{C}$)) on the performance of adsorption process. The response function (dye removal efficiency (%)) was further optimized to reach a

desired value by Response Optimizer. Data analysis and optimization procedure were performed using the statistical software "Statistica". After the optimization of adsorption process by response optimizer, the isotherm, kinetic and thermodynamic parameters of MB and AB25 removal were investigated by using prepared carbon nanomaterials.

2.6. Kinetics of adsorption process

Kinetics study was important as it describes the uptake rate of adsorbate. The rate and mechanism of the dye adsorption process onto adsorbent could be elucidated based on kinetic studies. In order to elucidate the adsorption kinetics, the pseudo-first-order and pseudo-second-order models were applied.

$$q_t = q_e [1 - \exp(-k_1 t)] \quad (4)$$

$$q_t = \frac{k_2 q_e^2 t}{1 + k_2 q_e t} \quad (5)$$

Where; k_1 and k_2 are pseudo-first-order and pseudo-second-order adsorption rate constants, respectively.

2.7. Dye sorption isotherms

The dye sorption capacity of the prepared material at different initial concentrations at equilibrium can be illustrated by the adsorption isotherms. Adsorption isotherms describe how the adsorbate interacts with adsorbents and give a thorough understanding of the nature of interaction. Several isotherm equations have been developed and employed for such analysis and the two important isotherms of Langmuir and Freundlich isotherms were applied.

2.7.1. Langmuir isotherm model

Langmuir's isotherm was used for monolayer adsorption on a surface containing a finite number of identified sites with negligible interaction between adsorbed molecules and assumes uniform energies of adsorption on the surface. In addition the maximum adsorption depends on the saturation level of monolayer (Elkady et al., 2015). The Langmuir isotherm is represented by the following linear equation:

$$\frac{q_e}{C_e} = \frac{1}{K_L q_m} + \frac{C_e}{q_m} \quad (6)$$

Where; q_e is the solid-phase dye concentration in equilibrium with the liquid-phase concentration C_e expressed in mole L^{-1} , q_m is the maximum monolayer adsorption capacity (mg g^{-1}), and K_L is an equilibrium constant (L mol^{-1}). A straight line with slope of $1/q_m$ and intercept of $1/q_m K_L$ is obtained when C_e/q_e is plotted against C_e . The separation factor (R_L) is a dimensionless constant which is an essential characteristic of the Langmuir model. The equation of R_L is expressed as:

$$R_L = \frac{1}{1 + K_L C_0} \quad (7)$$

Where C_0 (mg L^{-1}) is the highest studied initial dye concentration, ($C_0 = 200\text{ mg L}^{-1}$).

R_L indicates if the isotherm is unfavorable when $R_L > 1$, linear at $R_L = 1$, favorable at $0 < R_L < 1$, or irreversible at $R_L = 0$ (Elkady et al., 2016).

2.7.2. Freundlich isotherm model

Adsorbents that follow the Freundlich isotherm equation are assumed to have a heterogeneous surface consisting of sites with different adsorption potentials (Elkady et al., 2014), and each type of site is assumed to adsorb molecules, as in the Langmuir equation:

$$\ln q_e = \ln K_f + \frac{1}{n} \ln C_e \quad (8)$$

Where; K_f is constant (function of the energy of adsorption and temperature) and n is a constant related to adsorption intensity, by plotting $\ln q_e$ versus $\ln C_e$ which gave a straight line with slope of $1/n$ and intercept of $\ln K_f$. The magnitude of the "n" shows an indication of the favorability of adsorption (Gopinath et al., 2009). In general, if "n" is greater than 1, that means adsorbate is favorably adsorbed on the adsorbent whereas if "n" is lower than 1, that illustrates the adsorption process is chemical in nature (Elkady et al., 2016).

2.8. Adsorption thermodynamics

Adsorption thermodynamics experiments were performed at the optimum condition obtained by RSM for various temperatures (25, 35, 45 and 55 °C). Thermodynamic parameters were calculated by the following equations where K_D is the equilibrium partition constant, ΔG (kJ mol⁻¹) is the Gibbs free energy change, R (8.314 J mol⁻¹ K⁻¹) is the universal gas constant, T (K) is the temperature, ΔH (kJ mol⁻¹) is the enthalpy change and ΔS (kJ mol⁻¹ K⁻¹) is the entropy change.

$$K_D = \frac{q_e}{C_e} \quad (9)$$

$$\Delta G = -RT \ln K_D \quad (10)$$

$$\ln K_D = \frac{\Delta S}{R} - \frac{\Delta H}{RT} \quad (11)$$

The values of ΔG were calculated from the K_D values for each temperature, the values of ΔH and ΔS were calculated from the slope and intercept of the plot of $\ln K_D$ versus $1/T$, respectively (Gopinath et al., 2009; Abd Elhafez et al., 2017).

3. Results and discussion

3.1. Chemical composition of PET

The elemental analysis of PET waste is revealed that this plastic polymers are as a precursor in the preparation of graphene, especially due to its high carbon content and absence of inorganic matter and other impurities in their composition. This is an important property of this material for the presence of inorganic compounds could exert undesirable effects on processes such as adsorption of solutes in solution, catalysis, etc.

3.2. Characteristics of the prepared graphene

The SEM micrograph of the synthesized graphene is shown in Fig. 2-a. It exhibits the fiber network morphology with void space in between which can provide access to the porosity. On the other hand, different sizes that suggest a progressive consumption of material probably due to the fact that activation affect not only the surface but also the inner parts of the material. Meanwhile, as illustrated in Fig. 2-b the TEM image shows the presence of few-layers of graphene as relatively transparent sheets entangled and rippled with each other, graphite deposits are also observed. Energy Dispersive X-ray (EDX) is used to analyze the elemental composition of graphene as shown in Fig. 2-c. The elemental composition consisted of high amount carbon and traces of oxygen.

The XRD diagrams of the prepared sample are shown in Fig. 3-a. The disordered structure is reflected by the broad X-ray diffraction peaks centered at approximately 26, 42.3 and 44.3 2θ which correspond to the (002), (100) and (101) reflections, respectively for graphene. It is typical for highly amorphous graphite like carbons (Zhang et al., 2016; Sergienko et al., 2009). The broad (002) peak, in particular, encompasses diffuse sets of inter-layer distances which, on average, are larger than those in crystalline graphite (typically 0.344–0.355 nm). The presence of the (101) peak suggests a stacking order of graphene sheets (Shen and Lua, 2013).

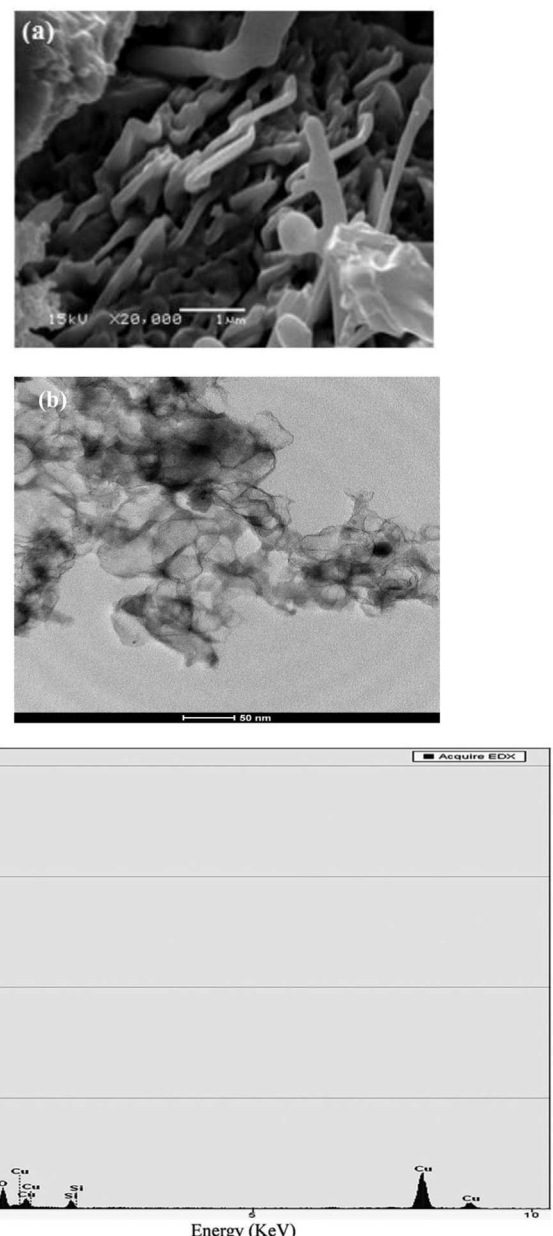


Fig. 2. (a) SEM image, (b) TEM image, c) EDX analysis of the synthesized graphene.

Raman spectroscopy is also widely used to analyze carbon materials and provided information about defects density, disorder structures, and doping levels. Generally, the Raman spectrum of graphene is characterized by two main features, the G mode, arising from the first order scattering of the E_{2g} phonons of sp^2 C atoms (usually observed at 1596 cm^{-1}) and the D mode, which attributed to the vibration of carbon atoms with dangling bonds for the in-plane terminated disordered graphite component, (at 1360 cm^{-1}). Fig. 3-b shows the Raman spectrum of the prepared graphene. The figure is typical for a hard carbon, with a broad band at $1331\text{--}1338\text{ cm}^{-1}$ representing a highly disordered (D) graphite arrangement (imperfect structure of amorphous carbons) and a band at $1573\text{--}1599\text{ cm}^{-1}$, characteristic of a more ordered graphitic (G) structure. When the bond lengths and angles of graphene are modified by strain, caused by the interaction with other graphene layers or due to external disorder, the hexagonal symmetry of graphene is broken (Malard et al., 2009; Ni et al., 2008). The G-band is, therefore, highly sensitive to strain effects in sp^2 nano-carbons and can be used to investigate any modification to the flat geometric structure of graphene, such as the strain induced by external

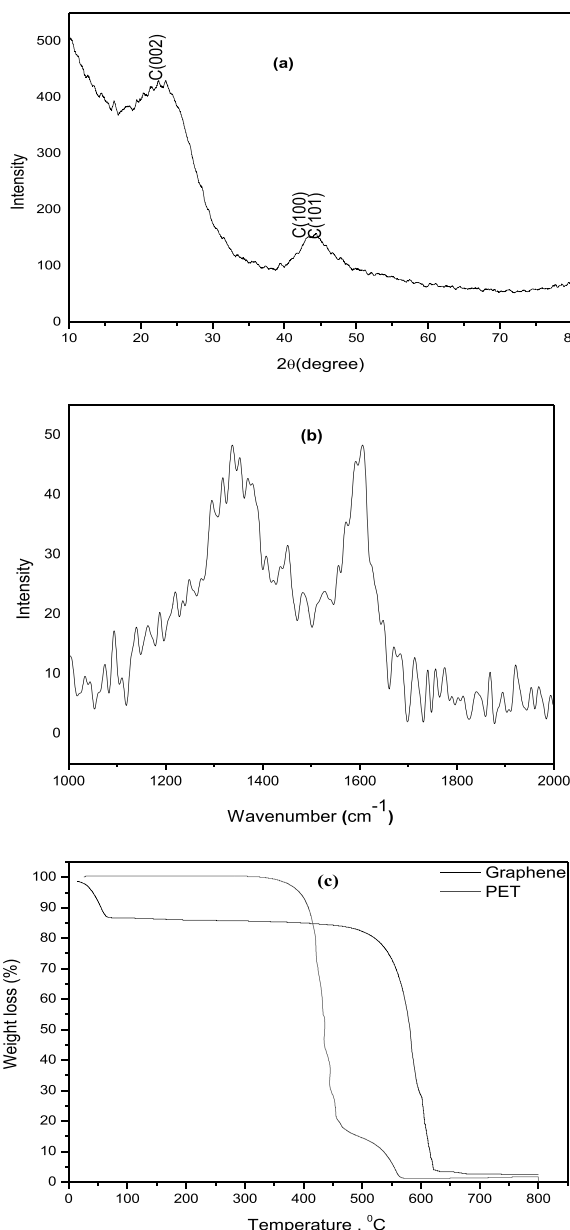


Fig. 3. a) XRD pattern and b) Raman spectra of the synthesized graphene, and c) TGA of PET and graphene.

forces, by one graphene layers on another in few layer graphene. The intensity ratio of the D and G-bands (I_D/I_G) is quantifying the relative levels of disordered structure and it is a good indicator of sample quality (Sergienko et al., 2009). However, the intensity ratio of the D and G bands is 1.13 for prepared graphene.

Fig. 3-c depicts the TGA of the PET bottle as a precursor and synthesized graphene. It shows that the degradation process of PET mainly occurs in one step. The temperature region is from ambient temperature to 800 °C under air atmosphere. As can be observed, PET showed no significant weight loss until 350 °C and only 13 wt% weight loss is seen from 25 to 100 °C which can be related to the loss of physically adsorbed water and the loss of volatile compounds (Hamad et al., 2014). Generally, PET and synthesized graphene thermally stable up to 360 and 485 °C, respectively. As expected, this sample is totally decomposed at high temperature (> 500 °C) and the ash content is quite low (about 1.74% and 2.46%) since the PET polymer is essentially composed of organic matter. The formation of carbon species during the thermal decomposition of PET may be regarded to a competition between a

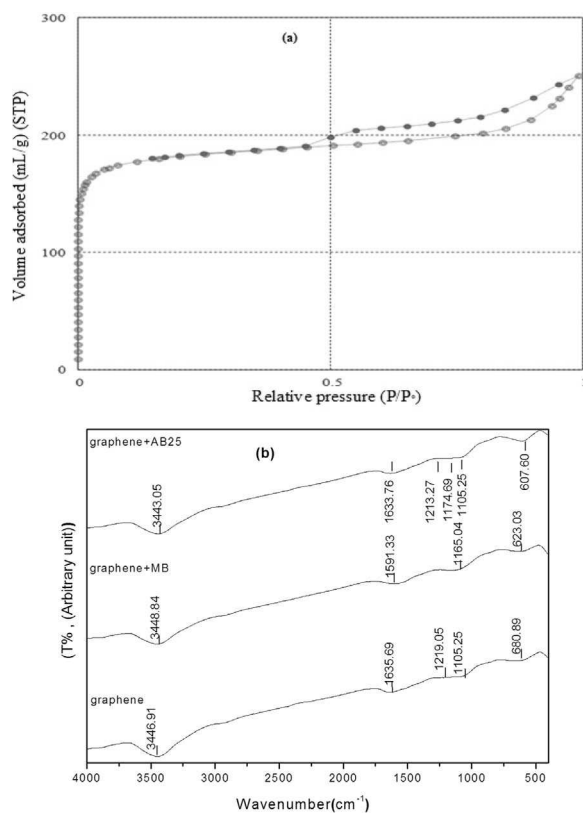


Fig. 4. (a) N_2 adsorption–desorption isotherms for prepared graphene at 77 K, and (b) FTIR spectra before and after adsorption of MB and AB25.

chain scission to generate volatile species and a condensation process to form carbon structure (Yuan et al., 2008). It is much easier for aromatic polymers to convert into polyhexagonal carbon layers compared with aliphatic polymers. Subsequently the aromatic (rich in benzene) property of PET makes condensation much easier, which leading to the almost simultaneous occurrence of chain scission and condensation rather than the aliphatic polymer (Lian et al., 2011).

The BET surface area of the PET is lower than $2\text{ m}^2/\text{g}$ and the synthesized graphene is $721.7\text{ m}^2/\text{g}$ (Table S2). Pore size is one of the main specifications for which adsorbents are selected for a particular application. As shown in Fig. 4-a, the N_2 adsorption and desorption at 77 K of graphene increased rapidly at low relative pressure, and at high relative pressure the adsorption volume stabilized, the shape of adsorption isotherms evolves from an isotherm exhibiting a very closed knee, which is classified as type I according to IUPAC classification that indicates the presence of large fractions of micropores (Gao et al., 2013). Furthermore, the D_{ap} value for graphene is 2.1007 nm as shown in Supplemental Table S2, which is very near to 2.0 nm indicating a great development of micropores whereas micropores ($< 2\text{ nm}$) and mesopores ($2\text{--}50\text{ nm}$) are based on the classification adopted by IUPAC (Gao et al., 2013). The BET surface area, mean pore diameter and total pore volume values are indicated that the prepared graphene has appropriate properties for the removal of dye molecules from waste water.

3.3. An exploratory adsorption study by FTIR

The existence of several functional groups peaks is estimated before and after adsorption of MB and AB25 dyes using FTIR that shown in Fig. 4-b. The graphitization of PET waste by thermal decomposition can be confirmed due to the presence of IR absorption peak around 1600 cm^{-1} corresponding to the in plane $C=C$ vibration, which is an intrinsic characteristic of sp^2 graphitic materials (Hu et al., 2017). As shown, graphene has four characteristic peaks at 3447 , 1636 , 1219 , and 1105 cm^{-1} , which may be attributed to the stretching vibration of O–H,

C=O of carboxyl groups, esters C—O—C ethers or phenol groups, and alkoxy C—O, respectively (El-Remaily and Hamad, 2015; Adel et al., 2016; Yu et al., 2016). That is evidenced; the prepared graphene consists of several surface functional groups such as oxygen surface groups are frequently in graphene which affect positively on the adsorption ability of organic pollutants in liquid solution.

As shown in Fig. 4-b (the results summarized in Supplementary Table S3), many significant differences occurred for graphene after adsorbing MB and AB25 [by mixing 5 mg of prepared graphene with 25 mL of 100 mg L⁻¹ dye solution in a mechanical shaker at a temperature of 25 °C for 30 min and an agitation speed of 200 rpm]. For instance, there are distinct and significant changes in the adsorption peak frequencies of OH, C=C, C=O and C—O—C suggesting that, such ionize the functional groups on the adsorbent surface are able to link and interact with the dye molecule. Moreover, the mechanism of adsorption can be deduced by its dependence on such functional groups especially the hydroxyl group. The changes in the FTIR spectrum are the clue of the formation of multiple carbon-carbon bond structures as well as the elimination of oxygen and hydrogen atoms which originally present (Gao et al., 2013).

3.4. Adsorption studies

The structure of MB and AB25 used in the present study is given in Table S1. The pKa of the functional groups associated with MB and AB25 renders them charged depending on the pH used. On the other hands, AB25 possesses a sulfonic group that imparts negative charge resulting in the repulsion between graphene and the dye molecule and hence lower adsorption is observed as compared to MB.

3.4.1. Effect of contact time

As shown in Fig. 5-a the q_t value increased rapidly in the beginning, then increased slowly and finally became constant over a certain time. This can be due to the fact that, there are free surface sites available for adsorption at the initial adsorption stage (Yu et al., 2016). At the further stages, the remaining unoccupied surface sites are hard to be utilized due to repulsive forces between the dye molecules adsorbed onto adsorbent and those in the solution. The adsorption of MB dye on graphene reached equilibrium after 30 min. So, 30 min is chosen to be the optimum contact time with adsorption capacity 481 mg g⁻¹. While for AB25 it is evident as per Fig. 5-a, the rates of adsorption are fast up to 25 min and then gradually increased between 30 to 50 min. Based on experimental results; there is no significant change in the adsorption capacity after 50 min for AB25; that may refer to the small number of vacant sites are available. The maximum percentage of AB25 removal at the equilibrium time is 90% with adsorption capacity 460 mg g⁻¹.

As shown, the color removal of MB dye is quicker than AB25 on the graphene surface. This is may be due to the fact that polar functional groups at the opening of pores adsorb water through hydrogen bonds while the anionic dye molecules suffer columbic repulsion with oxygen-containing functional groups (carboxyls, carbonyl etc.) present on graphene.

3.4.2. Effect of initial dye concentration

It is evident from Fig. 5-b that the adsorption is highly dependent on initial dye concentration. The percentage dye adsorption drops with increasing initial dye concentration from 50 to 200 mg L⁻¹ at contact time equal 30 min for MB and 50 min for AB25 at room temperature. This may be attributed to the repulsive forces between the dye molecules to the adsorbent surface and the bulk phase. At lower concentrations, all dyes concentration present in the adsorption sites can interact with the surface of graphene because of the ratio of available binding sites to the initial dye is larger (Ali et al., 2016). However, at higher initial dye concentration, the ratio is low because the adsorption site is saturated and it will impede the movement of dye toward the vacant surface sites on the adsorbent surface (Ali et al., 2016).

3.4.3. Effect of adsorbent dosage

It is indicated from Fig. 5-c that the percentage dye removal is enhanced as the adsorbent dose increased. The main reason for this behavior may be accounted to the greater availability the number active sites for dye-surface interactions as a result of increase the surface area, pore volume and the number of binding sites (Ali et al., 2016; Bangash and Alam, 2009). Another reason may be attributed that the aggregation of surface area of graphene that is available for adsorption of dye and increase the diffusion path length (Abd Elhafez et al., 2017). The optimum dosage to achieve 96% MB dye removal is recorded as 0.2 mg/mL. While, that value achieved 90% for AB25.

3.4.4. Effect of solution temperature

As shown in Fig. 5-d, the percentage dye removal increases with increasing solution temperature. This behavior indicates that the dye adsorption process is an endothermic process that give prediction in the presence of weak attractive forces between surface of graphene and the dye molecule that evident adsorption mechanism of MB and AB25 onto graphene is considered as a mainly chemisorption process (Yu et al., 2016; Elkady et al., 2016). But the percentage dye removal is almost unchanged at temperature higher than 35 °C for MB adsorption. Therefore, 35 °C is chosen as the best temperature of the adsorption process using the prepared material. The adsorption capacity of AB25 increased significantly with the increasing temperature indicating that the AB25 dye adsorption at higher temperatures is favored.

Generally, these results may be attributed to the rise of solution temperature, which accelerates the rate of diffusion of dye molecules from the solution bulk to the adsorbent surface across the external boundary layer and in the internal pores of the adsorbent. Also, the increasing of temperature facilitates the attraction of dye ions to the surface of graphene and increase the rate of ion exchange process due to the activation of graphene adsorbent material at high temperature (Elkady et al., 2016). However, as the temperature increases, the mobility of dye molecules increased with the creation of new active sites and the thickness of boundary layer surrounding the adsorbent decreased, which in turn decreased the mass transfer resistance of adsorbate in the boundary layer with temperature.

3.4.5. Effect of pH

The initial pH value of the dye solution is one of the most significant factors influencing on the adsorption capacity because it can influence the surface charge of the adsorbent as well as the surface binding sites and the degree of ionization of the dye (Abd Ellatif and Ibrahim, 2009; Ali et al., 2016; Elkady et al., 2016). Graphene as adsorbent may contain a large number of active sites and the dye ion uptake can be related to the active sites and also to the chemistry of dye solution. The impact of solution pH values on the removal of dyes is determined over a pH range of 2–12.

It is found out that, the removal percentage of MB increased with increasing the solution pH and the optimum pH value for MB adsorption is 12 (Fig. 5-e). This phenomenon may be explained by the fact that, the cationic dye becomes positively charged when it is dissolved in water. Thus, in acidic medium the positively charged surface of graphene hinders the adsorption of the cationic MB (Han et al., 2014). As a result, when the pH of the solution increased, adsorption of MB increased due to an increase in the electrostatic attraction between the positive dye molecules and the adsorbent surface which is negatively charged. However, graphene has a positive charge at low pH values due to the presence of functional groups containing the remaining oxygen. Moreover, a low pH value means a relatively high concentration of protons, which competes strongly with MB cationic molecules for the adsorption sites on the surface. As a result, the removal of MB dye decreases at low pH values. On the other hand, as the pH value increases, the surface charge becomes more negative sequentially and the removal of MB increases.

On the other side, the experiment results showed variations in the

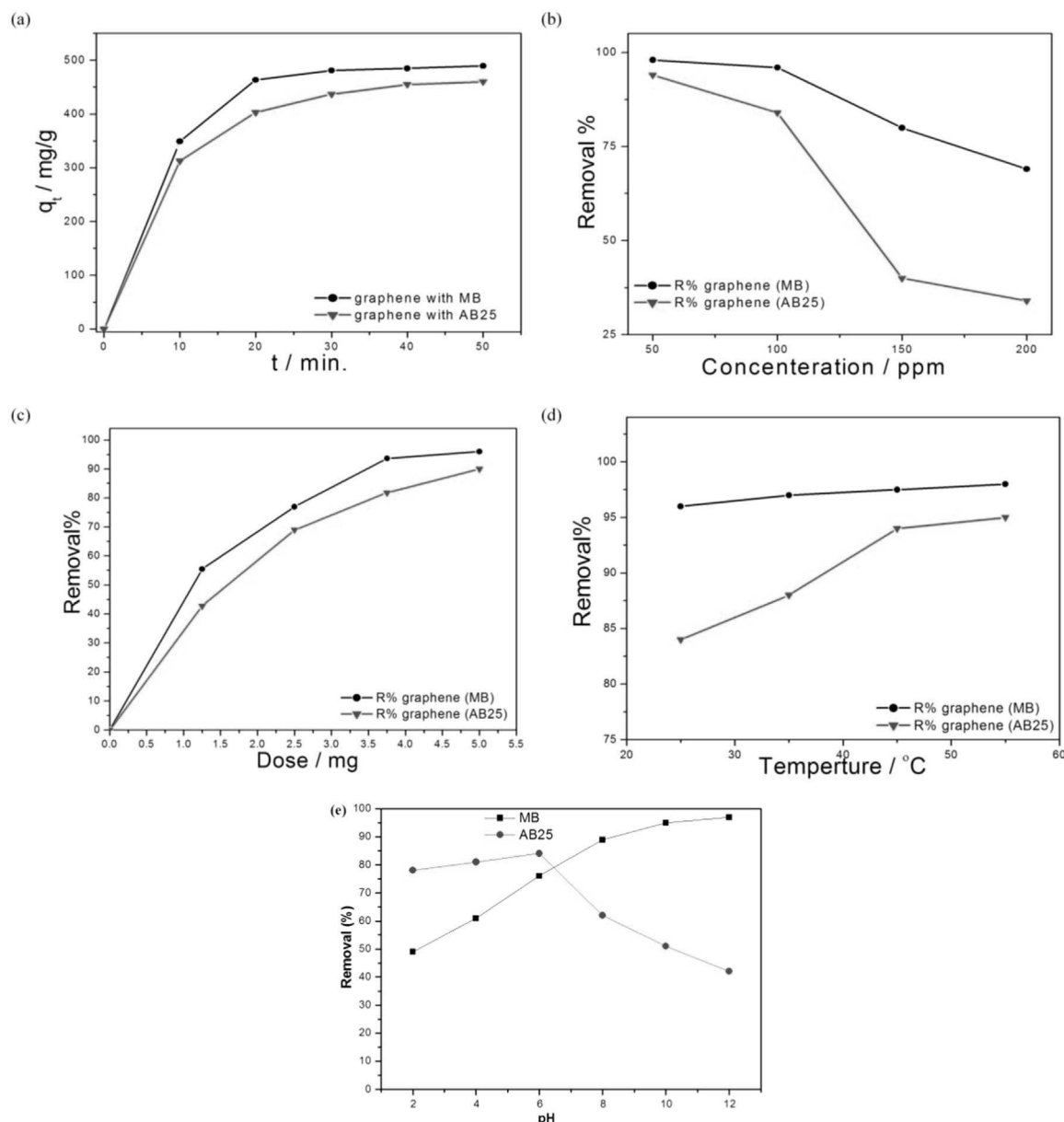
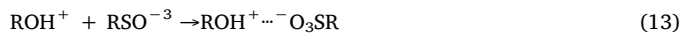
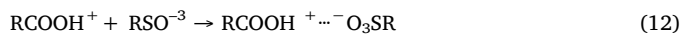


Fig. 5. Effect of processing parameters variation on MB and AB25 decolorization process onto graphene: (a) effect of contact time [Conditions: C_0 : 100 mg L⁻¹; dose of adsorbent: 0.2 mg/mL; at 25°C.]; (b) effect of initial dye concentration [at dose of adsorbent: 0.2 mg/mL; at 25°C.]; (c) effect of adsorbent dosage [at C_0 = 100 mg L⁻¹; at 25°C.]; (d) effect of dye solution temperature [at C_0 = 100 mg L⁻¹; dose of adsorbent: 0.2 mg/mL]; (e) effect of pH [C_0 = 100 mg L⁻¹; dose of adsorbent: 0.2 mg/mL at 25°C.].

AB25% removal at pH values of 2–12. It is noticed that the percentage removal of AB25 increased from pH 2–6 before it decreased gradually until pH 12. The maximum percentage removal of AB25 observed at pH 6 is 84%. The high percentage removal of the AB25 solution at acidic pH may be attributed to the electrostatic interactions between the positively charged adsorbent and the negatively charged AB25 dye anions (Hanafiah et al., 2012). Therefore, the attraction between sulfonate groups and positively charged adsorbent surface can be represented by the following equations:



The positively charged adsorbent is generated due to the hydrophobic nature of the adsorbent which tended to adsorb positive hydrogen ions on the surface when immersed in water (Ali et al., 2016). Generally, the positive charge in an acidic medium and the negative charge in basic medium have become developed on the surface of

adsorbent. Therefore, the adsorbent surface can attract the negatively charged functional groups located on AB25 dye molecules at lower pH and hence increases the adsorption capacity and decrease at higher pH. Hence, anionic dye removal by adsorption increases at low pH and decreases at high pH.

3.5. Optimization using RSM

The adsorption processes are performed according to Box-Behnken design which identified the best levels of the variables as time (min.), dye concentration (mg L⁻¹) and temperature (°C) as illustrated in Supplementary Table S4 for MB and AB25 dyes.

The quadratic model explained the statistical relationship between the selected variables and the response in terms of coded factors is the best fitted with the following equations.

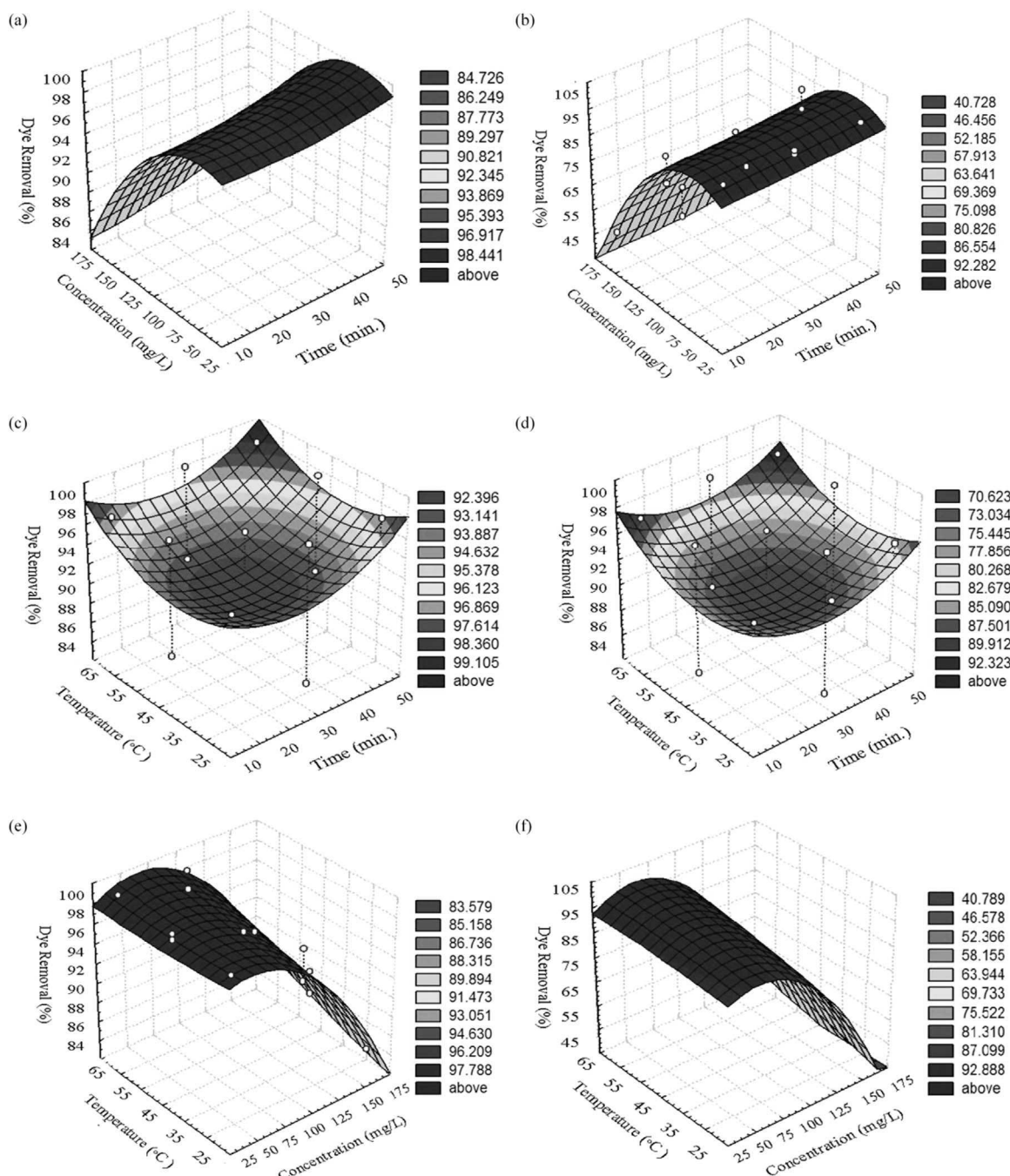


Fig. 6. Response surface plots for removal efficiency (%) of MB and AB25 onto graphene: effect of time/initial dye concentration for a)MB and b) AB25 [at dose of adsorbent: 0.2 mg/mL; at 25°C]; effect of time/temp for c) MB and d)AB25 [at $C_0 = 100 \text{ mg L}^{-1}$; at dose of adsorbent: 0.2 mg/mL]; effect of temp./initial conc. for e) MB and f) AB25 [at time:50 min; dose of adsorbent: 0.2 mg/mL].

$$\begin{aligned} Y_{\text{MB}} = & 95.98 + 1.01625X_1 - 5.53875X_2 + 1.0875X_3 + 0.5975X_1^2 \\ & - 3.5425X_2^2 + 0.415X_3^2 + 0.44X_1X_2 - 0.3025X_1X_3 + 1.0925X_2X_3 \end{aligned} \quad (14)$$

$$\begin{aligned} Y_{\text{AB25}} = & 88.97 + 1.555X_1 - 23.95125X_2 + 4.02875X_3 - 0.12875X_1^2 \\ & - 17.56125X_2^2 - 0.78625X_3^2 + 0.67X_1X_2 - 0.85X_1X_3 + 2.6175X_2X_3 \end{aligned} \quad (15)$$

where Y is the response (yield of removal) and X_1 , X_2 , and X_3 are contact time, dye concentration, and solution temperature, respectively.

The results of the Box-Behnken design can be presented in 3D presentations with contours. The 3D surface plots show the type of

interaction between the tested variables which allow obtaining the optimum conditions (Kousha et al., 2015). These plots of the second-order polynomial equation with two variables keeping constant and the other two variables within the determined experimental ranges are given in Fig. 6. The maximum predicted value is represented by the surface plots.

Fig. 6(a and b) indicates the simultaneous effect of contact time and dye concentration on dye removal efficiency for prepared graphene. The dye removal efficiency decreased with an increase in dye concentrations from 50 to 150 mg L^{-1} and the maximum efficiency was obtained with 50 mg L^{-1} initial concentrations for both dyes. Furthermore, the removal efficiencies for MB are between 91% and 99%, which achieved only after the maximum 30 min process that reveals the

high performance of the prepared graphene at studied conditions. While for AB25 the removal efficiencies lie between 70% and 97% and that carried out after 30 min.

Fig. 6(a, b, c and d) exhibit the effect of contact time, the removal efficiency increases with an increase in contact time and then remained approximately constant after 50 min. This observation revealed that in the beginning, the dye molecules are adsorbed externally and the adsorption rate increased rapidly. When the external surface became saturated, the dye molecules adsorbed into the porous structure of the graphene and finally, at some point in time, reached a constant value where no more dye is adsorbed from the solution.

The fitted surface plots of dye removal efficiency (%) versus the combined effect of initial dye concentration and solution temperature is also shown in Fig. 6(e and f). However, by investigating the combined effect of initial dye concentration and solution temperature on dye removal efficiency, it was realized that when the initial dye concentration is low, the optimum temperature is obtained at lower degree, probably due to the existence of a smaller number of dye molecules in the solution to be adsorbed on graphene. But, at highly concentrated solutions, the effect of heating is less efficient.

In this respect, the solver function of the Microsoft Excel tools was used to estimate the optimal levels of the three components. This optimal levels were obtained from the maximum point of the polynomial model to achieve 99% removal efficiency for MB were 35 min contact time, 71.7 mg L^{-1} dye concentration at solution temperature 45°C . While 95% dye removal for AB25 obtained at contact time 35 min, dye concentration of 70.58 mg L^{-1} and 45°C of solution temperature. Thereby, these results emphasize the necessity and value of an optimization process.

As illustrated in Table S4 of model validations, the agreement between the obtained and estimated removal efficiency showed that using response surface method to design the experiments can be considered as an effective choice in the optimization of process parameters besides its uses as an experimental design and statistical analysis.

3.6. Kinetic models and adsorption mechanism

To understand the adsorption process mechanism, the determination of the efficiency and control the residual time of adsorption process, the three kinetic models are used to test the experimental data, the pseudo-first-order and the pseudo-second-order and intra-particle diffusion equations. These models are helpful for the design of the sorption process and adsorption mechanism of determination the controlling steps, such as mass transport and chemical reaction. Kinetic models are tested for the kinetics of MB and AB25 dye sorption processes at various initial concentrations ($50, 100, 150$ and 200 mg L^{-1}) using the prepared graphene. The kinetic rate constants are calculated using the conventional rate expressions.

The pseudo-first-order kinetic model is more suitable for low concentration of solute. It can be written in the following form:

$$\ln(q_e - q_t) = \ln q_e - k_1 t \quad (16)$$

Where q_e is the amount of dye adsorbed at saturation per gram of adsorbent (mg g^{-1}), q_t is the amount of dye adsorbed at time t per gram of adsorbent (mg g^{-1}), and $k_1 (\text{min}^{-1})$ is the rate constant of the pseudo first-order adsorption. By plotting $\ln(q_e - q_t)$ versus time, the rate constants and q_e for MB and AB25 sorption on the prepared graphene can be calculated (Fig. S1). The calculated dye sorption capacities, the reaction rate constants, and the linear correlation coefficients R^2 values for the different studied dye concentrations were investigated in Table 1. The pseudo first order assumes that the adsorption capacity is limited by only one process or mechanism acting on one class of adsorbing sites (Abd Elhafiz et al., 2017). Comparing the calculated dye sorption capacities with the experimental capacity values, it was realized that the calculated values from the pseudo-first-order equation were far from their comparative experimental values as well as the

Table 1

Parameters and determination coefficients of the kinetic models for MB and AB25 dyes adsorption on prepared graphene.

	MB Initial concentrations (ppm) adsorbed on graphene				AB25 Initial concentrations (ppm) adsorbed on graphene			
	50	100	150	200	50	100	150	200
$q_{e,\text{exp}} (\text{mg/g})^*$	246	468	587	743	232	439	546	718
<u>Pseudo-</u> <u>1st- order</u>								
$q_{e,\text{cal}} (\text{mg/g})$	321	671	968	1297	720	1135	1895	4354
$k_1 (\text{min}^{-1})$	0.167	0.162	0.136	0.109	0.267	0.201	0.191	0.196
R^2	0.998	0.993	0.994	0.983	0.953	0.905	0.901	0.920
<u>Pseudo-</u> <u>2nd- order</u>								
$q_{e,\text{cal}} (\text{mg/g})$	241	481	610	687	248	455	561	710
$k_2 (\text{min}^{-1})$	0.004	0.002	0.0017	0.001	0.004	0.002	0.0018	0.0014
R^2	0.999	0.999	0.999	0.999	0.999	0.999	0.999	0.999

Note: * equilibrium time for MB removal equal 30 min, while for AB25 removal equal 50 min.

numerous sorption sites and mass transfer may be included at the sorption mechanism. So, the pseudo-first-order reaction kinetic model was not adequate to describe MB and AB25 dye sorption on the prepared graphene.

The pseudo-second-order kinetic model is dependent on the solute amount adsorbed on the surface of adsorbent and the adsorbed amount at equilibrium. The model parameters and the correlation coefficient (R^2) values for different initial concentrations were listed in Table 1 and Fig. S2. As it can be seen, the R^2 values obtained are consistently higher than those of the pseudo-first-order. In addition, the q_e calculated values are in a harmony with the experimental q_e values ($q_{e,\text{exp}}$). These results indicated that the adsorption perfectly obeys the pseudo-second-order model, meaning that the controlling rate step is chemisorption. Moreover, the result showed that the rate of adsorption for both dyes depended on the availability of adsorption sites on the surface of graphene as adsorbent material, whereas the dye concentration increased the k_2 values was decreased. This may be due to the higher competition for the adsorption site at a high dye concentration compared to low dye concentration (Chen et al., 2011).

To test the diffusion mechanism of MB and AB25 onto the prepared graphene, an intraparticle diffusion model has been used at different initial dye concentrations using the following form:

$$q_t = k_i t^{0.5} + C \quad (17)$$

Where; $k_i (\text{mg g}^{-1} \text{ min}^{-1/2})$ intraparticle diffusion rate constant which is the slope of the straight line of q_t versus $t^{1/2}$ and C is the value of the intercept which is a constant reflecting the significance of the boundary layer or mass transfer effect. As shown in Fig. 7 all the plots have the same general aspect, whereas the diffusion mechanism of the adsorption processes is generally divided into three steps for each curve from larger pores to micropores. In the first step, the external surface adsorption or diffusion in macropores occurred at the outer material surfaces which are followed by the second step, which is controlled by intraparticle diffusion; it is the gradual adsorption step. Lastly, the third step is the slowest step which represents the final equilibrium step. As listed in Table S5, k_i increased with increasing dye concentration, as a result of the fact that multitude dye molecules interacted with active sites on adsorbent which caused high adsorption intensity at a high initial concentration. For all initial concentrations, $k_{i,1}$ is larger than $k_{i,2}$, which indicates that the free path available for diffusion became smaller and the pore dimensions decreased (Wang et al., 2016). The $k_{i,3}$

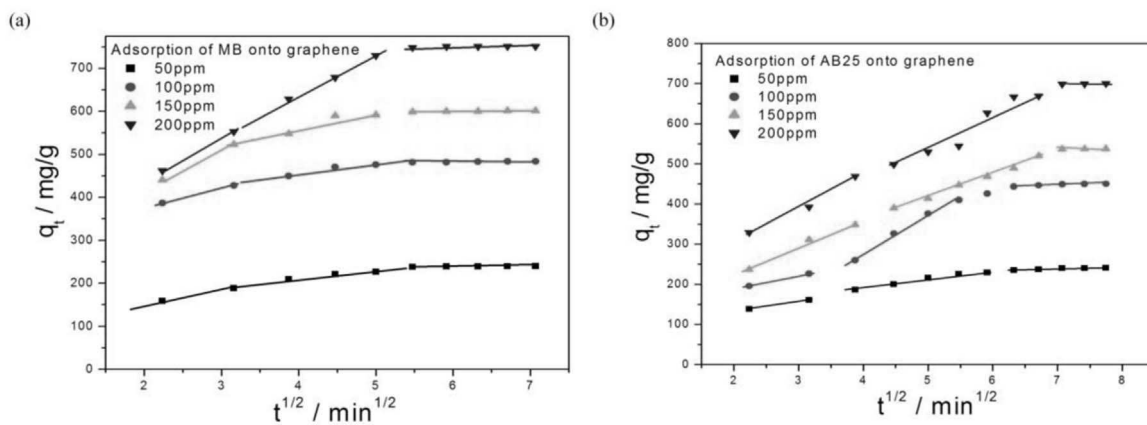


Fig. 7. Intra-particle diffusion kinetic model fit for the adsorption of (a)MB and (b) AB25 onto graphene. [Conditions: dose of adsorbent was 0.2 mg/mL; at 25 °C].

is significantly lower than the others, which confirmed that the third step is the slowest step.

3.7. Adsorption isotherms

The analysis of the isotherm data is urgent to develop an equation which represents the results used for the design. Adsorption equilibrium is traditionally evaluated by adsorption isotherms. It is obtained from experimental data using Langmuir and Freundlich adsorption isotherm models at different initial concentrations and two different temperatures (25 °C and 55 °C). According to the correlation coefficients and parameter values which summarized in Table 2, the R^2 of Langmuir model was very close to 1 and larger than Freundlich model which suggests that the adsorption was a process which occurred in a homogeneous surface. Thus, with the consideration of R^2 and the error functions, it was concluded that the Langmuir model best represented the adsorption data. In addition, the values of R_L at low temperatures were higher than those at high temperatures as shown in Fig S3. It can be deduced that the adsorption behavior was more effective at high temperatures (Gao et al., 2013) and the adsorption process was more irreversible. From Freundlich model, the values of $1/n_F$ which are a measure of adsorption intensity or surface heterogeneity fluctuate between 0 and 1 and that elucidate more heterogeneity as the values get closer to zero. Table 2 shows the values of $1/n_F$ at different concentrations at temperature 25 and 55 °C. It can be seen that all the values of $1/n$ are smaller than 1. However, the results also indicate that adsorption of both dyes is effective using Freundlich isotherm model.

3.8. Adsorption thermodynamics

The adsorption thermodynamics provided some useful information

Table 2

Adsorption isotherm parameters for the adsorption of MB and AB25 dyes onto prepared graphene at adsorbent dosage 0.2 mg/mL.

Temperature °C	MB adsorption onto graphene		AB25 adsorption onto graphene	
	25 °C	55 °C	25 °C	55 °C
Langmuir isotherm				
q_m (mg/g)	761.3	867.2	642.9	641.4
k_L (L/mg)	0.284	0.782	0.247	1.364
R^2	0.996	0.999	0.995	0.999
R_L	0.014	0.010	0.019	0.005
Freundlich isotherm				
K_F (mg/g)	183.745	245.145	200.463	368.353
$1/n_F$	0.335	0.338	0.317	0.204
R^2	0.996	0.976	0.992	0.998

on energy changes of the adsorption process. The thermodynamic parameters were summarized in Table 3. The negative values of ΔG showed that both dye adsorbent systems were spontaneous in nature. Furthermore, the decrease in the values of ΔG with the increasing temperature showed clearly that the adsorption was more spontaneous at higher temperatures (Wu et al., 2015b). The positive values of ΔH indicate an endothermic nature of the process. On the other hand, the positive values of ΔS indicate an increase in randomness in the solid and solution interface during the adsorption process (Yu et al., 2014). However, the positive value of ΔS can demonstrate a result of “solvent-replacement” phenomenon, where the dye molecules need to replace the water molecules on the adsorbent surface in order to be adsorbed (Kooh et al., 2016; Zhao et al., 2016).

4. Conclusions

This study involved the preparation of graphene via thermal dissociation of Poly-ethylene-terephthalate waste. The results revealed that the prepared graphene has a relatively high surface area and micropore volumes and it was found out to be a promising adsorbent for dye removal from aqueous solutions.

The adsorption efficiency of MB and AB25 is increased with increasing the solution temperature and dose of adsorbent and decrease with increasing initial dye concentration. While the amount of dye adsorbed was increased with increasing contact time at all initial dye concentrations. Furthermore, the adsorption processes reached equilibrium within 30 and 50 min for MB and AB25 respectively which represent short time duration. The adsorption of MB was favored at alkaline medium and the optimum pH value was found to be 12, while AB25 adsorption was favored at acidic medium. Whereas, RSM optimization results indicated that solution temperature, and dye concentrations are the most important variables in the removal of MB and AB25 dyes. In kinetic study, the pseudo-second order kinetic model was found to be well suited for the entire adsorption process of MB and AB25. Adsorption kinetic was generally controlled by different mechanisms, of which the most limiting are the diffusion mechanisms, including film diffusion and intra-particle diffusion. All equilibrium data obtained at different temperatures fit perfectly with Langmuir and Freundlich isotherm models. The negative values of ΔG and positive values of ΔH and ΔS indicate that the dyes adsorption process is spontaneous, endothermic and an increase in randomness occurs at the solid or solution interface. The overall results showed that the prepared graphene from thermal dissociation of PET waste bottles is an effective and low-cost adsorbent for the removal of MB and AB25 from aqueous solutions.

Table 3

Thermodynamics parameters of prepared graphene on the removal of 100 ppm of MB and AB25 at temperature ranged from 25 to 55 °C.

Temperature °C	MB adsorption onto graphene				AB25 adsorption onto graphene			
	25 °C	35 °C	45 °C	55 °C	25 °C	35 °C	45 °C	55 °C
ΔG(kJ/mole)	-11.3	-12.1	-13.6	-14.8	-9.8	-10.4	-11.8	-12.6
ΔH(kJ/mole)	18.9				17.6			
ΔS(J/mole K)	45.8				38.7			

Appendix A. Supplementary material

Supplementary data associated with this article can be found in the online version at <http://dx.doi.org/10.1016/j.ecoenv.2017.07.014>.

References

- Abd Elhafez, S.E., Hamad, H.A., Zaatout, A.A., Malash, G.F., 2017. Management of agricultural waste for removal of heavy metals from aqueous solution: adsorption behaviors, adsorption mechanisms, environmental protection and techno-economic analysis. *Environ. Sci. Poll. Res.* 24, 1397–1415.
- Abd Ellatif, M.M., Ibrahim, A.M., 2009. Adsorption, kinetic and equilibrium studies on removal of basic dye from aqueous solutions using hydrolyzed oak sawdust. *Desalination Water Treat.* 6, 252–268.
- Adel, M., Mohamed, M.A.A., El-Maghraby, A., El-Shazly, O., El-Wahidy, E.F., 2016. Synthesis of few-layer graphene-like nanosheets from glucose: new facile approach for graphene-like nanosheets large-scale production. *J. Mater. Res.* 31 (4), 455–467.
- Ali, R.M., Hamad, H.A., Hussein, M.M., Malash, G.F., 2016. Potential of using green adsorbent of heavy metal removal from aqueous solutions: adsorption kinetics, isothermal, thermodynamic, mechanism and economic analysis. *Ecol. Eng.* 91, 317–332.
- Bangash, F.K., Alam, S., 2009. Adsorption of acid blue 1 on activated carbon produced from the wood of *Ailanthus altissima*. *Braz. J. Chem. Eng.* 26, 275–285.
- Bassyouni, D.G., Hamad, H.A., El-Ashtoukhy, E.-S.Z., Amin, N.K., El-Latif, M.M.A., 2017. Comparative performance of anodic oxidation and electrocoagulation as clean processes for electrocatalytic degradation of diazo dye Acid Brown 14 in aqueous medium. *J. Hazard. Mater.* 335, 178–187.
- Bazargan, A., McKay, G., 2012. A review e synthesis of carbon nanotubes from plastic wastes. *Chem. Eng. J.* 195–196, 377–391.
- Box, G., Behnken, D.W., 1960. Some new three level designs for the study of quantitative variables. *Technometrics* 2, 455–475.
- Chen, H., Zhao, J., Dai, G., 2011. Silkworm exuviae-A new non-conventional and low-cost adsorbent for removal of methylene blue from aqueous solutions. *J. Hazard. Mater.* 186, 1320–1327.
- Ciardelli, G., Corsi, L., Marcucci, M., 2001. Membrane separation for wastewater reuse in the textile industry. *Conser. Recycl.* 31, 189–197.
- Deng, J., You, Y., Sahajwalla, V., Joshi, R.K., 2016. Transforming waste into carbon-based nanomaterials. *Carbon* 96, 105–115.
- Dutt, K., Soni, R.K., 2013. A review on synthesis of value added products from polyethylene terephthalate (PET) waste. *Polym. Sci. Ser. B* 55, 430–452.
- El Essawy, N., Konsowa, A.H., Elnoubey, M., Farag, H.A., 2016. A novel one step synthesis for carbon based nanomaterials from polyethyleneterephthalate (PET) bottles. *J. Air Waste Manag. Assoc.* 1–13. <http://dx.doi.org/10.1080/10962247.2016.1242517>.
- Elkady, M.F., El-Sayed, E.M., Farag, H.A., Zaatout, A.A., 2014. Assessment of novel synthesized nanozirconium tungstovanadate as cation exchanger for lead ion decontamination. *J. Nanomat.* 2014, 1–11.
- Elkady, M.F., Hassan, H.S., El-Sayed, E.M., 2015. Basic violet decolorization using alginate immobilized nanozirconium tungstovanadate matrix as cation exchanger. *J. Chem.* 2015, 1–10.
- Elkady, M., Shokry, H., Hamad, H., 2016. Effect of superparamagnetic nanoparticles on the physicochemical properties of nano hydroxyapatite for groundwater treatment: adsorption mechanism of Fe(II) and Mn(II). *RSC Adv.* 6, 82244–82259.
- El-Remaily, M.A.A.A., Hamad, H.A., 2015. Synthesis and characterization of highly stable superparamagnetic CoFe₂O₄ nanoparticles as a catalyst for novel synthesis of thiazolo [4,5-b]quinolin-9-one derivatives in aqueous medium. *J. Mol. Catal. A: Chem.* 404, 148–155.
- Fathy, M., Hamad, H., Kashyout, A., 2016. Influence of calcination temperatures on the formation of anatase TiO₂ nano rods with a polyol mediated solvothermal method. *RSC Adv.* 6, 7310–7316.
- Forgacs, E., Cserh'ati, T., Oros, G., 2004. Removal of synthetic dyes from wastewaters: a review. *Environ. Int.* 30, 953–971.
- Gao, J.J., Qin, Y.B., Zhou, T., Cao, D., Xu, P., Hochstetter, D., Wang, Y., 2013. Adsorption of methylene blue onto activated carbon produced from tea (*Camellia sinensis* L.) seed shells: kinetics, equilibrium, and thermodynamics studies. *J. Zhejiang Univ.-Sci. B (Biomed. Biotechnol.)*.
- Gopinath, K.P., Murugesan, S., Abraham, J., Muthukumar, K., 2009. *Bacillus* sp. mutant for improved biodegradation of Congo red: random mutagenesis approach. *Bioresour. Technol.* 100, 6295–6300.
- Hamad, H., Abd El-latif, M., Kashyout, A., Sadik, W., Feteha, M., 2014. Study on synthesis of superparamagnetic spinel cobalt ferrite nanoparticles as layered double hydroxides by co-precipitation method. *Russ. J. Gen. Chem.* 84, 2031–2036.
- Hamad, H.A., Abd El-latif, M.M., Kashyout, A.B., Sadik, W.A., Feteha, M.Y., 2015a. Synthesis and characterization of core-shell-shell magnetic (CoFe₂O₄–SiO₂–TiO₂) nanocomposites and TiO₂ nanoparticles for the evaluation of photocatalytic activity under UV and visible irradiation. *New J. Chem.* 39 (4), 3116–3128.
- Hamad, H., Abd El-latif, M., Kashyout, A., Sadik, W., Feteha, M., 2015b. Optimizing the preparation parameters of mesoporous nanocrystalline titania and its photocatalytic activity in water: physical properties and growth mechanisms. *Process Saf. Environ. Prot.* 98, 390–398.
- Hamad, H.A., Sadik, W.A., Abd El-latif, M.M., Kashyout, A.B., Feteha, M.Y., 2016. Photocatalytic parameters and kinetic study for degradation of dichlorophenol-indophenol (DCPIP) dye using highly active mesoporous TiO₂ nanoparticles. *J. Environ. Sci.* 43, 26–39.
- Han, Z., Zhu, Z., Wu, D., Wu, J., Liu, Y., 2014. Adsorption kinetics and thermodynamics of acid blue 25 and methylene blue dye solutions on natural sepiolite. *Synth. React. Inorg. Met.-Org. Nano-Met. Chem.* 44, 140–147.
- Hanafiah, M.A., Ngah, W.S., Zolkafly, S.H., Teong, L.C., Abdul Majid, Z.A., 2012. Acid Blue 25 adsorption on base treated Shorea dasypyllea sawdust: kinetic, isotherm, thermodynamic and spectroscopic analysis. *J. Environ. Sci.* 24, 261–268.
- Hu, B., Huang, C., Li, X., Sheng, G., Li, H., Ren, X., Ma, J., Wang, J., Huang, Y., 2017. Macroscopic and spectroscopic insights into the mutual interaction of graphene oxide, Cu(II), and Mg/Al layered double hydroxides. *Chem. Eng. J.* 313, 527–534.
- Hu, B., Ye, F., Ren, X., Zhao, D., Sheng, G., Li, H., Ma, J., Wang, X., Huang, Y., 2016. X-ray absorption fine structure study of enhanced sequestration of U(LV) and Se(LV) by montmorillonite decorated with zero-valent iron nanoparticles. *Environ. Sci.: Nano* 2016 (3), 1460–1472.
- Idris, M.N., Ahmad, Z.A., Ahmad, M.A., 2011. Adsorption equilibrium of malachite green dye onto rubber seed coat based activated carbon. *Int. J. Basic Appl. Sci.* 11 (3), 38–43.
- Jin, Z., Wang, X., Sun, Y., Ai, Y., Wang, X., 2015. Adsorption of 4-n-nonylphenol and bisphenol-A on magnetite reduced graphene oxides: a combined experimental and theoretical studies. *Environ. Sci. Technol.* 49 (15), 9168–9175.
- Kooh, M.R.R., Dahri, M.K., Lim, L.B.L., Lim, L.H., 2016. Batch adsorption studies on the removal of acid blue 25 from aqueous solution using Azolla pinnata and soya bean waste. *Arab J. Sci. Eng.* 41, 2453–2464.
- Kousha, M., Tavakoli, S., Daneshvar, E., Vazirzadeh, A., Bhatnagar, A., 2015. Central composite design optimization of Acid Blue 25 dye biosorption using shrimp shell biomass. *J. Mol. Liq.* 207, 266–273.
- Kui, L., Xia, Z.G., Ke, W.X., 2012. A brief review of graphene-based material synthesis and its application in environmental pollution management. *Chin. Sci. Bull.* 57, 1223–1234.
- Lian, F., Xing, B., Zhu, L., 2011. Comparative study on composition, structure, and adsorption behavior of activated carbons derived from different synthetic waste polymers. *J. Colloid Interface Sci.* 360, 725–730.
- Malard, L.M., Pimenta, M.A., Dresselhaus, G., Dresselhaus, M.S., 2009. Raman spectroscopy in graphene. *Phys. Rep.* 473, 51–87.
- Mallakpour, S., Behravand, V., 2016. Manufacture and characterization of nanocomposite materials obtained from incorporation of D-glucose functionalized MWCNTs into the recycled poly(ethylene terephthalate). *Des. Monomers Polym.* 19, 283–289.
- Mendoza-Carrasco, R., Cuerda-Correa, E.M., Alexandre-Franco, M.F., Fernandez-Gonzalez, C., Gomez-Serrano, V., 2016. Preparation of high-quality activated carbon from poly ethylene terephthalate (PET) bottle waste. Its use in the removal of pollutants in aqueous solution. *J. Environ. Manag.* 181, 522–535.
- Mishra, S., Goje, A.Z., Zope, V.S., 2003. Chemical recycling, kinetics, and thermodynamics of poly (ethylene terephthalate)(PET) waste powder by nitric acid hydrolysis. *Polym. React. Eng.* 11, 79–99.
- Nakagawa, K., Namba, A., Mukai, S.R., Tamon, H., Ariyadejwanich, P., Tanthapanichakoon, W., 2004. Adsorption of phenol and reactive dye from aqueous solution on activated carbons derived from solid wastes. *Water Res.* 38, 1791–1798.
- Nasuha, N., Hameed, B.H., 2011. Adsorption of methylene blue from aqueous solution onto NaOH-modified rejected tea. *J. Chem. Eng.* 66, 783–786.
- Ni, Z.H., Yu, T., Lu, Y.H., Wang, Y.Y., Feng, Y.P., Shen, Z.X., 2008. Uniaxial strain on graphene: raman spectroscopy study and bandgap opening. *ACS Nano* 2, 2301–2305.
- Parra, J., Ania, C., Arenillas, A., Rubiera, F., Palacios, J., Pis, J., 2004. Carbonaceous materials from recycled PET [Materiales carbonosos obtenidos a partir del reciclado de PET]. *Boletín De. la Soc. Esp. De. Ceram. Y. Vidr.* 43, 547–549.
- Pajootan, E., Arami, M., Rahimdokht, M., 2014. Application of carbon nanotubes coated electrodes and immobilized TiO₂ for dye degradation in a continuous photocatalytic-electro-fenton process. *Ind. Eng. Chem. Res.* 53, 16261–16269.
- Rafatullah, M., Sulaiman, O., Hashim, R., Ahmad, A., 2010. Adsorption of methylene blue on low-cost adsorbents: a review. *J. Hazard. Mater.* 177, 70–80.
- Rahimdokht, M., Pajootan, E., Arami, M., 2016. Central composite methodology for methylene blue removal by *Elaeagnus angustifolia* as a novel biosorbent. *J. Environ. Chem. Eng.* 4, 1407–1416.

- Saha, B., Ghoshal, A., 2005. Thermal degradation kinetics of poly(ethylene terephthalate) from waste soft drinks bottles. *Chem. Eng. J.* 111, 39–43.
- Sergienko, R., Shibata, E., Kim, S., Kinota, T., Nakamura, T., 2009. Nanographite structures formed during annealing of disordered carbon containing finely-dispersed carbon nanocapsules with iron carbide cores. *Carbon* 47, 1056–1065.
- Shen, Y., Lua, A.C., 2013. A facile method for the large-scale continuous synthesis of graphene sheets using a novel catalyst. *Sci. Rep.* <http://dx.doi.org/10.1038/srep03037>.
- Sheng, G., Alsaedi, A., Shammakh, W., Monaque, S., Sheng, J., Wang, X., Li, H., Huang, Y., 2016a. Enhanced sequestration of selenite in water by nanoscale zero valent iron immobilization on carbon nanotubes by a combined batch, XPS and XAFS investigation. *Carbon* 99, 123–130.
- Sheng, G., Hu, J., Li, H., Li, J., Huang, Y., 2016b. Enhanced sequestration of Cr(VI) by nanoscale zero-valent iron supported on layered double hydroxide by batch and XAFS study. *Chemosphere* 148, 227–232.
- Sheng, G., Tang, Y., Linghu, W., Wang, L., Li, J., Li, H., Wang, X., Huang, Y., 2016c. Enhanced immobilization of ReO₄⁻ by nanoscale zerovalent iron supported on layered double hydroxide via an advanced XAFS approach: implications for TcO₄⁻ sequestration. *Appl. Catal. B: Environ.* 192, 268–276.
- Sivakumar, P., Palanisamy, P.N., 2009. Adsorption studies of basic red 29 by anion-conventional activated carbon prepared from Euphorbia antiquorum L. *J. Chem. Technol. Res.* 1, 502–510.
- Wang, H., Gao, H., Chen, M., Xu, X., Wang, X., Pan, C., Gao, J., 2016. Microwave-assisted synthesis of reduced graphene oxide/titania nanocomposites as an adsorbent for methylene blue adsorption. *Appl. Surf. Sci.* 360 (2016), 840–848.
- Wu, Z.-L., Liu, Q., Chen, X.-Q., Yu, J.-G., 2015a. Preconcentration and analysis of Rhodamine B in water and red wine samples by using magnesium hydroxide/carbon nanotube composites as a solid-phase extractant. *J. Sep. Sci.* 38, 3404–3411.
- Wu, Z.-L., Yang, H., Jiao, F.-P., Liu, Q., Chen, X.-Q., Yu, J.-G., 2015b. Carbon nanoparticles pillared multi-walled carbon nanotubes for adsorption of 1-naphthol: thermodynamics, kinetics and isotherms. *Colloids Surf. A: Physicochem. Eng. Asp.* 470, 149–160.
- Yu, J.-G., Zhao, X.-H., Yang, H., Chen, X.-H., Yang, Q., Yu, L.-Y., Jiang, J.-H., Chen, X.-Q., 2014. Aqueous adsorption and removal of organic contaminants by carbon nanotubes: review. *Sci. Total Environ.* 482–483, 241–251.
- Yu, J.-G., Yu, L.-Y., Yang, H., Liu, Q., Chen, X.-H., Jiang, X.-Y., Chen, X.-Q., Jiao, F.-P., 2015. Graphene nanosheets as novel adsorbents in adsorption, preconcentration and removal of gases, organic compounds and metal ions. *Sci. Total Environ.* 502, 70–79.
- Yu, L., Wu, X., Liu, Q., Liu, L., Jiang, X., Yu, J., Feng, C., Zhong, M., 2016a. Removal of phenols from aqueous solutions by graphene oxide nanosheet suspensions. *J. Nanosci. Nanotechnol.* 16, 12426–12432.
- Yu, J.-G., Yue, B.-Y., Wu, X.-W., Liu, Q., Jiang, X.-Y., Zhong, M., Li, H.-Y., Li, S.-S., Chen, X.-Q., 2016b. The covalently organic functionalization of graphene: methodologies and protocols. *Curr. Org. Chem.* 20, 1284–1298.
- Yuan, Y., Cabasso, I., Liu, H., 2008. Surface morphology of nanostructured polymer-based activated carbons. *J. Phys. Chem. B* 112, 14364–14372.
- Zhang, J., Wang, X., Qi, G., Li, B., Song, Z., Jiang, H., Zhang, X., Qiao, J., 2016. A novel N-doped porous carbon microsphere composed of hollow carbon nanospheres. *Carbon* 96, 864–870.
- Zhao, H., Qiu, F., Yan, J., Wang, J., Li, X., Yang, D., 2016. Preparation of economical and environmentally friendly graphene/palygorskite/TiO₂ composites and its application for the removal of methylene blue. *Appl. Clay Sci.* 121–123, 137–145.